PERFORMANCE OF STEEL PIPELINES BACKFILLED WITH CONTROLLED LOW-STRENGTH MATERIAL (CLSM) UNDER SEISMIC WAVE PROPAGATION AND REVERSE-SLIP FAULT RUPTURE

A DISSERTATION IN
Civil Engineering
and
Geosciences

Presented to the Faculty of the University
of Missouri-Kansas City in partial fulfillment of
the requirements for the degree

DOCTOR OF PHILOSOPHY

by
PRAPON SOMBOONYANON

B.E., King's Mongkhut Institute of Technology of Thonburi, 1999
B.S., University of Missouri-Kansas City, 2001
M.S., University of Missouri-Kansas City, 2003

Kansas City, Missouri
2019

PERFORMANCE OF STEEL PIPELINES BACKFILLED WITH CONTROLLED LOW-STRENGTH MATERIAL (CLSM) UNDER SEISMIC WAVE PROPAGATION AND REVERSE-SLIP FAULT RUPTURE

Prapon Somboonyanon, Candidate for the Doctor of Philosophy Degree

University of Missouri-Kansas City, 2019

ABSTRACT

Seismic events may drastically damage buried pipelines affecting economy and public safety. Traditionally, buried pipelines are bedded and backfilled with compacted soils, which is labor intensive, time consuming, and could be a safety hazard to workers. Many studies have shown that achieving a proper compaction level around pipelines can be a difficult task. Improper compaction can greatly reduce performance of the pipelines under loads.

Controlled Low-Strength Materials (CLSM) is a group of cementitious materials that can be used as an alternative to compacted soils to backfill pipelines. These mixtures are highly flowable in their fresh state and are solid in the final state providing a uniform support around pipelines. Although there is considerable research about the advantages of using CLSM to backfill pipelines from construction point of view, there is no research on the performance of pipelines embedded in CLSM subject to seismic loads. In this research, 3D FEA was conducted using ABAQUS software to determine the

performance of buried steel pipes backfilled with CLSM when subjected to seismic wave propagation and reverse-slip fault rupture.

Under seismic wave propagation, the study started by evaluating the ASCE guidelines and its design limitations. Then, several FE model parameters were evaluated for their effects on FE model results. After setting the model parameters to match the predicted stresses by the ASCE guidelines, the developed FE model was used to evaluate the pipe seismic performance with various soil and CLSM backfill materials. Both linear and non-linear material behavior were considered in this study.

Under seismic fault rupture, the study developed a 3D FE model matching results from a full-scale testing performed by others. Various FE model parameters were also evaluated. Then, the developed FE model was utilized to determine the pipe seismic performance of CLSM mixture compared to compacted soil backfill.

Results indicated that for 3D FEA pipe seismic analysis, FE model parameters can have a significant effect on the results. In addition, with a proper design buried steel pipe embedded in CLSM backfill with all its inherent advantages can perform as well as or better than soils in seismic prone areas.

APPROVAL PAGE

The faculty listed below, appointed by the Dean of the School of Graduate Studies, have examined a dissertation titled "Performance of Steel Pipelines Backfilled with Controlled Low-Strength Material (CLSM) under Seismic Wave Propagation and Reverse-Slip Fault Rupture," presented by Prapon Somboonyanon, candidate for the Doctor of Philosophy degree, and certify that in their opinion it is worthy of acceptance.

Supervisory Committee

Ceki Halmen, Ph.D., P.E., Committee Chair
Department of Civil and Mechanical Engineering

Ganesh Thiagarajan, Ph.D., P.E.
Department of Civil and Mechanical Engineering

John T. Kevern, Ph.D., P.E., FACI, LEED AP
Department of Civil and Mechanical Engineering

Jejung Lee, Ph.D.
Department of Geosciences

Tina M. Niemi, Ph.D., R.G.
Department of Geosciences

TABLE OF CONTENTS

LIST OF ILLUSTRATIONS

Figure Page

LIST OF TABLES

ACKNOWLEDGEMENTS

First of all, I would like to truly thank my advisor and committee chair, Dr. Ceki Halmen, for his continuous guidance, mentorship, and dedication throughout my long journey of this doctoral program. Without him, this dissertation would definitely have not been possible. I also highly appreciate the members of my dissertation committee for their inputs, recommendations, and constructive feedbacks throughout this process: Dr. Ganesh Thiagarajan, Dr. John Kevern, Dr. Jejung Lee, and Dr. Tina Niemi.

I would like to extend my deepest gratitude to my supervisors and executives at Burns & McDonnell for their understandings and encouragements throughout this doctoral degree as well as their continuous and ongoing supports along my career.

On a more personal note, I would like to thank my parents, Surapol and Phairin Somboonyanon, my sister, Narapat Somboonyanon, and my wife, Pantip Leetacheewa, for their unconditional love and tremendous sacrifice. My heartfelt appreciation also goes to George and Helen, Chris and Jak, and all of my friends and colleagues here in Kansas City. I cannot thank them enough for everything they have done to support me to reach this invaluable academic achievement.

CHAPTER 1

INTRODUCTION

1.1 General Overview and Background

1.1.1 Introduction

Buried steel pipelines are often used to transport materials such as oil, gas, and other fluids. According to [1], there is more than 2.4 million miles of energy pipelines network installed in the United States, the largest network in the world, with almost the entire system being buried pipelines. Buried pipelines extend into a wide range of geologic conditions as well as different seismic zones. Different seismic events such as permanent ground deformation, liquefaction, landslide, fault rupture, or wave propagation could cause failure of buried steel pipelines with drastic impacts on economy and public safety.

Traditionally, buried steel pipelines are bedded and backfilled with several layers of compacted soils, as shown in Figure 1.

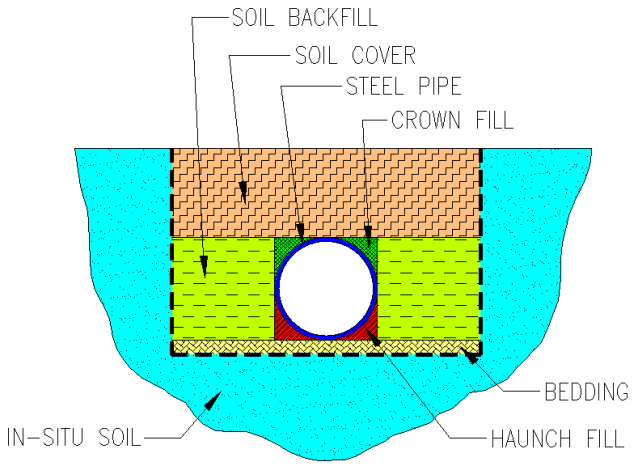

Figure 1: Conventional buried pipe installation

This construction method is labor intensive and time consuming. Many studies, e.g. [2], have shown that achieving a proper soil compaction level around pipelines, especially in the haunch zone, can be a very difficult task. Improper compaction could potentially result in pipe settlements and can greatly reduce performance of the pipelines under loads. In addition, a wider area of excavation would be required to accommodate workers and equipment for pipe installations, and with a limited working space it could be safety hazards on workers.

1.1.2 Controlled Low-Strength Material (CLSM)

With several drawbacks on the conventional pipe installation method, Controlled Low-Strength Material (CLSM) has been increasingly used as an alternative to compacted soils to backfill pipelines. Other CLSM applications include void filling, pavement base, structural fill, bridge approach backfill, etc. Figure 2 shows a typical pipe installation with CLSM backfill.

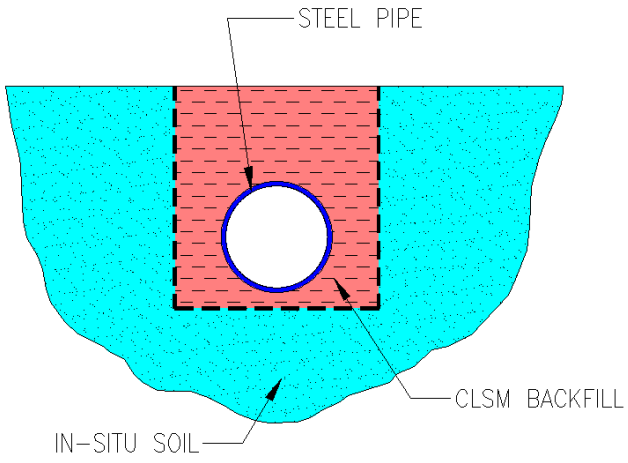

Figure 2: Buried pipe with CLSM backfill

CLSM, frequently referred to as flowable fill, is a group of self-consolidating cementitious materials that are highly flowable in their fresh state and are solid in the final state providing a uniform support to pipelines. CLSM mixtures typically consists of cementitious materials, fine and/or coarse aggregates, and water. There are a large number of studies that successfully include several waste materials and by-products in CLSM mixture such as fly ash, quarry fines, synthetic gypsum, foundry sand, cement kiln dust, wood ash, scrap tire, etc. [3-5]. As stated in the American Concrete Institute (ACI) committee 229 report [6], CLSM is being used more and more as a backfill material for buried pipes due to its inherent advantages compared to compacted soils. Some of the advantages include shorter construction time, less inspection required, ease of placement, improvement in worker safety and pipe settlement, and being environment-friendly materials. Although using CLSM a backfill material for underground pipelines has several benefits, their performance in seismic zones are not sufficiently evaluated.

1.1.3 Seismic Phenomena

There are several reports available, e.g. [7-9], regarding pipeline damages caused by different earthquake events. Seismic wave propagation and permanent ground deformations are among the causes of underground pipeline failures. Permanent ground deformations can occur in several forms, such as fault rupture, liquefaction, settlements, and landslide. Based on a study by Eguchi [10] evaluating the pipeline damages as a result of the 1971 San Fernando earthquake, it concluded that almost half of the total damage occurred in the areas where fault rupture was observed. Therefore, this study

mainly focused on buried pipelines subject to seismic wave propagation and seismic fault rupture.

1.1.3.1 Seismic Wave Propagation

An earthquake event generates seismic waves that propagate through the earth's crust. According to [11], there are two major wave type; 1) body waves and 2) surface waves. Body waves consist of P-wave, also known as compressional wave, and S-wave, or secondary wave. P-wave is the fastest of all wave types and can travel through any medium. S-wave is slower than P-wave and can only travel through solid medium. There are two types of surface waves; 1) Love waves and 2) Rayleigh waves. Just like its type, surface waves travel at the ground surface with side-to-side action for Love waves travel at the ground and with the combined actions, up-down and side-to-side, for Rayleigh waves. Figure 3 shows types of seismic waves.[12]

In this study, the selected earthquake event was Loma Prieta earthquake occurred on October 17, 1989 in San Francisco Bay area. The seismic ground acceleration records were obtained from Center for Engineering Strong Motion Data (CESMD) [13]. The earthquake was caused by a slip along San Andrea fault with the recorded magnitude of 6.9. Figure 4 shows time-history of ground displacement, velocity, and acceleration in all directions for this earthquake event at the record station on Eureka Canyon Road in Corralitos, California [13].

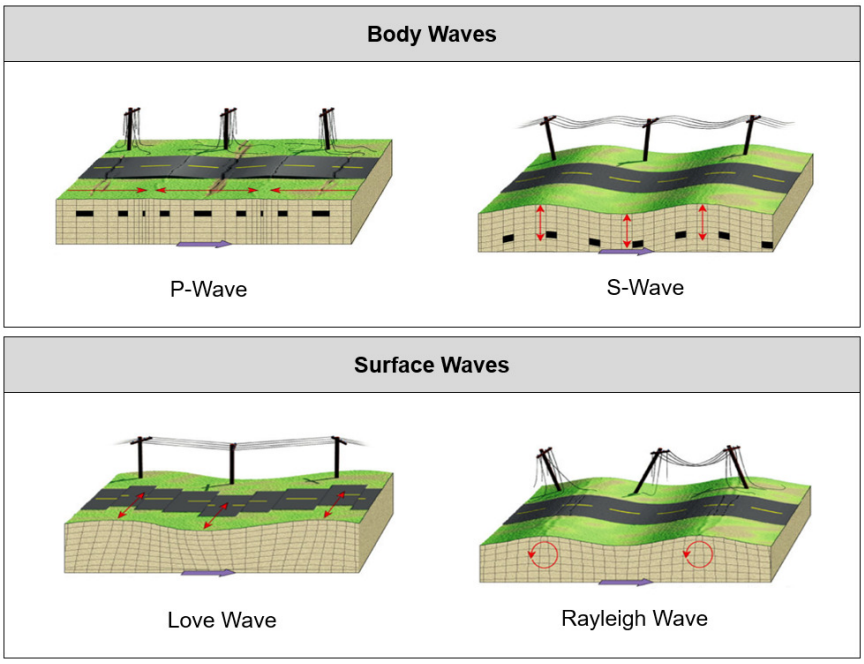

Figure 3: Types of seismic waves [12]

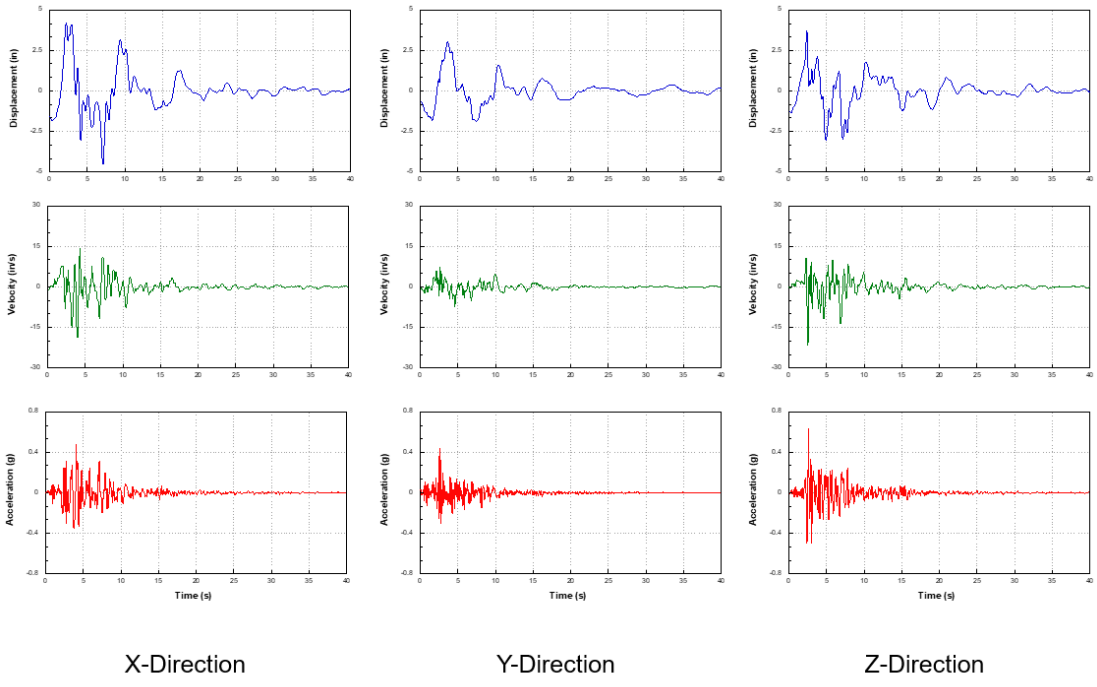

Figure 4: 1989 Loma Prieta earthquake seismic record [13]

1.1.3.2 Seismic Fault Rupture

Fault rupture is the displacement that happens as a result of a sudden movement of the earth's crust. Fault ruptures are categorized by the direction of movement, such as normal-slip, strike-slip, reverse-slip, and oblique-slip fault, as shown in Figure 5.

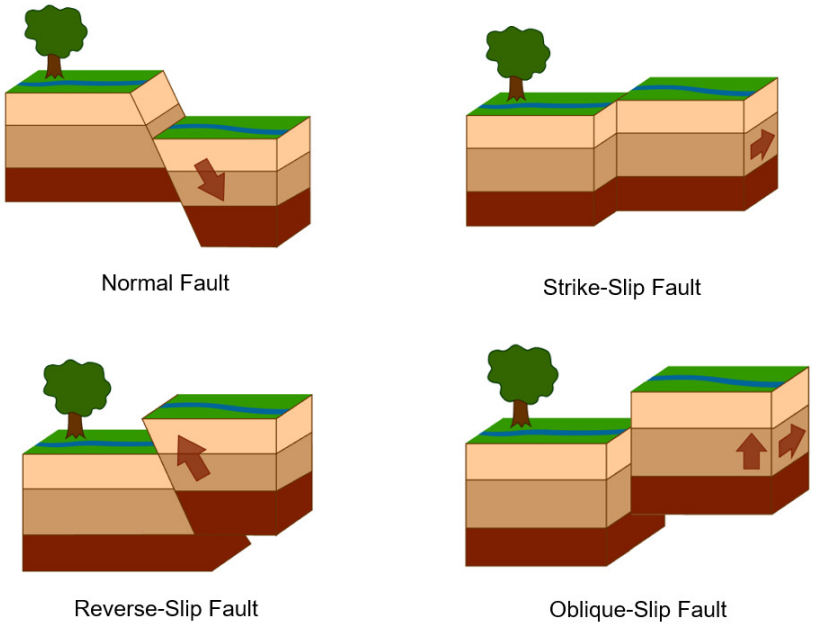

Figure 5: Seismic fault types [14]

Various researchers studied pipelines subjected to different fault rupture types. In 1975, Newmark and Hall [15] proposed a simplified analysis method for a pipeline subject to a strike-slip fault using a beam-type approach considering only pipe tensile strain. Their approach was extended by Kennedy et al. [16] in 1977 considering flexural deformations and soil-pipe interface lateral interactions. Wang and Yeh [17] further developed this analysis in 1985 with a beam on elastic foundation approach. In 1998,

Takada *et al.* [18] studied pipeline response to normal and reverse faults and found that pipelines are more vulnerable to reverse fault due to local buckling. Failure analysis of a pipe crossing a fault is very complex. It involves several factors such as soil-pipe interaction, material nonlinearity, large deformations, and local failures. Due to this complexity several researches, e.g. [19-21], also utilized a three-dimensional (3D) finite element analysis (FEA) approach to analyze performance of underground pipelines subjected to a fault rupture.

1.1.4 Finite Element Modeling

ABAQUS software was used in this study to create 3D FE models for analyzing buried steel pipelines embedded in CLSM when subjected to seismic wave propagation as well as reverse-slip fault rupture. Linear and nonlinear material behaviors were considered. For linear (or elastic) analysis, three material properties are required; 1) unit weight, 2) Young's modulus (E), and 3) Poisson's ratio (υ).[22] For nonlinear (or inelastic) analysis, three material constitutive models were considered; 1) Mohr-Coulomb plasticity model, 2) Drucker-Prager model, and 3) concrete damaged plasticity (CDP) model. According to [22], Mohr-Coulomb plasticity model uses the classical Mohr-Coulomb yield criterion. It allows the material to harden and/or soften isotropically, and is suitable in several geotechnical engineering applications. Drucker-Prager model is applicable for the material that becomes stronger as the pressure increases (or pressure-dependent yield). It also allows for volume change with inelastic behavior. Concrete damaged plasticity model is often used for modeling concrete or quasi-brittle materials. Seismic wave propagation was applied in FE models by using

body force that considers the mass of defined materials with applied ground acceleration time-history of the selected earthquake event in any direction (X, Y, or Z). For reverse-slip fault rupture, displacements were applied in the upward direction along the fault plane. In all FE models, seismic loads were applied after application of gravitational forces.

1.2 Research Objective

The main research objective was to improve earthquake resistance of buried pipelines preventing loss to human life as well as reducing economic impact by:

- Evaluating the use of CLSM mixtures to backfill pipelines with its inherent advantages for equal or better earthquake resistance compared to conventional compacted soil backfill.
- Providing recommendations on 3D FE modeling parameters and material properties of CLSM for optimum earthquake resistance.

1.3 Scope and Rationale

This study utilized finite element analysis in a 3D domain using ABAQUS software to determine the performance of buried steel pipes embedded in CLSM backfill compared to compacted soil backfill. At the beginning, literature review was conducted to evaluate studies previously performed regarding this subject. Then, buried pipes embedded in soil and CLSM backfills subject to two types of seismic failure modes were analyzed, 1) seismic wave propagation and 2) seismic reverse-slip fault rupture.

For buried pipes subject to seismic wave propagation, the study started by evaluating the existing ASCE guidelines for seismic design of buried pipelines and its

design limitations. The 3D FE models with elastic material behavior matching design assumptions in the ASCE guidelines were developed to investigate the seismic performance of a straight pipe axially free at both ends. Several FE model parameters were evaluated for their effects on a pipe stress prediction, including soil-pipe interaction, boundary condition, FE model dimensions, friction coefficients at interfaces, relationship between soil spring stiffness and material Young's modulus, and FE model dimension scale factor. After setting the FE model parameters to match the axial stress predicted by the ASCE guidelines, the developed FE model was then utilized to evaluate the pipe seismic performance of various soil and CLSM backfill materials. In addition, the developed FE model was used to investigate the pipe seismic performance of other conditions that are not addressed in the ASCE guidelines, such as the effect from three-directional seismic wave applied simultaneously or the effect from pipe having a rigid connection at one end. Next, the effect on the pipe axial stress from non-linear material behavior was investigated including the discussion on various FE model parameters in inelastic range, such as the use of soil spring stiffness or dashpot element at FE model boundaries.

For buried pipes subject to seismic reverse-slip fault rupture, the study first developed a 3D non-linear FE model with model parameters matching a full-scale laboratory testing performed by Jalali *et al.* [23]. Those model parameters included FE model dimensions, steel pipe diameter and thickness, pipe and soil backfill properties, boundary conditions, and total applied fault movement. Maximum pipe longitudinal strain, maximum pipe deformation, and pipe deformation shape were compared to

experimental data reported by [23] for FE result verifications. Various FE model parameters were evaluated for their effects on FE model results including CLSM trench continuity through a fault plane and CLSM-pipe interaction. Then the developed FE model was further utilized to evaluate the pipe seismic performance for pipes with CLSM backfilled compared to soil backfill. Other variables affecting the pipe seismic performance were also investigated, such as material shear strength, material Young's modulus, and pipe diameter-to-thickness ratio.

1.4 Research Significance

Although consequences of pipe failures during a seismic event could be catastrophic, the available ASCE guidelines are limited in assumptions and are only valid for buried pipes in compacted soil backfill under seismic wave propagation. This study discussed the effects of several parameters of 3D FE models on stress predictions and established an FE model matching the ASCE guideline. The developed FE model was then used to analyze the seismic performance of pipes with various CLSM backfills and provided a design tool to engineers to use in conditions that cannot be analyzed with the ASCE guidelines. In addition, this study evaluated the seismic performance of steel pipes embedded in CLSMs when subjected to a reverse-slip fault including the discussion on the effect of various FE model parameters. This type of analysis has not been previously performed. The research findings provided a more complete understanding of seismic performance of underground pipelines backfilled with CLSM and assist design engineers in specifying CLSM mixtures for backfilling applications.

CHAPTER 2

LITERATURE REVIEW

This chapter discusses research in the literature that has been previously conducted on using CLSM as a backfill material. The literature on a buried pipeline response under seismic loads is also reviewed. This chapter is divided into three sections that mainly focus on 1) CLSM backfill applications, 2) seismic performance of buried pipelines, and 3) conclusion.

2.1 CLSM Backfill Applications

CLSM as a backfill material has been used in several applications, such as pipe backfill, pavement base, and bridge abutment backfill. Many studies on CLSM backfill applications have been performed utilizing different analysis methods, including full-scale testing, numerical analysis, and finite element analysis. The literature was reviewed and is summarized below.

In 1997, Zhan and Rajani [24] utilized 2D plane strain FEA to determine performance of buried pipelines embedded in different backfill materials, including soil and CLSM, subjected to traffic loads. The research objectives were to compare FE model results to previously collected field test data and to assess the effect on pipe performance from various pipe embedment depths. One-half of FE models was created due to the model symmetry. The pipe was modeled as an elastic material, but nonlinear constitutive model Drucker-Prager was utilized for soil and CLSM backfill materials accounting for material nonlinearities. Soil-pipe interaction was modeled with a jointed material option in ABAQUS defining a material failure with parameters such as friction

angle, dilation angle, cohesion, and temperature. This approach is different from our FE modeling techniques and could have incurred additional errors due to variations in jointed material properties simulating this interface. Based on results, FE models predicted higher pipe hoop strain, which could be from 2D plane strain analysis. Results indicated that pipe embedded in CLSM yielded a lower stress and a decrease in pipe embedment depth compared to pipe embedded in conventional soil backfills.

Masada and Sargand [25] conducted a study on the structural performance of High Density Poly-Ethylene (HDPE) pipe using CLSM as a pipe backfill. The buried pipe was backfilled with several lifts of CLSM and was subjected to surcharge loads. This study included results from field experiment as well as results from FEA. Laboratory testing on CLSM properties was previously performed and were used for CLSM properties in FEA. It was assumed that there was no separation between CLSM and pipe considering fully bonding to the pipe from CLSM. This approach is different from our research that soil-pipe separation was considered. The assumption of no separation may be valid for some scenarios, e.g. under surcharge loads or small anticipated deflections/stresses, but it may not be applicable for an interface subjected to seismic loads since large ground movements are likely to occur. FE model parametric study was not performed. The results showed that FE models over-predicted the pipe deflections and stresses, which could have been caused by variations in CLSM material properties used in the field and in the FE models. Results also indicated that under loadings pipe installed in CLSM backfill experienced lower deflections and stresses compared to pipe installed in conventional soil backfill.

In 2014, Dezfooli *et al*. [26] carried out field tests on a large steel buried pipeline backfilled with CLSM subjected to compaction forces during installation. Three steel pipes, 84-inch pipe outside diameter (*D*), embedded in three different trench configurations were tested using CLSM as a pipe bedding and pipe backfill. Trench configurations included 1) trench width of (*D* + 36") backfilled with CLSM up to 0.3*D* for Test 1, 2) trench width of (*D* + 12") backfilled with CLSM up to 0.7*D* for Test 2, and 3) trench width of (*D* + 18") backfilled with CLSM up to 0.7*D* for Test 3. After CLSM backfill placement, the trenches were backfilled with compacted native soils on top of the CLSM layer up to the ground surface. 3D nonlinear finite element models were also developed in this study. Native soil materials were modeled using Mohr-Coulomb constitutive model and CLSM was modeled with Concrete Damaged Plasticity model. Lateral loads induced by compactions were calculated based on at-rest lateral pressure. Loads were then applied to FE models using the equivalent thermal loading based on material thermal expansion coefficients and followed by surcharge load. Field test results were in agreement with results obtained from the FE models indicating that the developed FE model could be further used to predict pipe performance in different backfill materials as well as different trench configurations.

Alizadeh *et al*. [27] performed a full-scale laboratory test of a bridge abutment backfilled with CLSM subjected to surcharge loads. The study also carried out a nonlinear 3D FEA to be compared with experimental results in terms of bearing pressure, vertical and lateral displacements, and axial forces in anchors. CLSM was modeled with Concrete Damaged Plasticity constitutive model. After the result verification, the

developed FE model was then used to evaluate the influence on structural performance of the bridge abutment from various CLSM curing age and curing temperature. Results showed that bearing pressure of the bridge abutment increased as CLSM cured longer and at higher temperatures, which is the influence from CLSM compressive strength. In our research, CLSM curing age and curing temperature were not considered. CLSM properties at 28-day were utilized.

In 2018, Abdel-Rahman *et al*. [28] conducted a study on buried pipes embedded in CLSM backfill subjected to traffic loads. Finite element analysis (FEA) in a 2D domain, plane strain, was utilized for this study. FE model dimensions were provided, but there was no discussion on the process used to select FE model dimensions. Mohr-Coulomb constitutive model was used for both CLSM backfill and in-situ surrounding soils. Mohr-Coulomb constitutive model is commonly used for considering material nonlinearities in several studies, especially for granular soils, and was also utilized in our FE models. Soil-pipe interaction was modeled with friction contact. This same soil-pipe interaction was implemented in our research. Two pipe types, concrete and flexible PVC pipe, were considered in the study. Results indicated that pipe vertical stress, horizontal stress, and bending moment on flexible PVC pipe from traffic loads were generally lower than concrete pipe.

2.2 Seismic Performance of Buried Pipelines

2.2.1 Buried Pipelines Subjected to Seismic Wave Propagation

Design guidelines are available for researchers to design buried pipeline subjected to seismic wave propagation. Other analysis methods, including numerical

analysis and finite element analysis, are also available for assessing buried pipeline performance. The literature was reviewed and are summarized below.

In 1984, American Society of Civil Engineers (ASCE) published the Guidelines for the Seismic Design of Oil and Gas Pipeline Systems [29]. The document provides a detailed background of seismic hazards and design guidelines and considerations for both aboveground and buried pipelines. For buried pipelines, different seismic failure modes are discussed including seismic wave propagation and permanent ground deformation. The analysis method outlined in ASCE guideline for pipes under seismic wave propagation was adopted from a study by Newmark [30]. This method assumes a straight buried pipe axially free at both ends. The analysis method was applicable only for pipelines embedded in soils. In addition, it cannot be used with pipelines subjected to three-directional seismic waves or pipelines rigidly connected to a structure at one end.

Lee *et al*. [31] analyzed buried steel pipeline under seismic wave propagation utilizing FEA for both straight pipe and pipe with bend configurations. Soil-pipe interaction was modeled with a series of nonlinear soil springs, which is different from our FE modeling techniques that use friction contact. Multi-directional seismic wave was also considered for various earthquake events. Only pipes embedded in soils were analyzed. The effect on pipe response from several FE model parameters, including pipe types, end conditions, soil characteristics, and pipe embedment depths was evaluated. Results showed that pipe strain at the fixed end was always higher than the pinned end,

and was approximately 10 times higher than the strain at the mid-length of the pipe. In addition, pipe strain decreased with a larger pipe embedment depth.

In 2010, Lee [32] performed a study on a flexible buried pipeline under traffic load and seismic wave propagation using FEA in a 3D domain. Parametric studies on FE model mesh size, pipe length, and pipe embedment were also performed. The study was limited to pipelines embedded in soils. Mohr-Coulomb constitutive model was utilized for surrounding soils. The study assumed fully bonded interface for soil-pipe interaction, which does not allow pipe sliding or separation. This soil-pipe interface assumption is not realistic and may be too conservative since all seismic loads from wave propagation would be transferred to the pipe. Results showed that as the pipe was installed with a greater embedment depth, the pipe settlement decreased under traffic loads. Also, pipe stress was generally higher at the fixed end compared to the free end.

Yang and Zhang [33] conducted a study on a concrete buried pipeline embedded in various soil types subjected to three-dimensional seismic wave propagation. This study also assumed that there is no slip between soil and pipeline whereas our research utilized friction contact allowing slip and separation. Although the study considered three-dimensional seismic wave, each seismic wave direction was applied independently to determine the effect on the pipe seismic response. They found that under seismic wave propagation, pipe axial stress is much higher compared to pipe bending stress. The analysis was performed using 3D FEA, but there was no discussion on how FE model dimensions were chosen for the study.

In 2014, Sahoo *et al*. [34] evaluated the seismic response of buried single pipe and buried two parallel pipes embedded in soils subjected to seismic wave propagation using 3D FEA. There was no discussion on how FE model dimensions were selected. Soil-pipe interaction was modeled with a jointed material considering cohesion, friction angle, and assumed strength reduction factor, similar to an approach utilized in the study by Zhan and Rajani [24]. Seismic wave excitation was applied only in one direction perpendicular to pipelines. The effect on seismic performance from pipe embedment depth and spacing between two parallel pipes was evaluated. For both pipe configurations, results indicated that pipe displacements and stresses decreased with greater pipe burial depths. For two parallel pipes installed at varying spacing, results showed that pipe stresses increased as pipe spacing increased. A study of buried pipelines subjected to permanent ground deformation was also included. It was modeled by applying lateral pipe bending, single curvature, in FE models. This assumption may be applicable only for pipes subjected to permanent ground deformation caused by liquefaction, settlements, or landslide but it would not be valid for seismic fault rupture because pipe deformation shape would be a double curvature instead.

Zhang and Wang [35] proposed a numerical model for analyzing buried pipeline subjected to seismic wave propagation. Their numerical model was an extension on the work originally conducted by Shinozuka and Koike and was revised to be consistent with the ASCE guidelines [29]. Zhang and Wang verified their numerical model with results from FEA. The study included three different pipe configurations including 1) a straight pipe, 2) a pipe with 90 degree right-angle bend, and 3) a pipe with tee connection. The

pipe was connected with a series of soil springs as computed from the ASCE guidelines. The study was only limited to buried pipe embedded in soils and did not consider multi-direction seismic wave. Results predicted by the proposed numerical model agreed well with FEA results. It was also found that strain in a straight pipe dominated the design with a small ground strain where there is no slippage between soil and pipe. At a larger ground strain where slippage occurs, maximum strain is located near pipe bends and tees.

2.2.2 Buried Pipelines Subjected to Seismic Fault Rupture

Permanent ground deformation, specifically caused by seismic fault rupture, is among the sources to buried pipeline failures. A large number of studies have been conducted on buried pipelines subjected to various seismic fault rupture types, such as normal-slip, strike-slip, reverse-slip, and oblique-slip fault. In 1998, Takada *et al*. [18] studied pipeline response to normal and reverse faults and found that pipelines are more vulnerable to reverse fault due to pipe local buckling failure. Therefore, the literature, mainly focusing on buried pipelines subjected to reverse-slip fault rupture, was reviewed and are summarized below.

In 2011, Joshi *et al*. [36] proposed a FE model to analyze buried pipelines under reverse fault motion. The pipe was modeled using linear beam elements supported by a series of nonlinear soil springs representing soil-pipe interaction. Pipe internal pressure was not considered in this study. Also, pipe local buckling and large deformation were ignored due to a limitation on beam elements representing steel pipes. The influences on pipe response from pipe crossing angle, fault dip angle, soil spring characteristic, pipe diameter, and pipe embedment depth were determined. Results showed that pipe strain

increased as pipe crossing angle increased, with the maximum values at the angle of 90º. Pipe compressive strain was lower for pipe backfilled with loose soil compared to dense backfill. In addition, pipe compressive strain increased as pipe embedment depth increased.

Tarinejad *et al*. [21] studied seismic response of buried steel pipelines embedded in soils subjected to reverse-slip fault rupture using a nonlinear 3D FEA. Gravitational forces were first applied to FE models followed by internal pipe pressure before applying seismic faulting. Mohr-Coulomb constitutive model and friction contact were adopted for FE models, which are the same as our FE modeling techniques. The study neither provides a discussion on selected FE model dimensions nor FE model result verification. Results showed that at the same amount of fault movement, pipe with a higher D/t ratio exhibited a lower pipe displacement and had less elements that went beyond elastic range. In addition, pipe stresses decreased as fault angle increased. Although pipe internal pressure, equal to 40% of pipe maximum design pressure, was considered, the study did not discuss its effect of pipe performance.

In 2016, Zhang *et al*. [37] studied a seismic performance of buried pipelines embedded in soil backfill in rock stratum subjected to reverse faulting. The study was carried out utilizing 3D FEA. Shell elements were employed for steel pipelines. FE model dimensions were provided but there was no discussion on the process used to select these dimensions. The FE models were applied with gravity and internal pressure loadings, simultaneously, at the beginning. Then, seismic reverse faulting was applied to the models. Material nonlinearities were considered in this study using Mohr-

Coulomb constitutive model for both soil and rock. Although friction contact was utilized on all interfaces, only one value of friction coefficient was specified. Our research defined different friction coefficients for different material interfaces. The effects on pipe strain and deformation from pipe internal pressure, total fault displacement, pipe wall thickness, and pipe embedment depth were determined and discussed. Results showed that as internal pressure increased, pipe wall wrinkles appeared in more locations, which could be an influence of increasing pipe stiffness. Also, pipe deformation and stress increased as fault displacement increased.

Jalali *et al*. [23] conducted a full-scale laboratory testing on 4" and 6" buried steel pipes installed in a sand split-box subjected to 0.6 meter vertical movement along an inclined plane simulating seismic reverse fault rupture. A nonlinear 3D FEA was also carried out. Results from FE models were compared to experimental results. Material nonlinearities were modeled using Mohr-Coulomb constitutive model. In addition, friction contact was utilized for soil-pipe interaction. Our research uses the same FE modeling techniques. The study was limited to steel pipes embedded in soil. Both pipes are 4 mm thick having diameter to thickness ratio (*D*/t) of 26 and 38, for 4" and 6" pipe, respectively. Experimental results showed that both pipes exhibited "diamond-shape" buckled section matching FE results. Results also showed that pipe with lower D/t ratio experienced higher strain, but reached the pipe buckling at a larger fault movement. FE results slightly over predicted the maximum pipe longitudinal strains but simulated similar pipe buckled locations to experimental results.

Xu and Lin [38] utilized a FEA based on Vector Form Intrinsic Finite Element (VFIFE) method to assess buried pipe performance subjected to reverse fault rupture. The pipe was modeled as 3D triangular shell elements near the fault plane connected with beam elements elsewhere along the pipe. The shell elements were used to capture severe deformation. In our research, 8-node brick elements were utilized for steel pipelines. A study by Sadowski and Rotter [39] indicated that using shell elements generally reduced computational runtime up to a pipe radius to thickness ratio of 25, but both brick and shell elements provided a comparable result accuracy. Pipeline failure was identified based on three different criteria 1) ultimate tensile strain, 2) local buckling, and 3) pipe distortion at the cross-section. Soil-pipe interaction was modeled by connecting pipe elements with a series of soil springs. FE model results were compared to experimental data available from other studies. After the result validation, the developed models were utilized to evaluate the effect on pipe performance from pipe crossing angle and fault dip angle. Results showed that higher pipe deformation and pipe stress occurred as pipe crossing angle increased, with the maximum values at the angle of 90º. In addition, pipe axial stress was higher with a smaller fault dip angle while pipe bending stress decreased.

In 2017, Liu *et al*. [40] investigated buckling failure of buried steel pipelines subjected to reverse fault rupture using FEA. Two buckling failure modes as defined in Canadian Standards Association (CSA), CSA Z662 [41]. The pipe was modeled with elbow elements available in ABAQUS software, which is similar to shell elements but allows more complex deformation pattern. The nonlinear soil springs connected to the

pipe were used to simulate soil-pipe interaction. The pipe internal pressure was applied and followed by seismic reverse faulting. FE model results were verified with experimental data available from other studies. The effects on pipe performance from FE model parameters, including fault dip angle, pipe wall thickness, and pipe embedment depth, were also evaluated. Results indicated that pipe vertical displacement and maximum compressive strain increased as fault dip angle increased. In addition, pipe vertical displacement decreased while maximum compressive strain increased with a greater pipe burial depth.

2.3 Summary

Review of literature shows that CLSM has been used as a backfill material in various applications such as pipe backfill, pavement base, and bridge abutment backfill. Finite element analysis, both in 2D and 3D domain, is utilized in several studies to analyze structural performance with CLSM backfills. All studies only considered static loads, such as surcharge or construction loads, but there is no study on CLSM applications performed with seismic loads. Several material constitutive models have been used to represent CLSM behavior including Drucker-Prager, Mohr-Coulomb, and Concrete Damaged Plasticity models with Mohr-Coulomb model being the most common. According to [22], Mohr-Coulomb plasticity available in ABAQUS software is used with the linear elastic material model. It allows the material to harden and/or soften isotropically and is often used in several geotechnical engineering applications. It describes material shear stress in terms of material cohesion, normal stress, and angle of internal friction, as expressed in Eq. (1) and Figure 6.

$$\tau = c + \sigma \tan(\emptyset) \qquad \text{Eq. (1)}$$

Where: τ = shear stress on the failure plane

c = material cohesion

σ = normal stress on the failure plane

ϕ = angle of internal friction

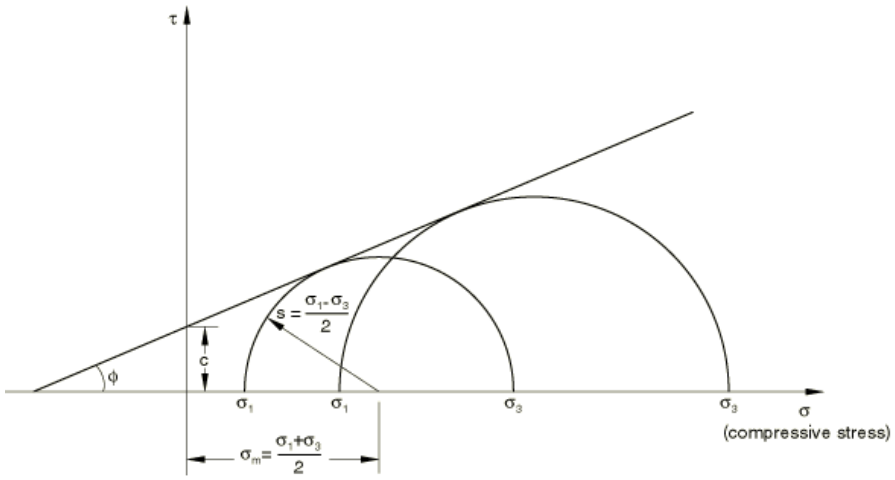

Figure 6: Mohr-Coulomb plasticity model [22]

For studies on CLSM as a pipe backfill material, various assumptions were taken on the soil-pipe interaction. Some studies considered no slip or separation assuming full bonding between CLSM and pipe. The assumption may be applicable for some scenarios, e.g. under surcharge loads or small anticipated deflections/stresses, but it may not be valid for large ground movement, e.g. under seismic loads. Several studies considered friction contact that allows slip and separation, which is more realistic behavior and was adopted in our research.

For buried pipelines subjected to seismic wave propagation and seismic fault rupture, specifically reverse-slip fault, a large number of studies are available, but all of them only considered pipes embedded in soils. No study has been performed for pipes embedded in CLSM under seismic loads. In addition, researchers utilized 3D FEA for analyzing the performance of buried pipelines subjected to seismic loading conditions, but there is a significant variation in FE model dimensions used in those studies. The process used to select FE model dimensions and their effects on the results are typically not discussed. Furthermore, several studies with FEA approach without conducting a full-scale laboratory validated their results with experimental data conducted by others before the verified FE models were used for further analysis. This approach was also adopted in our research.

CHAPTER 3

BURIED PIPELINES SUBJECT TO SEISMIC WAVE PROPAGATION

3.1 Introduction

This chapter focuses on seismic performance of pipelines embedded in CLSM when subjected to seismic wave propagation. This study utilized a 3D finite element model to compare the seismic performance of pipelines embedded in CLSM to the performance of pipelines embedded in compacted soils. The study was carried out in two phases, 1) with the design assumptions that all materials, including steel pipe, backfill material, and in-situ soil, remain in elastic range when subjected to seismic wave propagation, and 2) with the design assumptions accounting for non-linear material plasticity (inelastic range).

3.2 Research Methodology with Elastic Materials

The study started with the evaluation of available design guidelines for designing pipelines when subjected to seismic wave propagation. Then, FE models in 3D domain were developed using ABAQUS software for a buried steel pipe in soil backfill with the same design assumptions of the ASCE guidelines [29], i.e. infinitely long pipe with free ends. The effects of model parameters, such as soil-pipe interaction, boundary condition, FE model dimensions, friction coefficients at interfaces, and soil spring used at boundaries, on the pipe axial stress predictions were evaluated. Later, the FE model parameters were set to obtain similar stress predictions as [29] for pipes buried in soils. The developed model with set parameters was further used to evaluate 1) the seismic performance of pipes embedded in CLSM backfills, 2) the effect on pipe seismic

performance from seismic wave applied three directions simultaneously, and 3) pipe end conditions. A pipe axial stress value was mainly used to evaluate the seismic performance of pipelines. A lower pipe axial stress indicates a better pipeline performance under seismic wave propagation.

3.2.1 ASCE Guidelines

There are several design guidelines available for designing buried steel pipes under various seismic failure modes such as permanent ground deformation, liquefaction, landslide, or fault rupture. However, there are only a few design guidelines available for the buried pipes subject to seismic wave propagation. These guidelines are all either modified or adopted from ASCE Guidelines for the Seismic Design of Oil and Gas Pipeline Systems [29] dated back in 1984 which is based on a study by Newmark [30].

When a buried pipeline is subject to seismic wave propagation, seismic forces get transferred to the pipeline through friction at the soil-pipe interface. According to [29], for an infinitely long pipe free on both ends, the maximum force transfer occurs at the maximum seismic ground strain, ε_g, given by Eq. (2), and the maximum friction force per unit length, t_u, at soil-pipe interface for a cohesionless soil can be determined from Eq. (3):

$$\varepsilon_g = \frac{V_{max}}{\alpha_\varepsilon C} \qquad \text{Eq. (2)}$$

$$t_u = \frac{\pi}{2} D H \gamma (1 + K_o) \tan\delta \qquad \text{Eq. (3)}$$

Where: ε_g = maximum seismic ground strain

V_{max} = maximum ground velocity

C = seismic wave-propagation velocity

α_ε = ground strain coefficient

t_u = maximum friction force per unit length

K_o = coefficient of soil pressure at rest

H = depth from the ground surface to center of the pipeline

D = Pipeline outside diameter

γ = effective unit soil weight

δ = interface angle of friction

Based on [29], Goodling [42] provided a set of equations to determine the maximum axial force of the pipeline, F_{max}, for a straight configuration free at both ends, given by Eq. (4):

$$F_{max} = t_u \, L' \qquad \text{Eq. (4)}$$

Where: F_{max} = maximum axial force of the pipeline

L' = effective friction length

It should be noted that the ASCE guidelines are only applicable for pipes embedded in soils and cannot be used for different backfill materials such as CLSM. Another limitation of the ASCE guidelines is that they are only valid for an infinitely long pipe free at both ends and under one directional wave propagation. In addition, the ASCE guidelines cannot be used to estimate stresses if the pipe is rigidly connected to a structure at one end or if the pipe is subject to seismic waves in three directions simultaneously.

3.2.2 3D Finite Element Models

In this study, FE models in 3D domain were developed to investigate various effects on the pipe performance subject to seismic wave propagation as outlined earlier. The developed 3D FE model generally consists of a steel pipeline component embedded in a trench of backfill material surrounded by in-situ soil. A steel pipeline was modeled using linear hexahedral element (C3D8R) whereas backfill material and in-situ soil were modeled using linear wedge elements (C3D6). Smaller mesh sizes, as small as 0.25D (where D is the pipe outside diameter), were specified for the steel pipeline and backfill materials for more accurate results. Larger mesh sizes, as large as 2D, were defined for in-situ soil where no results were extracted. Half-sized models were used due to model symmetry to minimize computational run-time. Figure 7 shows an example of a developed FE model consisting of all model components.

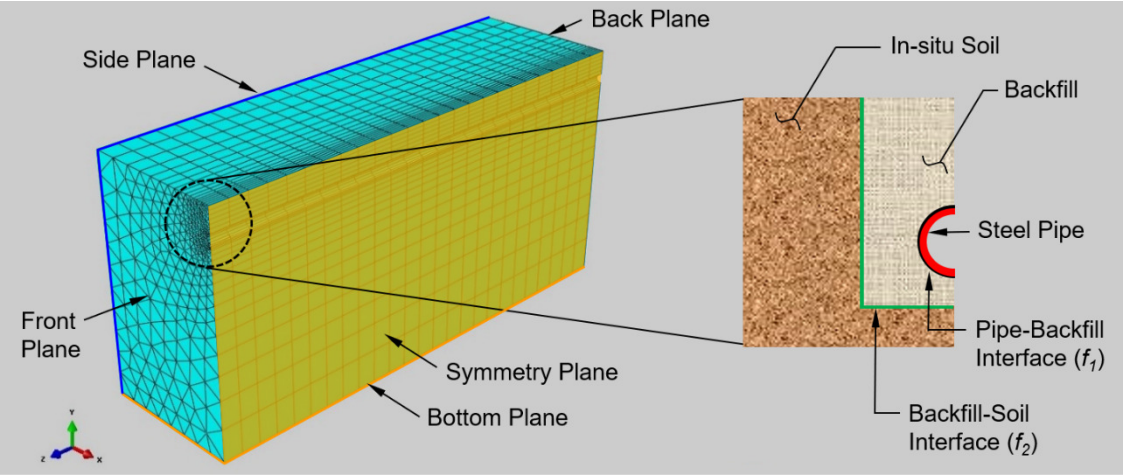

Figure 7: Developed 3D FE model for pipe subject to seismic wave propagation

FE model parameters that were used in this study are listed below:

- Equations provided in the ASCE guidelines assume elastic material properties. Therefore, steel pipeline, backfill, and in-situ soil material properties were kept in elastic range.
- Steel pipe: API-5LX-60 Grade 60 steel pipe with a 609.6 mm [24 in.] in pipe outside diameter, 9.53 mm [0.375 in.] in thickness, and pipe embedment depth of 1524 mm [60 in.] to the top of the pipe.
- Backfill trench dimensions: full width trench of 1828.8 mm [72 in.], or 3*D* (1.5*D* was modeled due to model symmetry) and trench depth of 2438.4 mm [96 in.], or 4*D*.
- Properties of soil and CLSM as backfill materials investigated in this study are summarized in Table 1. Properties of four soil types, Soil (S1) thru Soil (S4), were based on a study by Yang and Zhang [33], and three selected CLSM mixtures, CLSM (C1) thru CLSM (C3), were evaluated by Shah [4].
- Load applications: all FE models were subject to the same seismic ground acceleration time-history of 1989 Loma Prieta earthquake event from a record station on Eureka Canyon Road in Corralitos, California obtained from Center for Engineering Strong Motion Data (CESMD) [13] after application of gravitational forces.
- Boundary condition for the bottom plane of FE models: pinned boundary condition restraining displacement in all direction was placed at the bottom plane, as shown in Figure 7, to simulate bedrock condition.

Table 1: Soil and CLSM properties [4, 33]

ID	Material Description as Listed in References	Density kg/m^3 [lbf/ft^3]	Young's Modulus MPa [kip/in^2]	Poisson Ratio
Soil (S1)	Loosely Compacted Soil	1650 [103]	6.3 [0.91]	0.20
Soil (S2)	Loosely Compacted Sandy Silt	1910 [119.2]	12.9 [1.87]	0.25
Soil (S3)	Loosely Compacted Sandy Silt	1950 [121.7]	15.3 [2.22]	0.20
Soil (S4)	Loosely Compacted Sandy Silt	2100 [131.1]	20.27 [2.94]	0.25
Soil (T1)	Pseudo Soil Evaluating Eq. (5)	2025 [126.4]	17.79 [2.58]	0.25
CLSM (C1)	Mix Identity – S3	2000 [124.9]	689.5 [100]	0.13
CLSM (C2)	Mix Identity – P2″	1811 [113.1]	1379 [200]	0.21
CLSM (C3)	Mix Identity – S2″	1798 [112.2]	2757.9 [400]	0.24

3.2.3 FE Model Parametric Study

Various researchers used 3D FE model approach to analyze buried pipelines under seismic wave propagation. However, review of the literature, e.g. [32-34, 43], showed that there are significant variations in model dimensions used by researchers to evaluate buried pipelines with 3D FEA. The process used to select model dimensions and their effects on the results as well as how results compare to those obtained from available design guidelines are typically not discussed. In this study, a total of seven (7)

FE model parameters was evaluated to investigate their effects on the pipe axial stress prediction. These parameters include:

- Soil-pipe interaction
- Boundary condition
- FE model dimensions, width and depth
- FE model length with various friction coefficients
- Friction coefficients at interfaces
- Relationship between soil spring used at boundaries and material Young's modulus
- FE model dimension scale factor

The ASCE guidelines for an infinitely long pipe with a constant pipe cross section under seismic wave propagation assume the peak axial stress to be uniformly distributed along the entire pipe length. Therefore, a uniform pipe axial stress distribution along the pipe was expected from FE model results with elastic materials.

3.2.3.1 Soil-Pipe Interaction

Based on the literature review performed earlier, two types of soil-pipe interaction are commonly used for analyzing pipes subject to seismic wave propagation by 3D FEA, 1) tie constraint, and 2) friction interface, as shown in Figure 8. Tie constraint assumes that soil and pipe are fully bonded. There is no slippage or separation between soil and pipe under seismic loads. On the other hand, friction interface only allows seismic loads to transfer from soil to pipe by friction. The friction interface allows pipe slippage as well as separation from soil mass. Table 2 summarizes FE model variables used in the study of soil-pipe interaction.

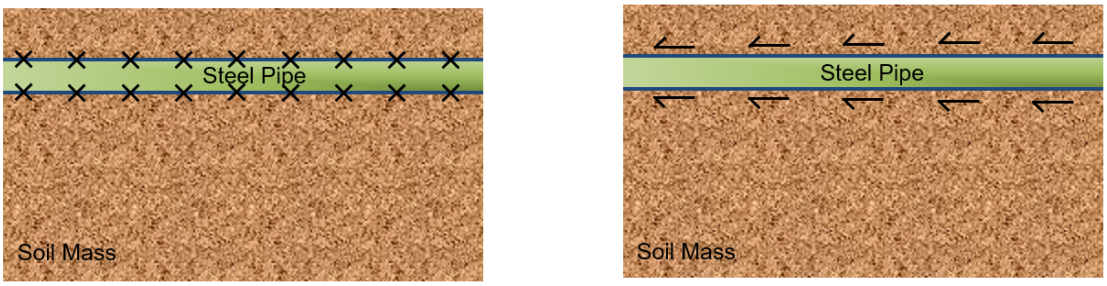

Figure 8: Soil-pipe interaction types

Table 2: FE model variables evaluated for soil-pipe interaction

FE Model Constants	
Model:	Steel pipe embedded in Soil (S2) backfill
Boundary Condition:	Pin at the bottom and roller support at all other planes
FE Model Variables	
FE Model Width, W_d :	20*D*, 30*D*, and 40*D*
FE Model Depth, D_d :	10*D*, 15*D*, 20*D*, and 25*D*
FE Model Length, L_d :	50*D* and 100*D*
Soil-Pipe Interface:	1. Tie constraint (fully bonded) 2. Friction interface with coefficient of friction (f_1) = 0.5

D = pipe outside diameter

3.2.3.2 Boundary Condition

FE model boundary condition used in the previous FE model parametric study, soil-pipe interaction, was the pin type at the bottom plane and the roller type at all other planes (front, back, and side planes as shown in Figure 7). Another type of boundary condition evaluated in this study was soil spring, as shown in Figure 9, with FE model

variables summarized in Table 3. Results provided from the two types of boundary condition were compared to determine a uniform pipe axial stress distribution along the pipe.

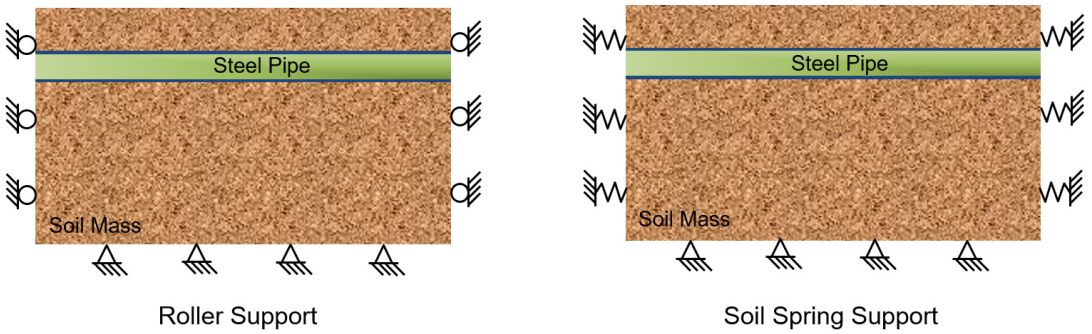

Figure 9: Boundary condition types

Table 3: FE model variables evaluated for boundary condition

FE Model Constants	
Model:	Steel pipe embedded in Soil (S2) backfill
Soil-Pipe Interface:	Friction interface with coefficient of friction (f_1) = 0.5
FE Model Dimensions:	W_d = 20D, D_d = 35D, and L_d = 150D
FE Model Variables	
Boundary Condition:	1. Roller type 2. Spring type with stiffness (k) = 52.54 kN/m [300 lb/in]

3.2.3.3 FE Model Width and Depth

Table 4 and Table 5 show FE model variables evaluated on the effect on FE model results from FE model width and FE model depth, respectively.

Table 4: FE model variables evaluated for model width

FE Model Constants	
Model:	Steel pipe embedded in Soil (S2) backfill
FE Model Length, L_d :	50*D*
Soil-Pipe Interface:	Friction interface with coefficient of friction (f_1) = 0.5
Boundary Condition:	Spring type with stiffness (k) = 52.54 kN/m [300 lb/in]
FE Model Variables	
FE Model Depth, D_d :	10*D* and 15*D*
FE Model Width, W_d :	20*D*, 30*D*, and 40*D*

Table 5: FE model variables evaluated for model depth

FE Model Constants	
Model:	Steel pipe embedded in Soil (S2) backfill
FE Model Length, L_d :	150*D*
Soil-Pipe Interface:	Friction interface with coefficient of friction (f_1) = 0.5
Boundary Condition:	Spring type with stiffness (k) = 52.54 kN/m [300 lb/in]
FE Model Variables	
FE Model Width, W_d :	20*D*, 30*D*, and 40*D*
FE Model Depth, D_d :	10*D*, 15*D*, 20*D*, 25*D*, 30*D*, 35*D*, 40*D*, and 45*D*

3.2.3.4 FE Model Length

Table 6 and Table 7 show FE model variables evaluated on the effect on FE model results from FE model length for pipe embedded in soil backfill and in CLSM backfill, respectively. Various soil-pipe and CLSM-pipe friction coefficients were also evaluated in this parametric study.

Table 6: FE model variables evaluated for model length for soil backfill

FE Model Constants	
Model:	Steel pipe embedded in Soil (S2) backfill
FE Model Dimensions:	$W_d = 20D$, $D_d = 20D$
Boundary Condition:	Spring type with stiffness (k) = 52.54 kN/m [300 lb/in]
FE Model Variables	
Soil-Pipe Interface:	Friction interface with coefficient of friction (f_1) = 0.3, 0.5, 0.7, and 0.9
FE Model Length, L_d :	50D, 75D, 100D, 125D, 150D, 175D, and 200D

Table 7: FE model variables evaluated for model length for CLSM backfill

FE Model Constants	
Model:	Steel pipe embedded in CLSM (C3) backfill
FE Model Dimensions:	$W_d = 30D$, $D_d = 25D$
Boundary Condition:	Spring type with stiffness (k) = 105.08 kN/m [600 lb/in]
FE Model Variables	
CLSM-Pipe Interface:	Friction interface with coefficient of friction (f_1) = 0.3, 0.5, 0.7, and 0.9
FE Model Length, L_d :	50D, 75D, 100D, 125D, 150D, 175D, 200D, 300D, 400D, and 500D

3.2.3.5 Friction Coefficients at Interfaces

Under seismic wave propagation, seismic loads are transferred to buried pipelines through friction. As shown in Figure 7, in case of buried pipe with soil backfill, only friction coefficient of soil-pipe interface (f_1) was evaluated. When CLSM is used as a backfill material, there are two interfaces with different friction coefficients that can

affect the pipe axial stress; 1) CLSM-pipe (f_1) and 2) CLSM-soil (f_2). Effects of varying friction coefficients of both interfaces on pipe axial stresses were evaluated in this study with FE model variables evaluated shown in Table 8.

Table 8: FE model variables evaluated for friction coefficients for CLSM backfill

FE Model Constants	
Model:	Steel pipe embedded in CLSM (C3) backfill
FE Model Dimensions:	$W_d = 30D$, $D_d = 25D$, and $L_d = 200D$
Boundary Condition:	Spring type with stiffness (k) = 105.08 kN/m [600 lb/in]
FE Model Variables	
CLSM-Pipe Interface:	Friction interface with coefficient of friction (f_1) = 0.3, 0.5, 0.7, and 0.9
Soil-CLSM Interface:	Friction interface with coefficient of friction (f_2) = 0.2, 0.4, 0.6, and 0.8

3.2.3.6 Relationship between Material Young's Modulus and Soil Spring Stiffness

To achieve a uniform pipe axial stress distribution along the pipe, the study further evaluated a relationship between material Young's modulus (E) and soil spring stiffness value (k) used at the FE model boundaries (front, back, and side planes as shown in Figure 7). Four selected soil types (Soil S1 thru S4) with different densities, Young's modulus, Poisson ratios, cohesion, and friction angles were investigated based on a study from [33]. In-situ soil spring stiffness placed at FE model boundaries for steel pipe embedded in CLSM backfills was also investigated. Three selected CLSM mixtures (CLSM C1 thru C3) as evaluated by [4] were used for this study. The three selected

CLSM mixtures consist of fly ash, gypsum, quarry waste, and water with the following proportions:

- CLSM (C1) - Mix Identity S3: water to fly ash ratio (W/FA) of 0.61 and 15% gypsum of fly ash by weight.
- CLSM (C2) - Mix Identity P2″: water to fly ash ratio (W/FA) of 0.80 and 15% gypsum of fly ash by weight.
- CLSM (C3) - Mix Identity S2″: water to fly ash ratio (W/FA) of 0.80 and 10% gypsum of fly ash by weight.

All soil and CLSM properties evaluated in this parametric study are summarized and listed in Table 1. Table 9 and Table 10 show FE model variables evaluated on the relationship between material Young's modulus and soil spring stiffness value for pipe embedded in soil backfill and in CLSM backfill, respectively.

Table 9: FE model variables evaluated for boundary soil spring for soil backfill

FE Model Constants	
Soil-Pipe Interface:	Friction interface with coefficient of friction (f_1) = 0.5
FE Model Dimensions:	W_d = 30D, D_d = 25D, and L_d = 200D
FE Model Variables	
Model:	Steel pipe embedded in Soil (S1) thru (S4) backfills
Boundary Condition:	Soil (S1): spring stiffness (K) ranging from 17.51 kN/m [100 lb/in] to 157.61 kN/m [900 lb/in] Soil (S2): spring stiffness (K) ranging from 122.59 kN/m [700 lb/in] to 700.51 kN/m [4000 lb/in] Soil (S3): spring stiffness (K) ranging from 175.13 kN/m [1000 lb/in] to 875.63 kN/m [5000 lb/in] Soil (S4): spring stiffness (K) ranging from 280.2 kN/m [1600 lb/in] to 1225.89 kN/m [7000 lb/in]

Table 10: FE model variables evaluated for boundary soil spring for CLSM backfill

FE Model Constants	
Soil-Pipe Interface:	Friction interface with coefficient of friction (f_1) = 0.5
FE Model Dimensions:	W_d = 30D, D_d = 25D, and L_d = 200D
FE Model Variables	
Model:	Steel pipe embedded in CLSM (C1) thru (C3) backfills
Boundary Condition:	Spring stiffness (K) ranging from 105.08 kN/m [600 lb/in] to 315.23 kN/m [1800 lb/in]

3.2.3.7 FE Model Dimension Scale Factor

Larger FE model dimensions increase the computational run-time necessary for an analysis. In this study, the effect of changing the FE model dimensions while keeping the dimension scale factor (SF) ratios constant was evaluated for pipe embedded in soil

backfill (Soil S2). The developed FE model was scaled down and up by multiplying all dimensions with 0.75 and 1.25, respectively. Overall FE model dimensions, pipe outside diameter and thickness, pipe embedment depth, and trench dimensions were all scaled. The soil spring stiffness placed at boundaries and soil-pipe friction coefficient remained unchanged. This parametric study may allow engineers to minimize the computational run-time of FE model analysis by scaling the model and understanding the FE model size effects on model results. Table 11 shows FE model variables evaluated in this study.

Table 11: FE model variables evaluated for scale factor for soil backfill

FE Model Constants	
Model:	Steel pipe embedded in Soil (S2) backfill
Soil-Pipe Interface:	Friction interface with coefficient of friction (f_1) = 0.5
Boundary Condition:	Spring type with stiffness (k) = 245.18 kN/m [1400 lb/in]
FE Model Variables	
FE Model Dimensions:	(SF = 0.75) $W_d = 22.5D$, $D_d = 18.75D$, and $L_d = 150D$ (SF = 1.00) $W_d = 30D$, $D_d = 25D$, and $L_d = 200D$ (SF = 1.25) $W_d = 37.5D$, $D_d = 31.25D$, and $L_d = 250D$

3.2.4 Pipe Seismic Performance of Various Backfill Materials

After evaluating the effects of different FE model parameters, the parameters of the FE model were set to obtain a similar uniform axial peak stress along the pipe as predicted by the ASCE guidelines for pipes buried in soils. This FE model with set parameters to match the ASCE values was then used to evaluate the pipe seismic performance of four soils (Soil S1 thru S4) and three CLSM mixtures (CLSM C1 thru

C3) with their properties as listed in Table 1. This study was conducted to address one of the limitations from using the ASCE guidelines that it cannot be used for buried pipe embedded in CLSM. A pipe axial stress value was mainly used to evaluate the seismic performance of pipelines. A lower pipe axial stress indicates a better pipeline performance under seismic wave propagation.

3.2.5 Effect from One- and Three-Directional Seismic Wave

For computing pipe axial stress under seismic wave propagation, equations provided in the ASCE guidelines only accounts for one directional wave propagation. The developed FE model was further utilized to evaluate the effect on the pipe seismic performance subject to three-directional seismic wave applied simultaneously. Pipes embedded in soil backfill, Soil (S2), and CLSM backfill, CLSM (C3), were investigated and compared to the pipe seismic performance when subjected to one-directional seismic wave.

3.2.6 Pipe End Conditions

In many instances, buried pipelines interconnect with other components such as above ground pipelines, storage structures, and support facilities. This pipe end condition is considered rigid. Additional limitation of the ASCE guidelines is that they are only valid for an infinitely long pipe free at both ends. The ASCE guidelines cannot be used to estimate stresses if the pipe is rigidly connected to a structure at one end. For this particular scenario, the developed FE model was used to investigate the effect on the pipe seismic performance. The effect from three-directional seismic wave applied simultaneously was also considered in conjunction with pipe end conditions.

3.3 Results and Discussions with Elastic Materials

3.3.1 ASCE Guidelines

For API-5LX-60 Grade 60 steel pipe with a 609.6 mm [24 in.] in pipe outside diameter (D), 9.53 mm [0.375 in.] in wall thickness, and pipe embedment depth (H) of 1524 mm [60 in.] to the top of the pipe, the pipe axial stress when subjected to the 1989 Loma Prieta earthquake was computed. According to [13], the peak ground acceleration recorded during this earthquake event was 0.643g with the maximum ground velocity, V_{max}, of 0.475 m/s [18.697 in/s] and the seismic wave velocity, C, of 462 m/s [1,515.7 ft/s]. Assuming dilatational wave only, ground strain coefficient, α_ε, is equal to 1.0. Using Eq. (2), the computed maximum ground strain, ε_g, for this earthquake event is equal to 0.0010279. From [33], soil unit weight, soil Young's Modulus, and Poisson ratio of a sandy silt soil were taken as 1910 kg/m^3 [119.24 lb/ft^3], 12.9 MPa [1871 psi], and 0.25, respectively, as listed as Soil (S2) in Table 1. Using Eq. (3) and Eq. (4), the calculated maximum friction force per unit length, t_u, was 29.523 kN/m [2.023 kip/ft] resulting in a peak axial stress of the steel pipeline of 50.13 MPa [7.270 ksi] for an effective friction length, L', of 60.96 m [200 ft].

This peak stress value was later used to set various parameters of the developed FE model using Soil (S2) to obtain a similar uniform axial stress. After adjustments of parameters the obtained uniform average pipe axial stress from the FE model with Soil (S2) was equal to 49.69 MPa [7.206 ksi]. Figure 10 shows the pipe axial stress along the pipe length obtained from the ASCE guidelines as well as from the developed FE model

for pipe embedded in Soil (S2) backfill. Results indicated that pipe axial stress prediction from the developed FE model matched well with the ASCE guidelines.

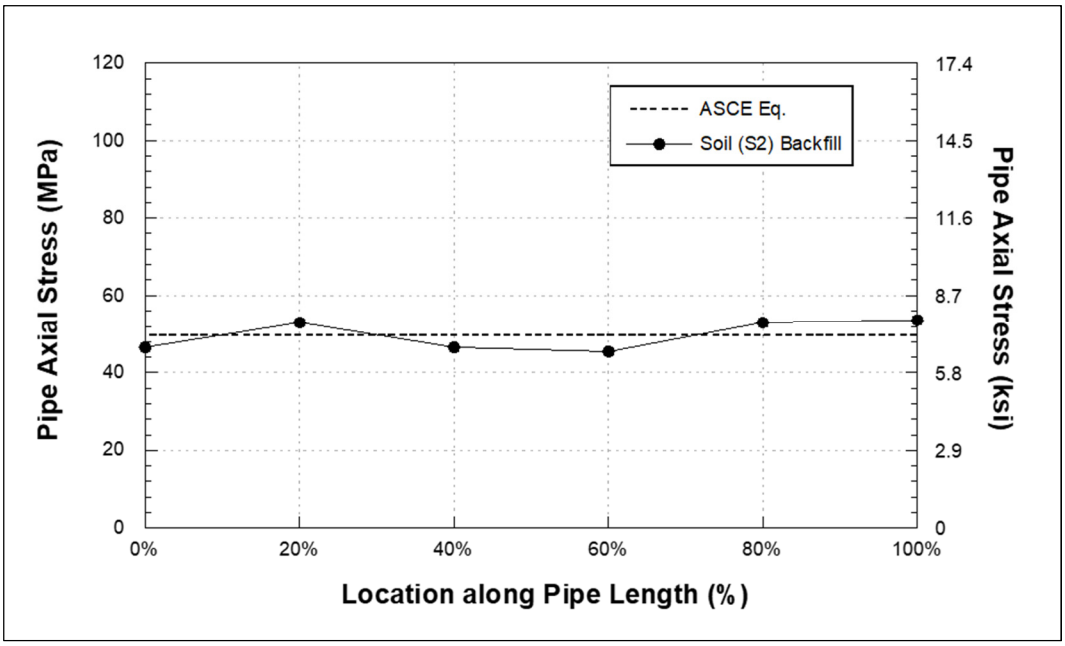

Figure 10: Pipe axial stress along the pipe obtained from the ASCE guidelines and the developed FE models

3.3.2 FE Model Parametric Study

3.3.2.1 Soil-Pipe Interaction

Two types of soil-pipe interaction, 1) tie constraint, and 2) friction interface, were evaluated with FE model variables as shown in Table 2. Figure 11, Figure 12, and Figure 13 show the pipe axial stress along the pipe length for FE models using tie constraint for soil-pipe interaction for FE model width (W_d) of 20D, 30D, and 40D, respectively, with various FE model depths (D_d), varying from 10D to 25D.

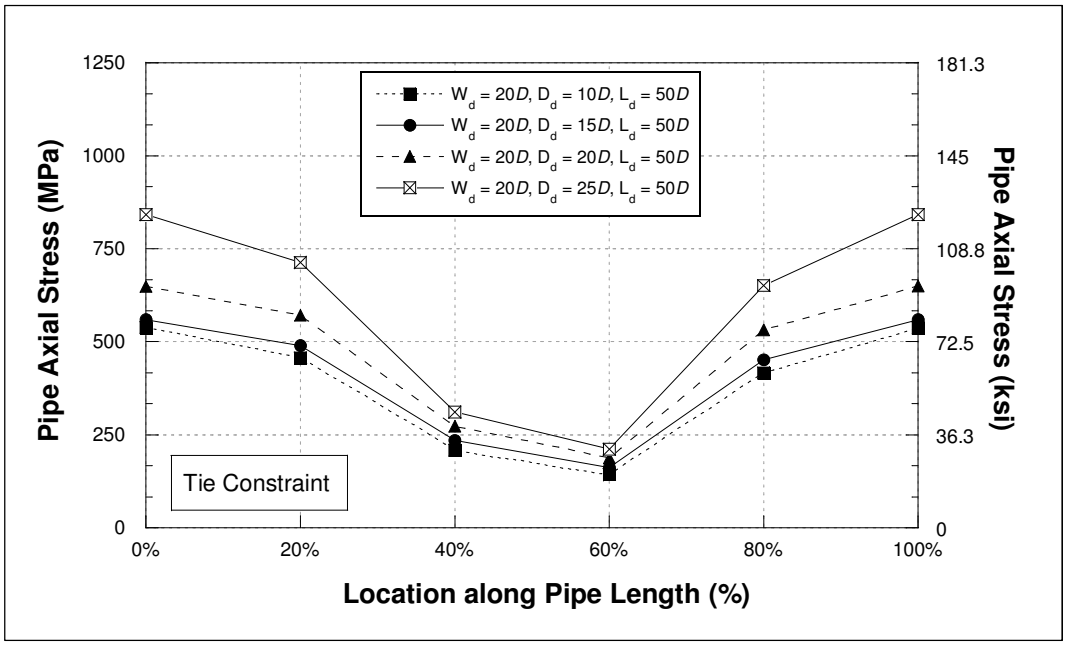

Figure 11: Pipe axial stress along the pipe using tie constraint for soil-pipe interaction with FE model width (W_d) of 20D for various FE model depth (D_d)

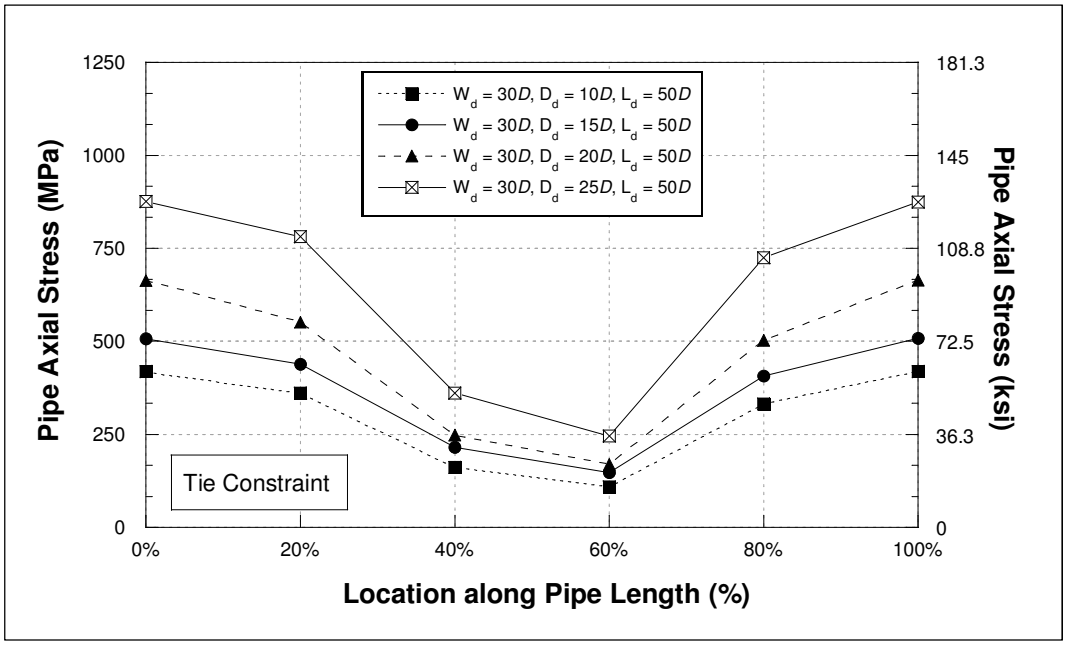

Figure 12: Pipe axial stress along the pipe using tie constraint for soil-pipe interaction with FE model width (W_d) of 30D for various FE model depth (D_d)

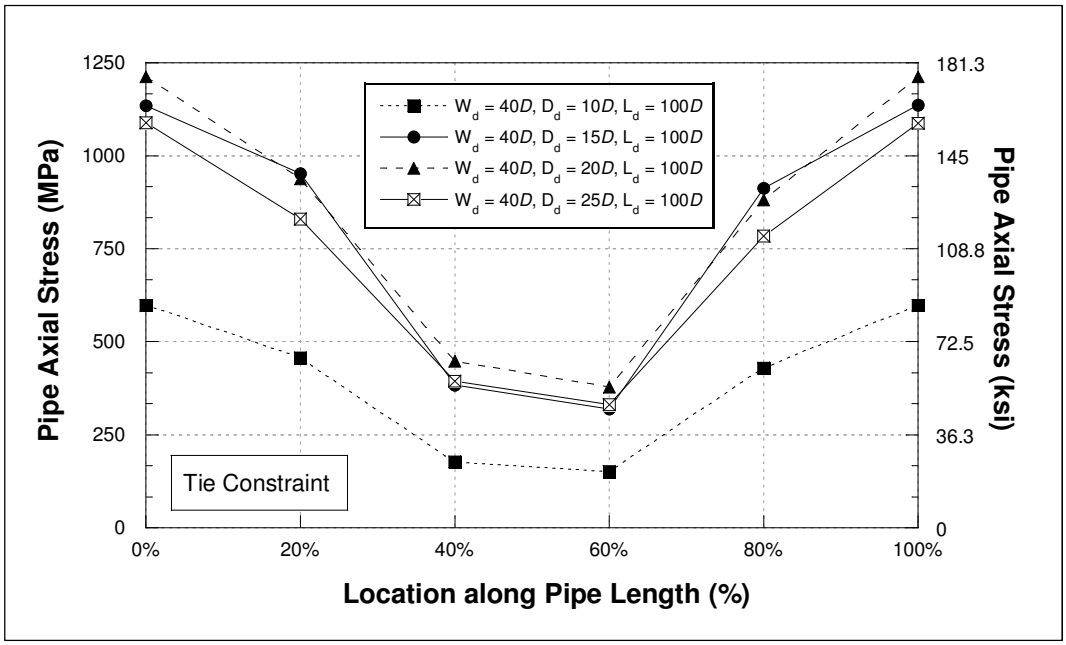

Figure 13: Pipe axial stress along the pipe using tie constraint for soil-pipe interaction with FE model width (W_d) of 40D for various FE model depth (D_d)

It should be noted that pipe axial stress with tie constraint for soil-pipe interaction was well beyond the ultimate steel strength because steel pipe materials used in the developed models was assumed to be elastic with no failure point defined. Although this may not be a realistic material behavior, the results were only used to evaluate the effect on uniform pipe stress distribution from the two types of soil-pipe interaction.

Figure 14, Figure 15, and Figure 16 show the pipe axial stress along the pipe length for FE models using friction interface for soil-pipe interaction for FE model width (W_d) of 20D, 30D, and 40D, respectively, with various FE model depths (D_d), varying from 10D to 25D. From the results for all FE model widths, the pipe axial stress using tie constraint for soil-pipe interaction were approximately 10-15 times higher than FE models with friction at both pipe end and mid-pipe locations. It was also observed that

when using friction interface for soil-pipe interaction stress variance among FE model depths were much less and average pipe axial stress was much closer to the value computed from the ASCE guidelines. Therefore, it was concluded that friction interface should be utilized for soil-pipe interaction.

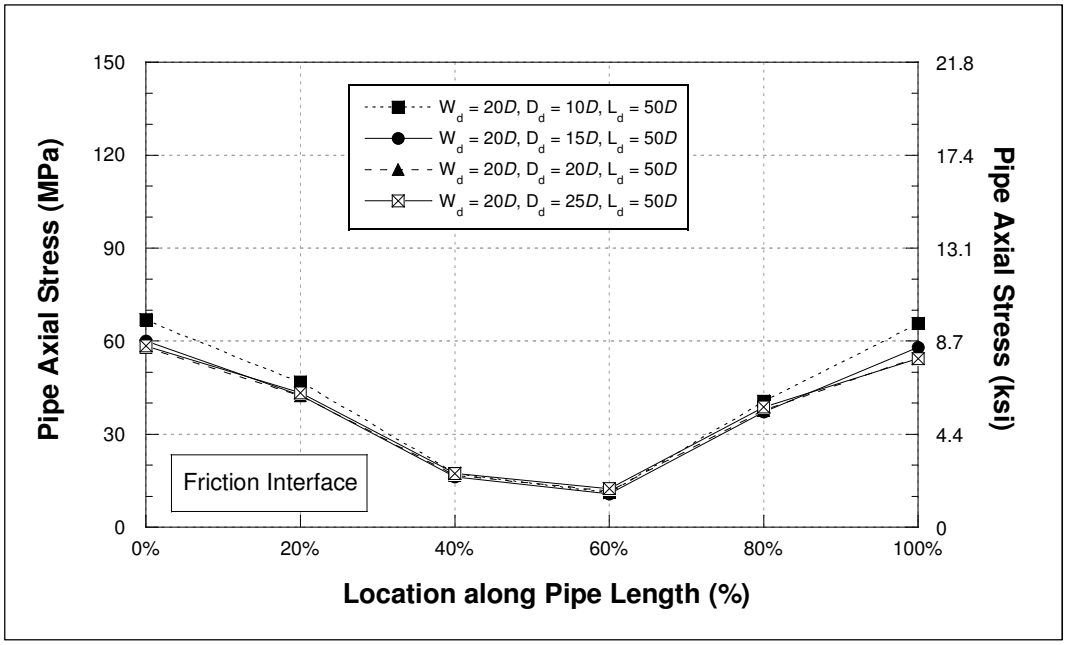

Figure 14: Pipe axial stress along the pipe using friction interface for soil-pipe interaction with FE model width (W_d) of 20D for various FE model depth (D_d)

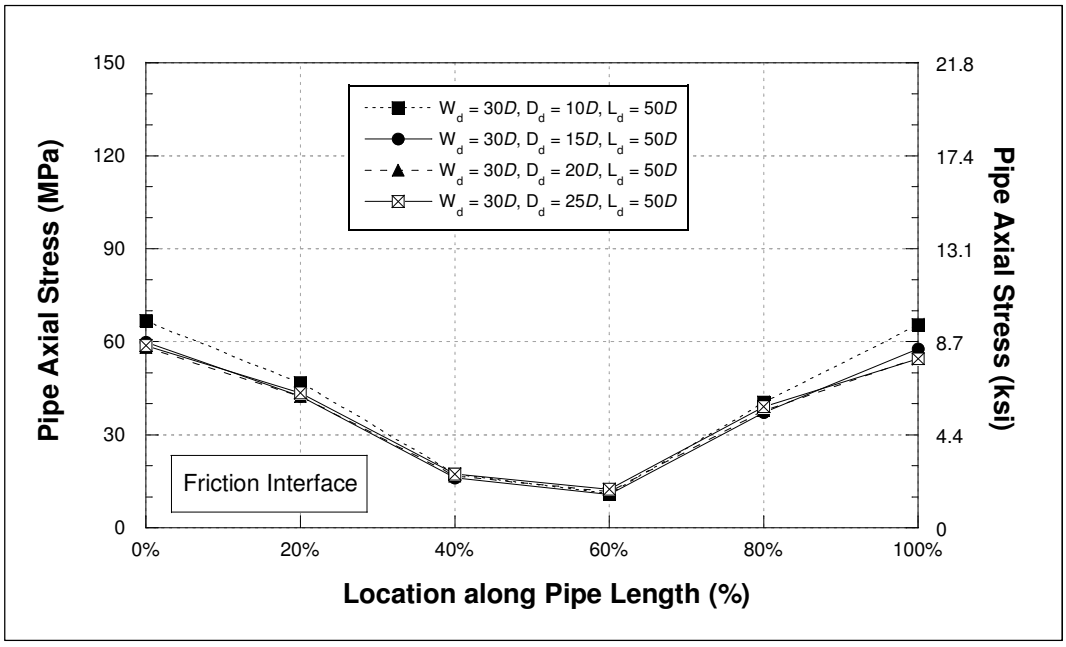

Figure 15: Pipe axial stress along the pipe using friction interface for soil-pipe interaction with FE model width (W_d) of 30D for various FE model depth (D_d)

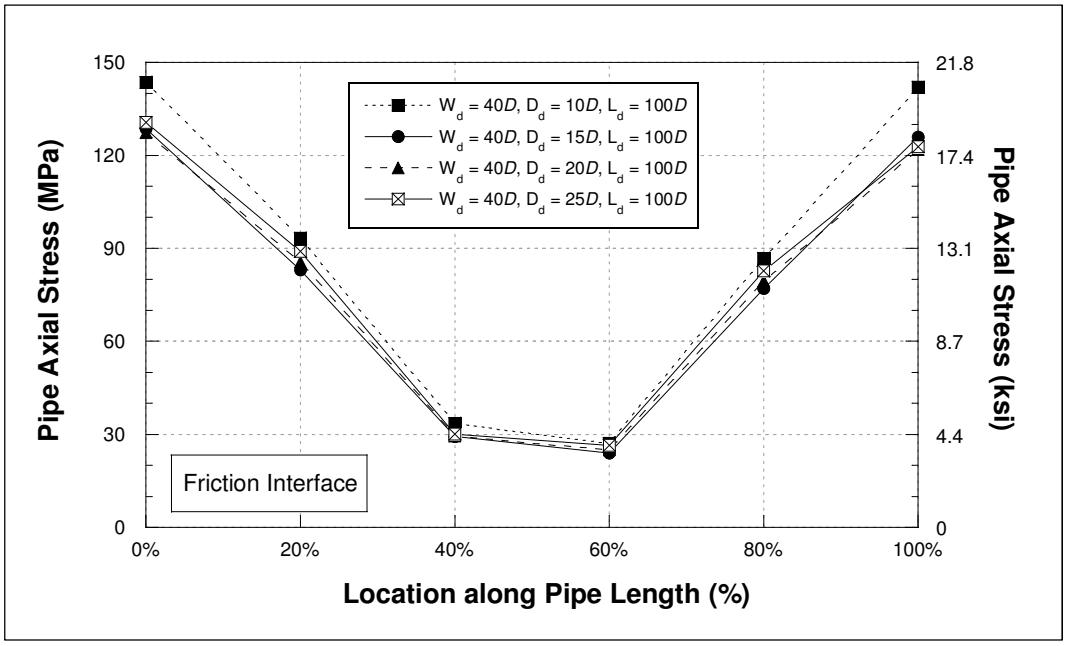

Figure 16: Pipe axial stress along the pipe using friction interface for soil-pipe interaction with FE model width (W_d) of 40D for various FE model depth (D_d)

3.3.2.2 Boundary Condition

Two types of boundary condition, 1) roller support, and 2) soil spring support, were evaluated with FE model variables as shown in Table 3. Figure 17 shows the pipe axial stress along the pipe length comparing between FE models using roller supports and soil spring supports. Results clearly indicated that using soil spring at boundaries provided a much more uniform axial stress along the pipe length. Therefore, it was recommended to use soil spring at all planes (front, back, and side planes) as a boundary condition for the developed FE models.

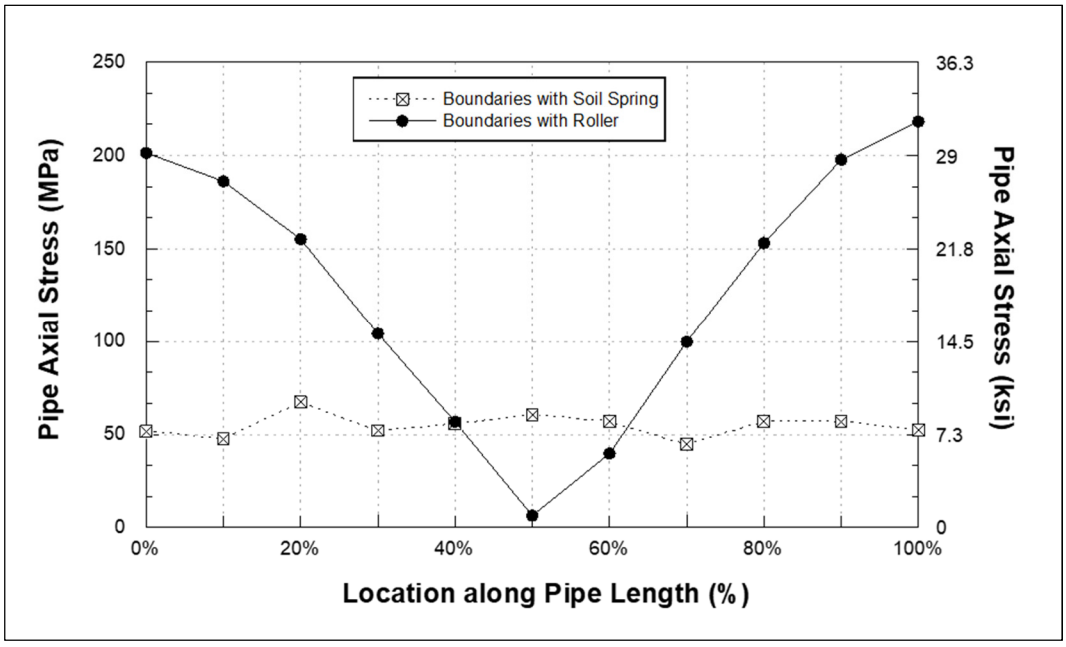

Figure 17: Pipe axial stress along the pipe for roller and soil spring supports

3.3.2.3 FE Model Width

Figure 18 and Figure 19 show the pipe axial stress along the pipe length for various FE model widths (W_d), 20D, 30D, and 40D. Two FE model depths (D_d), 10D and 15D, were evaluated in this parametric study. Results showed that stress variance along the pipe length among FE model widths evaluated was insignificant. Therefore, it was concluded that FE model width does not have a significant impact to FE model results. A minimum FE model width of 20D was recommended to minimize computational run-time.

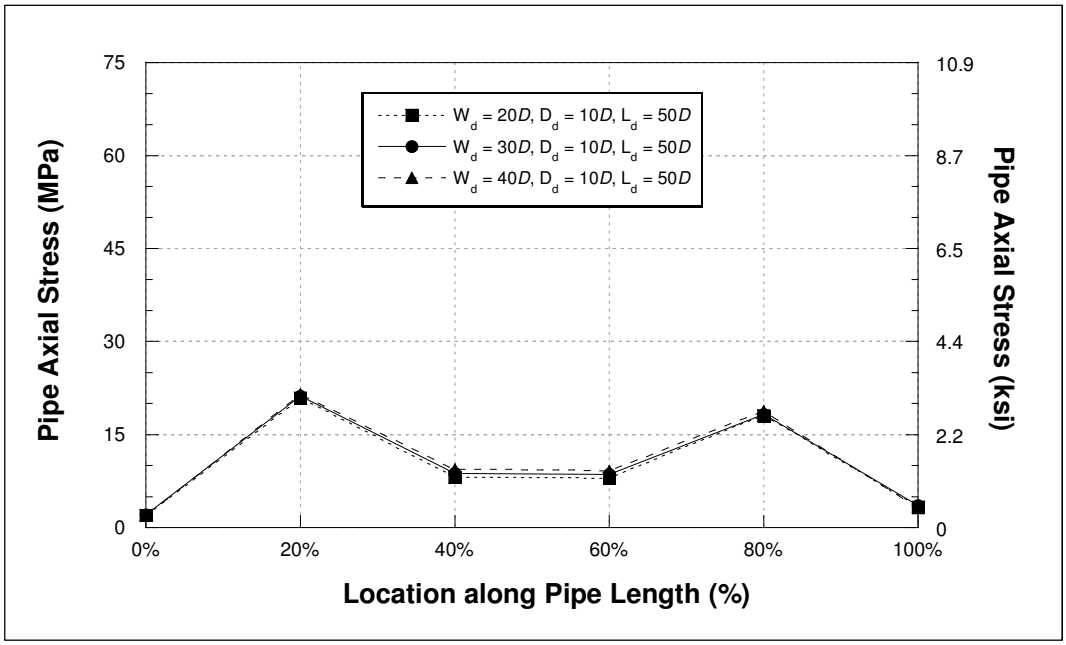

Figure 18: Pipe axial stress along the pipe with various FE model widths (W_d) for FE model depth (D_d) of 10D

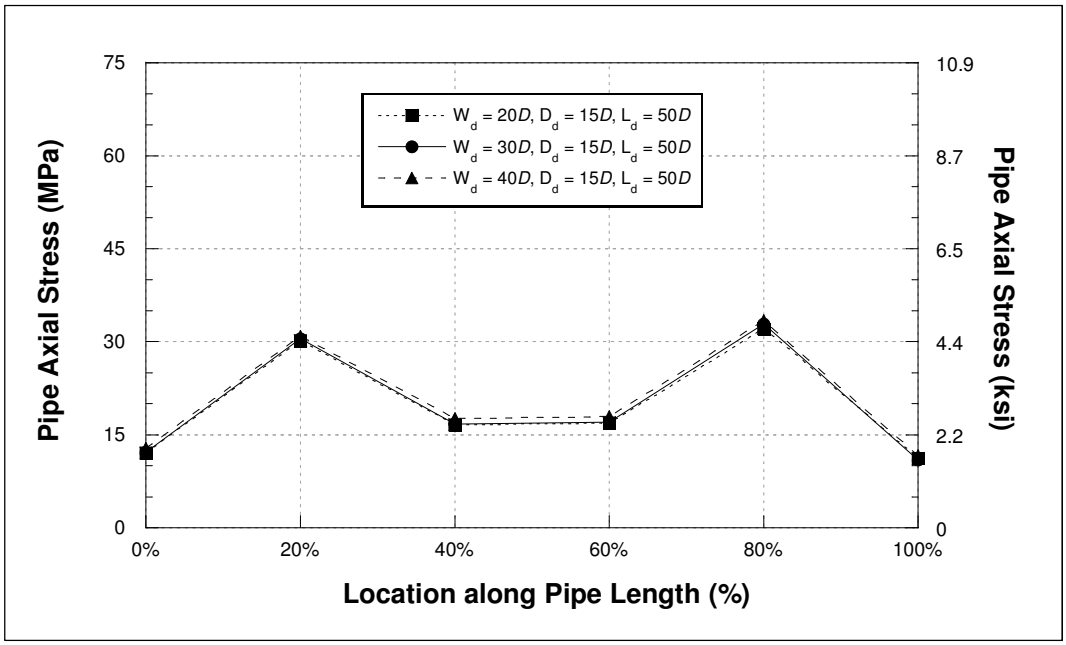

Figure 19: Pipe axial stress along the pipe with various FE model widths (W_d) for FE model depth (D_d) of 15D

3.3.2.4 FE Model Depth

Figure 20 shows the pipe axial stress at mid-pipe location for various FE model depths (D_d), varying from 10D to 45D. Three FE model widths (W_d), 20D, 30D, and 40D) were evaluated in this parametric study with a constant FE model length (L_d) of 150D. From the results, it was observed that the peak axial stress at mid-pipe location increased as the FE model depth increased and started to be constant after a certain model depth. It was also noted that the peak axial stress could be under estimated with a shallower FE model depth. Therefore, a minimum FE model depth of 35D was suggested.

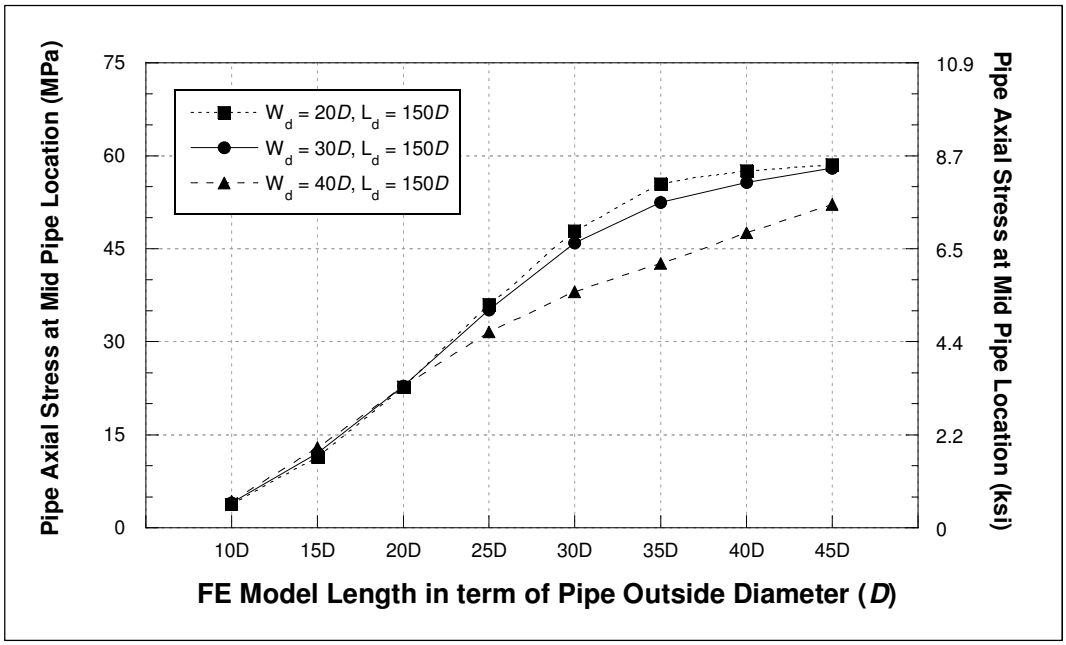

Figure 20: Pipe axial stress at mid-pipe location for various FE model depth (D_d)

3.3.2.5 FE Model Length

Figure 21 shows the pipe axial stress at mid-pipe location for various FE model lengths (L_d), varying from 50*D* to 200*D*, for piped embedded in soil backfill, Soil (S2). Four friction coefficients of soil-pipe interaction (f_1), 0.3, 0.5, 0.7, and 0.9, were evaluated in this parametric study.

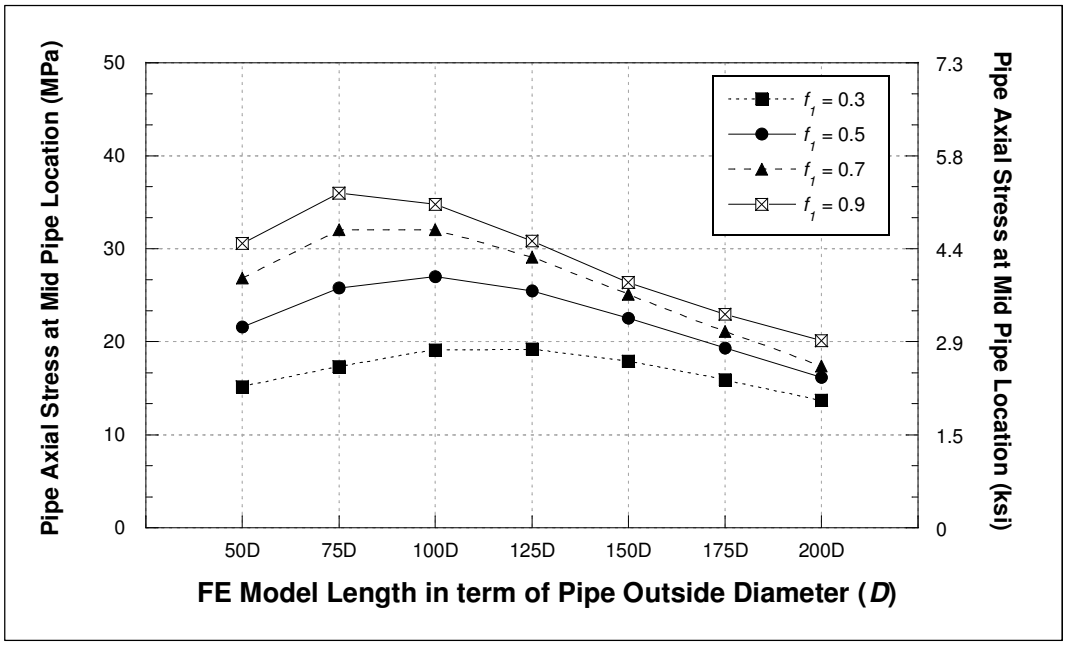

Figure 21: Pipe axial stress at mid-pipe location for various FE model lengths (L_d) for pipes embedded in soil backfill

As mentioned earlier, seismic loads are transferred to buried pipelines through friction for pipes subject to seismic wave propagation. Results showed that there is the critical FE model length required to completely transfer the load for each friction coefficient. The peak axial stress at mid-pipe location first increased with increasing FE model length and decreased after it reached the critical FE model length. It was observed that the critical FE model length decreased as the friction coefficient increased. In addition, the maximum pipe axial stress at the critical length increased as the friction coefficient increased. Therefore, it was recommended that a model should be created with a sufficient FE model length depending on soil-pipe friction coefficient to capture the peak axial stress that a pipeline could experience under seismic loads. For this study,

a minimum FE model length of 200*D* was used for all other investigations with soil backfill.

Figure 22 shows the pipe axial stress at mid-pipe location for various FE model lengths (L_d), varying from 50*D* to 500*D*, for piped embedded in CLSM backfill, CLSM (C3). The same set of selected CLSM-pipe friction coefficients (f_1) were investigated. The value of friction coefficient at CLSM-soil interface (f_2) was set equal to the CLSM-pipe friction coefficient.

Results showed that the pipe axial stress initially increased as the FE model length increased for all CLSM-pipe friction coefficients, similar to pipe embedded in soil backfill, and it remained constant after reaching the critical model length. Results also indicated that the maximum pipe axial stress increased with increasing CLSM-pipe friction coefficient. This is consistent with the ASCE guidelines, which state that seismic forces get transferred to the pipeline through friction at the soil-pipe interface. Unlike soil backfills, the critical FE model length did not vary with the CLSM-pipe friction coefficient. Based on results shown in Figure 22, it was decided to use a minimum FE model length of 200*D* for all other evaluations of CLSM backfills in this study.

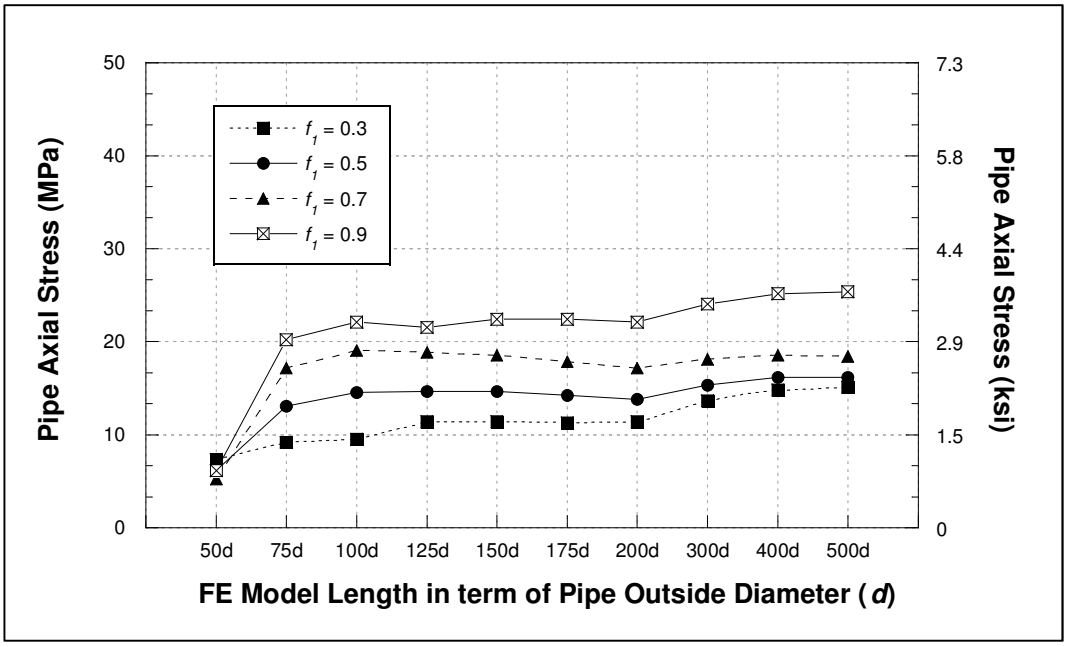

Figure 22: Pipe axial stress at mid-pipe location for various FE model lengths (L_d) for pipes embedded in CLSM backfill

3.3.2.6 Friction Coefficients at Interfaces

The effect of CLSM-soil coefficient of friction (f_2) on pipe axial stresses was also evaluated. Four values of CLSM-pipe friction coefficient (f_1); 0.3, 0.5, 0.7, and 0.9, were combined with four values of CLSM-soil friction coefficients (f_2); 0.2, 0.4, 0.6, and 0.8, in this parametric study for pipes embedded in CLSM backfill, CLSM (C3).

Figure 23 shows the average pipe axial stresses for various f_1 and f_2 combinations. Results showed that for the same CLSM-pipe friction coefficient (f_1), the average pipe axial stress increased as CLSM-soil friction coefficient (f_2) increased. Similarly, for the same CLSM-soil friction coefficient (f_2), the average pipe axial stress increased as CLSM-pipe friction coefficient (f_1) increased.

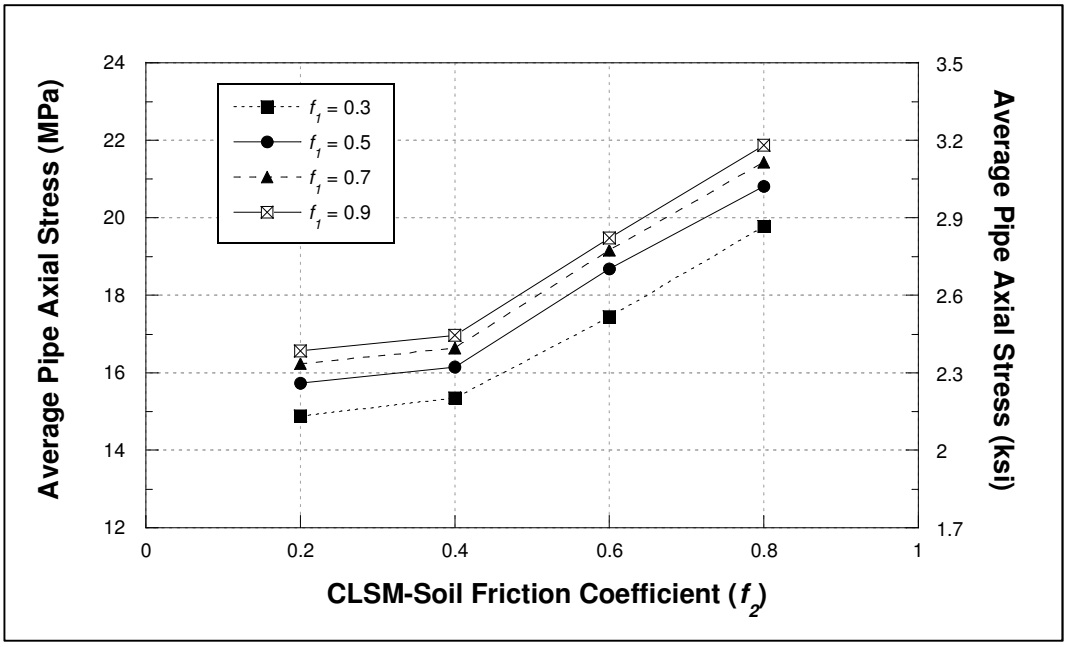

Figure 23: Effect on pipe axial stress from CLSM-pipe (f_1) and CLSM-soil (f_2) friction coefficients at interfaces

3.3.2.7 Relationship between Material Young's Modulus and Soil Spring Stiffness

Based on the results from the parametric study of FE model boundary condition, it showed that use of soil springs was necessary at the front, back and side boundary planes, as shown in Figure 7, to achieve a uniform pipe axial stress distribution along the pipe. In this study this issue was further investigated to establish a relationship between material Young's modulus (E) and soil spring stiffness value (K) used at the FE model boundaries to obtain a uniform stress distribution. Four soil backfills, Soil (S1) thru Soil (S4), and three CLSM mixtures, CLSM (C1) thru CLSM (C3), with different Young's modulus (E) values as shown in Table 1. Soil spring stiffness value (K) evaluated for each backfill material was summarized in Table 9 and Table 10 for soil and CLSM backfills, respectively.

For each backfill material, axial stresses along the pipe length (σ_x) were plotted for each *K* value. The average pipe stress ($\bar{\sigma}$) and stress variation, $(\sigma_x - \bar{\sigma})^2$, along the pipe were also calculated for each *K* value. Then, the summation of stress variance, $\sum(\sigma_x - \bar{\sigma})^2$, was plotted with the *K* value, as shown in Figure 24 a soil with *E* of 6.3 MPa [0.91 ksi], Soil (S1), and for a CLSM mixture with *E* of 689.5 MPa [100 ksi], CLSM (C1).

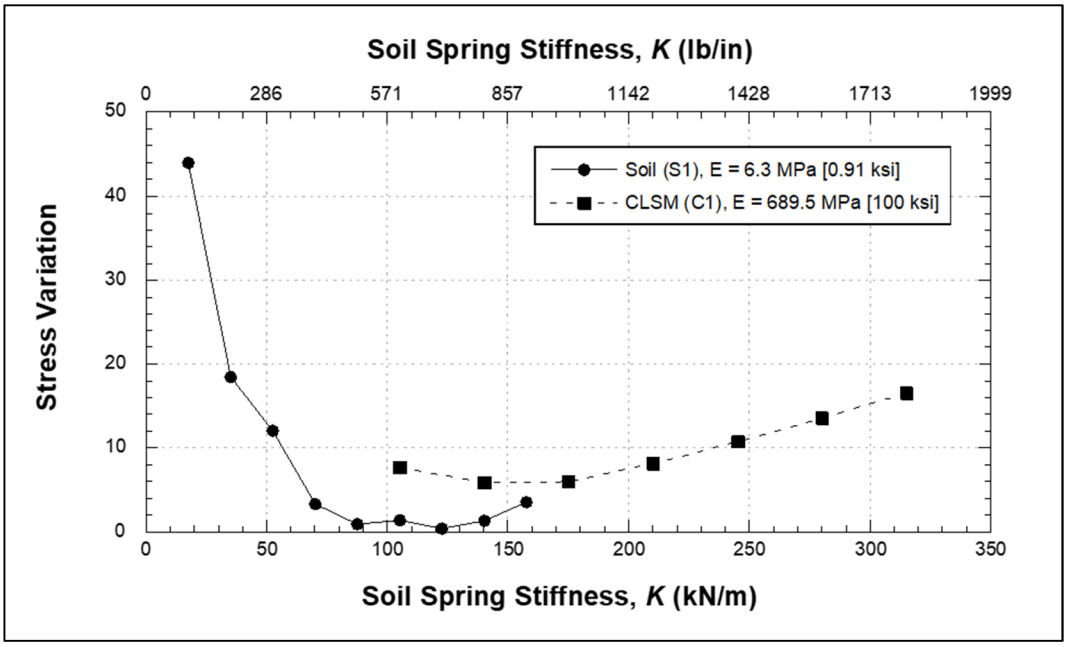

Figure 24: Stress variation curve for soil and CLSM backfills

Results showed that there was an optimum *K* value (K_{opt}) that resulted in the minimum stress variation along the pipe for each backfill material. Table 12 thru Table 15 show the summation stress variance for each *K* value evaluated for different soil

backfills investigated in this study. The optimum K value (K_{opt}) was selected based on the lowest value of the summation stress variance and was highlighted in those tables.

Table 12: Soil spring stiffness and sum of stress variance for Soil (S1)

Backfill Material	**Soil Spring Stiffness (K) lb/in**	**Avg. Pipe Axial Stress ($\bar{\sigma}$) kip/in^2**	**Sum of Stress Variance $\Sigma(\sigma_x - \bar{\sigma})^2$**
Soil (S1) E = 6.3 MPa [0.91 ksi]	100	6.192	43.980
	200	6.568	18.459
	300	6.727	12.065
	400	7.133	3.308
	500	7.352	0.934
	600	7.134	1.386
	700	7.379	0.426
	800	8.007	1.354
	900	8.289	3.594

* highlighted row indicates the optimum K value (K_{opt}) for this backfill material

Table 13: Soil spring stiffness and sum of stress variance for Soil (S2)

Backfill Material	**Soil Spring Stiffness (K) lb/in**	**Avg. Pipe Axial Stress ($\bar{\sigma}$) kip/in^2**	**Sum of Stress Variance $\Sigma(\sigma_x - \bar{\sigma})^2$**
Soil (S2) E = 12.9 MPa [1.87 ksi]	700	6.917	13.577
	800	6.854	13.328
	900	6.922	9.382
	1000	7.481	1.956
	1100	9.703	26.106
	1200	7.092	2.576
	1300	7.147	1.758
	1400	7.206	1.573
	4000	10.365	82.949

Table 14: Soil spring stiffness and sum of stress variance for Soil (S3)

Backfill Material	**Soil Spring Stiffness (K) lb/in**	**Avg. Pipe Axial Stress ($\bar{\sigma}$) kip/in^2**	**Sum of Stress Variance $\Sigma(\sigma_x - \bar{\sigma})^2$**
Soil (S3) E = 15.3 MPa [2.22 ksi]	1000	6.453	1.356
	1100	6.569	1.844
	1200	6.764	3.876
	1300	6.093	0.807
	1400	7.123	10.616
	1500	6.181	2.124
	1600	6.302	3.239
	1700	6.455	4.579
	5000	12.624	147.213

Table 15: Soil spring stiffness and sum of stress variance for Soil (S4)

Backfill Material	**Soil Spring Stiffness (K) lb/in**	**Avg. Pipe Axial Stress ($\bar{\sigma}$) kip/in^2**	**Sum of Stress Variance $\Sigma(\sigma_x - \bar{\sigma})^2$**
Soil (S4) E = 20.27 MPa [2.94 ksi]	1600	6.422	3.036
	1700	6.453	2.064
	1800	6.483	1.368
	1900	7.420	2.408
	2000	7.595	3.819
	2100	8.522	13.148
	2200	8.864	17.672
	7000	10.200	99.846

Next, the K_{opt} value obtained was plotted with soil Young's modulus (E), as shown in Figure 25. Results indicated that the K_{opt} value for a more uniform stress distribution along the pipe length increased with increasing E values for soil backfills. The observed empirical relationship between K_{opt} value and soil Young's modulus is given by Eq. (5) and Eq. (6) for metric and English units, respectively:

[for metric unit]: $K_{opt} = 13.24\,E + 46.382$ Eq. (5)

[for English unit]: $K_{opt} = 0.521\,E + 264.85$ Eq. (6)

Where: K_{opt} = soil spring stiffness placed at FE model boundaries (kN/m for metric unit; lb/in for English unit)

E = soil's Young's modulus (MPa for metric unit; lb/in^2 for English unit)

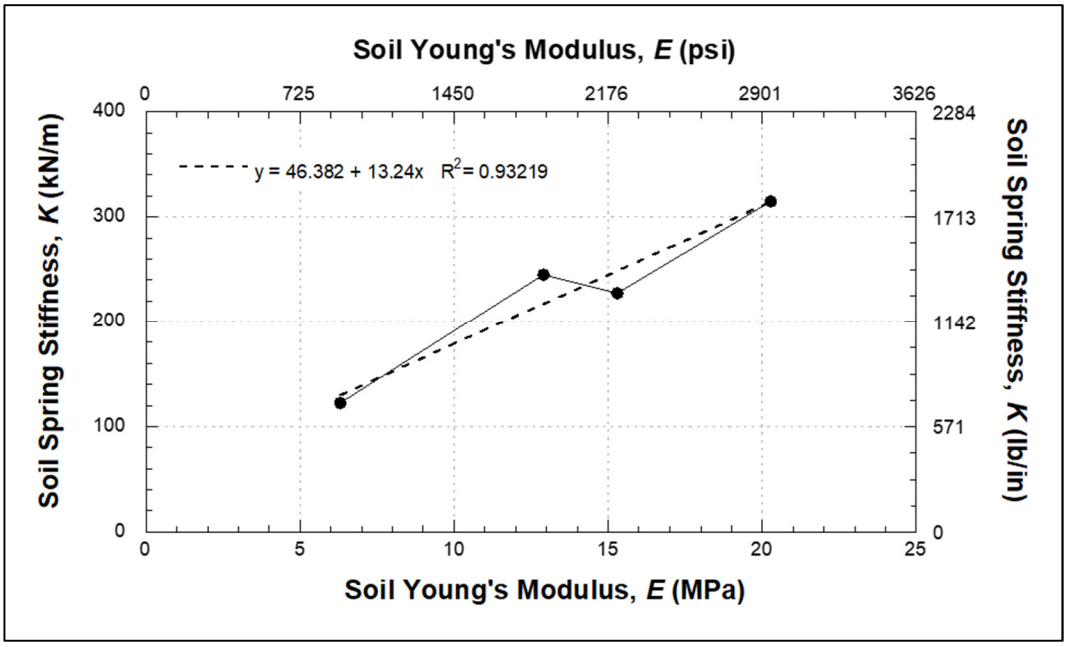

Figure 25: Relationship between soil Young's modulus and soil spring stiffness

The K_{opt} value for additional soil type, referred to as Soil (T1) as listed in Table 1, with E value of 17.79 MPa [2580.2 psi] was calculated using Eq. (5) to be 281.9 kN/m [1609.1 lb/in]. The soil properties and the computed K_{opt} value were then used in the developed FE model to evaluate the variation of axial stresses along the pipe. Figure 26 shows axial stresses plotted along the pipe for Soil (T1) using computed K_{opt} value at boundary planes. Results showed that a fairly uniform axial stress distribution along the pipe was achieved for Soil (T1) when its K_{opt} calculated using Eq. (5) was used in the developed FE model.

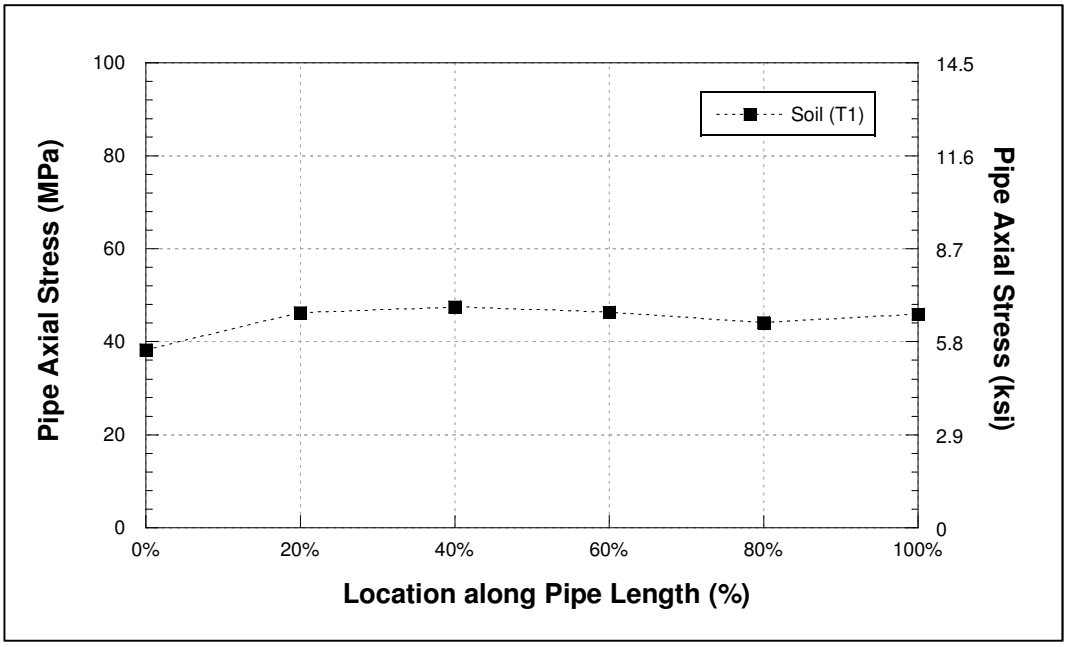

Figure 26: Evaluation of empirical relationship for Soil (T1)

Similar to the evaluation for soil backfills, three CLSM mixtures, CLSM (C1) thru CLSM (C3), with different Young's modulus (E) values were investigated for their relationship with soil spring stiffness utilized at FE model boundaries. Table 16 thru Table 18 show the summation stress variance for each K value evaluated for different CLSM backfills investigated in this study. The optimum K value (K_{opt}) was selected based on the lowest value of the summation stress variance and was highlighted in those tables.

Table 16: Soil spring stiffness and sum of stress variance for CLSM (C1)

Backfill Material	**Soil Spring Stiffness (K) lb/in**	**Avg. Pipe Axial Stress ($\bar{\sigma}$) kip/in²**	**Sum of Stress Variance $\Sigma(\sigma_x - \bar{\sigma})^2$**
CLSM (C1) E = 689.5 MPa [100 ksi]	600	4.149	7.683
	800	4.533	5.899
	1000	5.045	5.981
	1200	5.496	8.151
	1400	5.841	10.803
	1600	6.140	13.539
	1800	6.359	16.519

Table 17: Soil spring stiffness and sum of stress variance for CLSM (C2)

Backfill Material	**Soil Spring Stiffness (K) lb/in**	**Avg. Pipe Axial Stress ($\bar{\sigma}$) kip/in²**	**Sum of Stress Variance $\Sigma(\sigma_x - \bar{\sigma})^2$**
CLSM (C2) E = 1379 MPa [200 ksi]	600	3.329	2.127
	800	3.886	0.196
	1000	4.195	1.518
	1200	5.081	4.903
	1400	4.936	4.476
	1600	6.883	23.317
	1800	5.493	12.307

Table 18: Soil spring stiffness and sum of stress variance for CLSM (C3)

Backfill Material	**Soil Spring Stiffness (K) lb/in**	**Avg. Pipe Axial Stress ($\bar{\sigma}$) kip/in^2**	**Sum of Stress Variance $\Sigma(\sigma_x - \bar{\sigma})^2$**
CLSM (C3) E = 2757.9 MPa [400 ksi]	600	2.473	0.671
	800	2.879	1.209
	1000	3.248	3.166
	1200	3.593	5.158
	1400	3.880	7.499
	1600	4.256	11.463
	1800	4.440	14.173

Unlike Soils, the K_{opt} value for minimum stress variation along the pipe changed only slightly for the three CLSM mixtures evaluated with different E values. Therefore, it was concluded that the CLSM Young's modulus value was not a significant factor affecting the K_{opt} value. This could be due to the large difference in stiffness between the CLSM mixtures and the surrounding in-situ soil as well as an increase in system stiffness provided by CLSM trench surrounding the pipe. For all other investigations with CLSM backfills in this study, an average K_{opt} value of 140.2 kN/m [800 lb/in] was utilized.

3.3.2.8 FE Model Dimension Scale Factor

Figure 27 shows axial stresses along the pipe length for the FE model with Soil (S2) backfill and the two scaled models with factors of 0.75 and 1.25. The average pipe stress for the Soil (S2) backfill material was 49.69 MPa [7.206 ksi] and the average pipe

stresses for the down and up scaled models were 38.69 MPa [5.612 ksi] and 63.75 MPa [9.246 ksi], respectively.

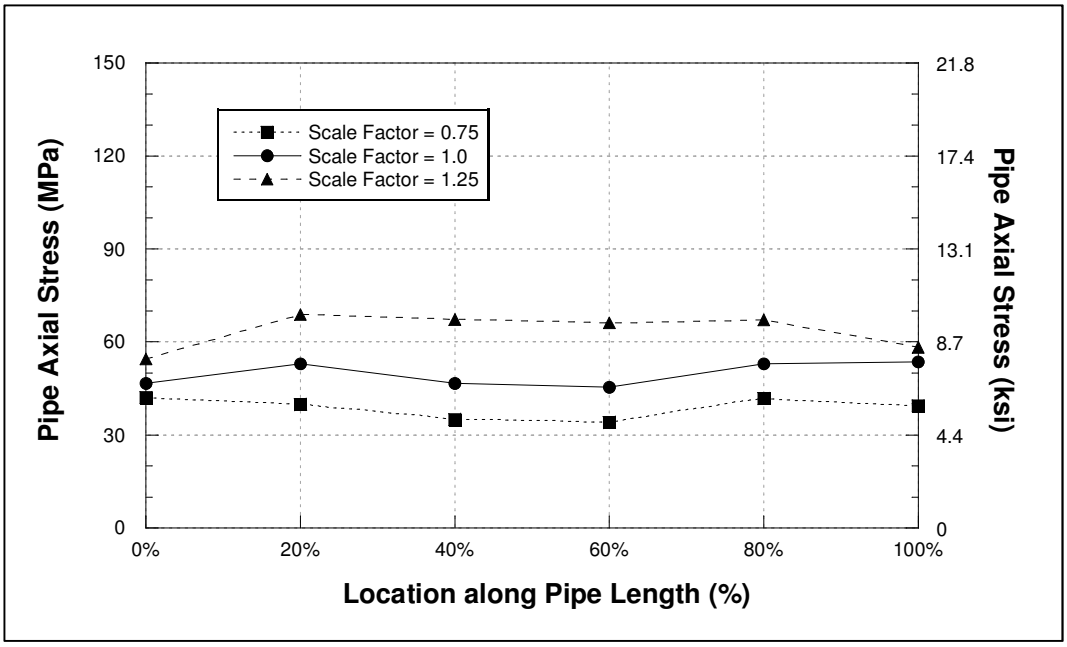

Figure 27: Pipe axial stress along the pipe for various FE model scale factors

The average pipe axial stress of the FE model scaled down with a factor of 0.75 was 78% of the average pipe axial stress of the original model. Similarly, the average pipe axial stress of the scaled up FE model with a factor of 1.25 was 128% of the average pipe axial stress of the original model. Results indicated that when the FE model dimensions are modified with a constant scale factor keeping the dimension ratios constant, the average pipe axial stresses changed with almost the same factor. This result can be used to minimize analysis run-time by using scaled down models.

3.3.3 Pipe Seismic Performance of Various Backfill Materials

After setting the FE model parameters such as soil spring stiffness at boundaries, minimum FE model length, and friction coefficient to match the axial stress predicted by the ASCE guidelines when using Soil (S2) as a pipe backfill material, this developed FE model was further utilized to evaluate the pipe seismic performance of other soil and CLSM backfill materials, as shown in Table 1. The pipe seismic performance is determined to be better when the pipe experiences the lower pipe axial stress under seismic loads. Figure 28 shows the plot of pipe axial stress along the pipe length for buried pipes subject to one directional seismic wave propagation for various backfill materials. It can be seen that pipe axial stresses were fairly uniform along the pipe length. Table 19 shows the average pipe axial stresses for various backfills.

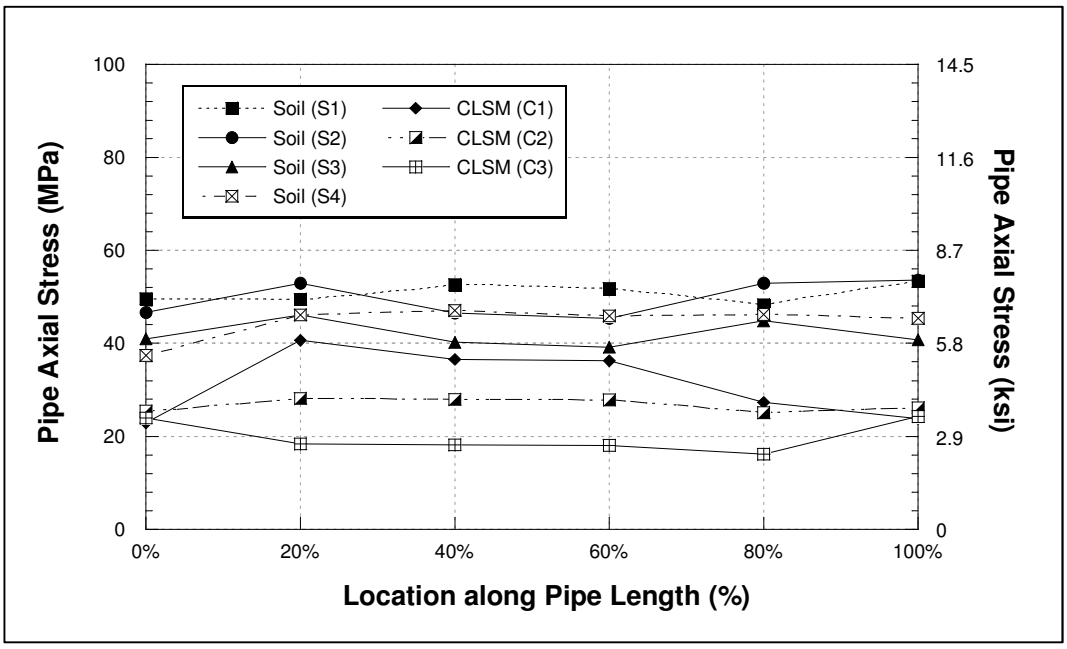

Figure 28: Pipe axial stress along the pipe for various backfill materials using K_{opt} at boundaries

Table 19: Summary of average pipe axial stress for various backfills

Pipe Config.*	Description	Average Pipe Axial Stress MPa [kip/in^2]	
		Subject to 1-Dir. Seismic Wave	Subject to 3-Dir. Seismic Wave
I	Computed from ASCE guidelines	50.13 [7.270]	---
I	FE model with Soil (S1) backfill	50.88 [7.379]	---
I	FE model with Soil (S2) backfill	49.69 [7.206]	60.94 [8.838]
I	FE model with Soil (S3) backfill	42.01 [6.093]	---
I	FE model with Soil (S4) backfill	44.70 [6.483]	---
I	FE model with Soil (T1) backfill	44.74 [6.489]	---
I	FE model with CLSM (C1) backfill	31.26 [4.533]	---
I	FE model with CLSM (C2) backfill	26.79 [3.886]	---
I	FE model with CLSM (C3) backfill	19.85 [2.879]	15.12 [2.198]
II	FE model with Soil (S2) backfill**	307.31 [44.572]	338.19 [49.051]
II	FE model with CLSM (C3) backfill**	126.55 [18.355]	127.20 [18.448]

* Pipe Config.: I = an infinitely long pipe free on both ends
II = a pipe free on one end and rigidly connected on the other end

** Pipe axial stress measured at rigid end

Results clearly showed that under one dimensional seismic wave propagation, use of CLSM as a backfill material lowered the pipe axial stresses compared to soil backfills. The pipe axial stresses decreased with increasing stiffness (Young's modulus) of the backfill materials. The change in pipe axial stresses between different CLSM mixtures was higher compared to the change between soil backfills. It should be noted that in this study the differences in Young's modulus value among evaluated CLSM mixtures are much higher compared to soils. Therefore, it was concluded that for the evaluated backfill materials, the pipes embedded in CLSM backfills have a higher pipe seismic performance compared to soil backfills.

3.3.4 Effect from One- and Three-Directional Seismic Wave

The FE models with Soil (S2) and CLSM (C3) backfills were also evaluated on the effect from three directional seismic wave propagation applied simultaneously. Figure 8 shows the pipe axial stresses under one and three directional wave propagation for pipes with the evaluated backfill materials.

As shown in Figure 29 and Table 19, for Soil (S2) backfill material, the average pipe axial stress increased from 49.69 MPa [7.206 ksi] to 60.94 MPa [8.838 ksi] when subjected to three directional seismic wave propagation, approximately 23% increase. For CLSM (C3) backfill material, the change in average pipe axial stresses when subjected to three directional wave propagation was very small. The average pipe axial stresses were 19.85 MPa [2.879 ksi] and 15.12 MPa [2.198 ksi] when subject to one and three directional seismic wave propagation, respectively.

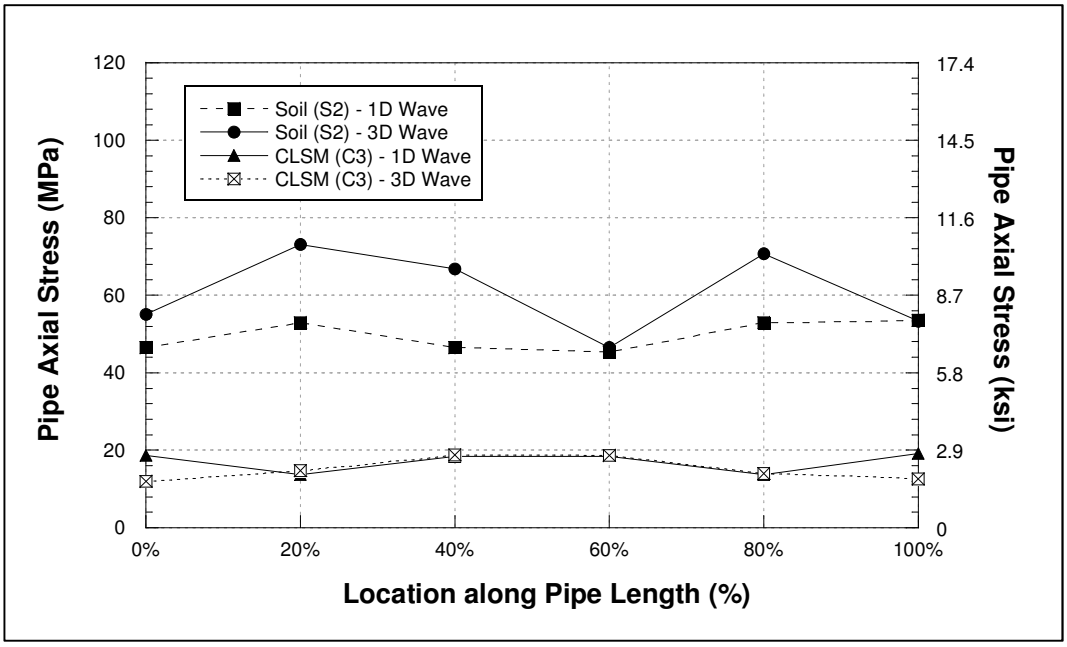

Figure 29: Effect on pipe axial stress from one- and three-directional seismic wave

Therefore, it was concluded that the effect from three-directional seismic wave has a higher impact to pipe seismic performance for the pipe with soil backfill, but does not have a significant impact for the pipe with CLSM backfill.

In addition to pipe axial stress, Figure 30 and Figure 31 show the horizontal and vertical bending stresses along the pipe, respectively, when subjected to one and three directional seismic wave propagation using backfill materials Soil (S2) and CLSM (C3). Results indicated that pipe horizontal and vertical bending stresses are approximately 20 times lower compared to the pipe axial stresses in both soil and CLSM backfills. Therefore, results suggested that buried pipes, even when subjected to three directional seismic wave propagation, would fail in pipe crushing rather than pipe bending failure.

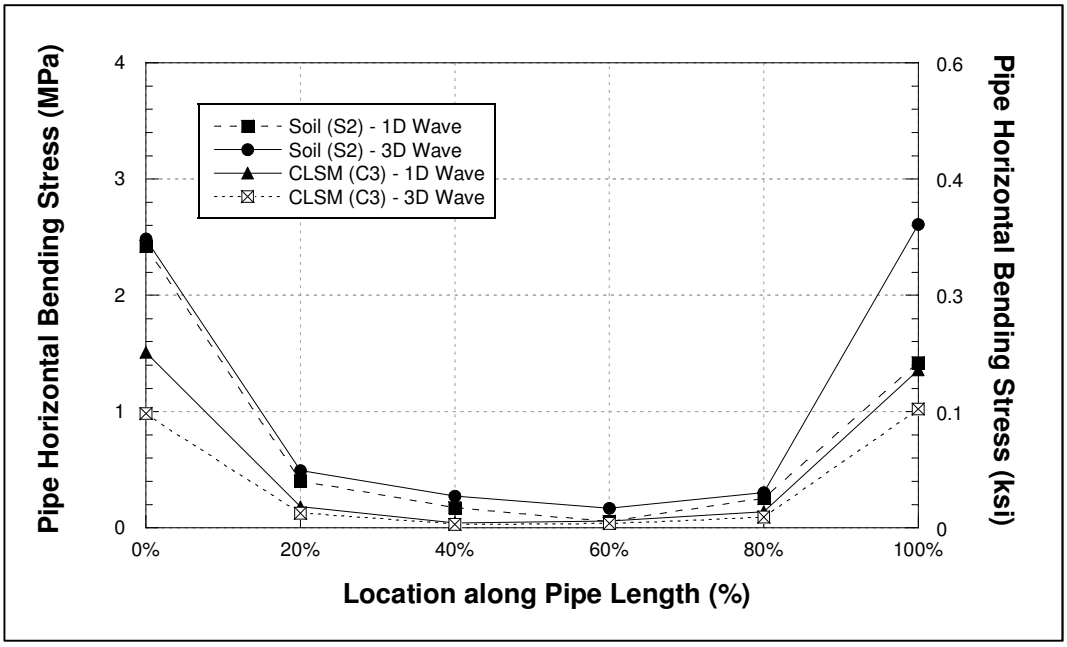

Figure 30: Effect on pipe horizontal bending stress from one- and three-directional seismic wave

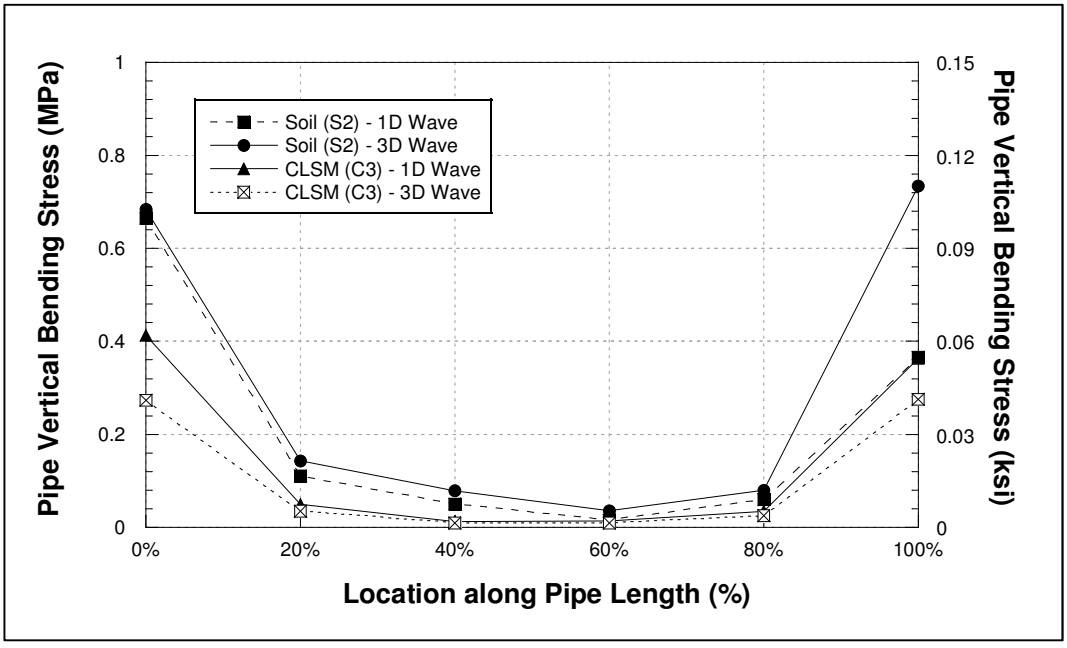

Figure 31: Effect on pipe vertical bending stress from one- and three-directional seismic wave

3.3.5 Pipe End Conditions

After matching the axial stress predicted by the ASCE guidelines for an infinitely long pipe free at both ends, the developed FE model was also used to evaluate the effect of having a rigid connection at one end of the pipe. Figure 32 shows the pipe axial stress along the pipe length for pipes rigidly connected to a structure at one end and embedded in backfill materials Soil (S2) and CLSM (C3). Pipe axial stresses are shown for both when subjected to one- and three directional seismic wave propagation.

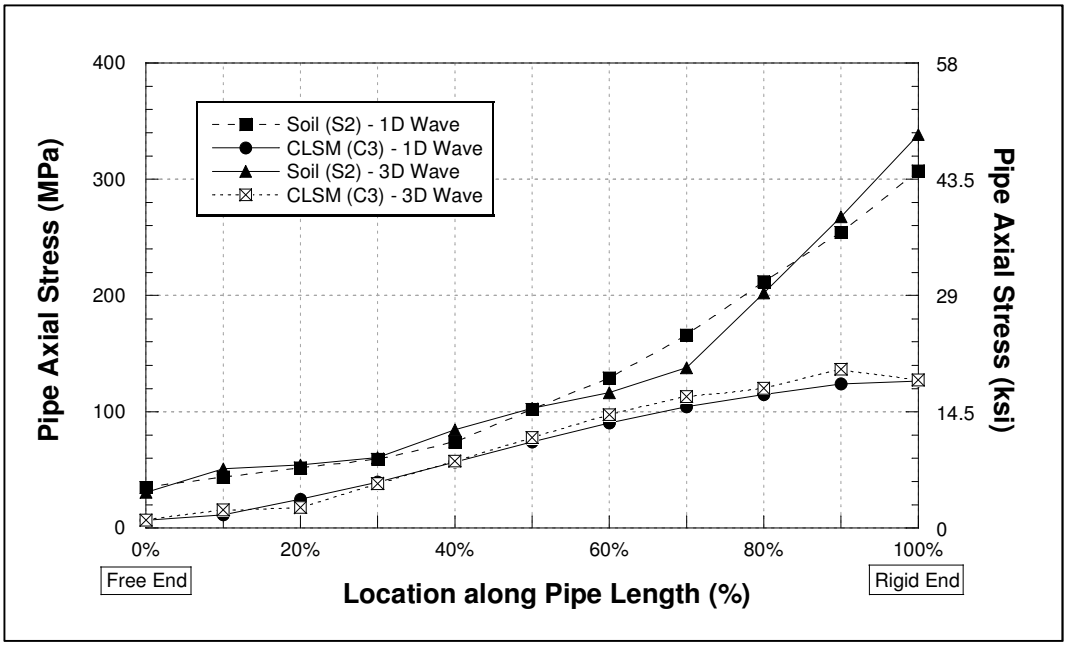

Figure 32: Pipe axial stress having one end rigidly connected to a structure

Results indicated that pipe axial stresses could be 5 to 7 times higher at the rigid connection compared to the free end of the pipe regardless of the type of backfill material. However, the pipe embedded in CLSM (C3) backfill exhibited significantly

lower axial stress compared to the pipe embedded in Soil (S2) backfill at the rigid connection end. The maximum axial stress values observed at the rigid connections for soil and backfill materials were summarized in Table 19. It was also observed that the effect of one- versus three-directional wave propagation on pipe axial stress was negligible compared to the effect of having a rigid connection at pipe end.

3.4 Research Methodology with Inelastic Materials

In the first phase of the study for buried pipelines subject to seismic wave propagation, all materials were considered to remain in elastic range under seismic loads. The second phase of this study was to evaluate the effect of non-linear material plasticity on the seismic performance for pipes embedded in soil and CLSM backfills. The study started with the development of FE models using recommended FE model parameters obtained from the first phase, such as soil-pipe interaction, boundary condition, and FE model dimensions. Various FE model parameters were investigated, including soil spring stiffness (K) and dashpot coefficient (c) utilized at FE model boundaries. Similar to the study with elastic materials, the goal was to achieve a uniform pipe axial stress distribution along the pipe with non-linear material behavior. Then, the developed FE model was further utilized to determine the seismic performance of pipes embedded in CLSM backfills compared to soil backfills in inelastic range. The inelastic pipe seismic performance was also compared to the performance in elastic range.

3.4.1 3D Finite Element Models

All the modeling techniques implemented earlier in the first phase were adopted for the second phase, including model element types, mesh sizes, and load applications.

The developed FE model was the same as shown in Figure 7. FE model parameters that were used in this study are listed below:

- Steel pipe material, pipe size and thickness, pipe embedment depth, and backfill trench dimensions were the same as that utilized in the first phase.
- 3D FE model dimensions: model width (W_d) of 30D, model depth (D_d) of 35D, and model length (L_d) of 200D.
- Boundary conditions: pinned boundary condition at the bottom plane and soil spring support at all other planes with the K value based on the material Young's modulus (E) as suggested previously.
- Load applications: all FE models were subject to the same seismic ground acceleration time-history of 1989 Loma Prieta earthquake record by [13] after application of gravitational forces.

3.4.2 Inelastic Material Properties

All materials considered in the second phase of the study accounted for non-linear material behavior. For the steel pipeline, an elastic-plastic material behavior with von Mises plasticity model was utilized with the stress-strain curve as shown in Table 20 and Figure 33.

Table 20: Stress-strain characteristics of steel pipeline [21]

$\sigma_1 = \sigma_y$ (MPa)	$\sigma_2 = \sigma_f$ (MPa)	E_1 (GPa)	E_2 (GPa)	Strain Limit	
				Elastic	Failure
490	531	210	1.088	0.0023	0.04

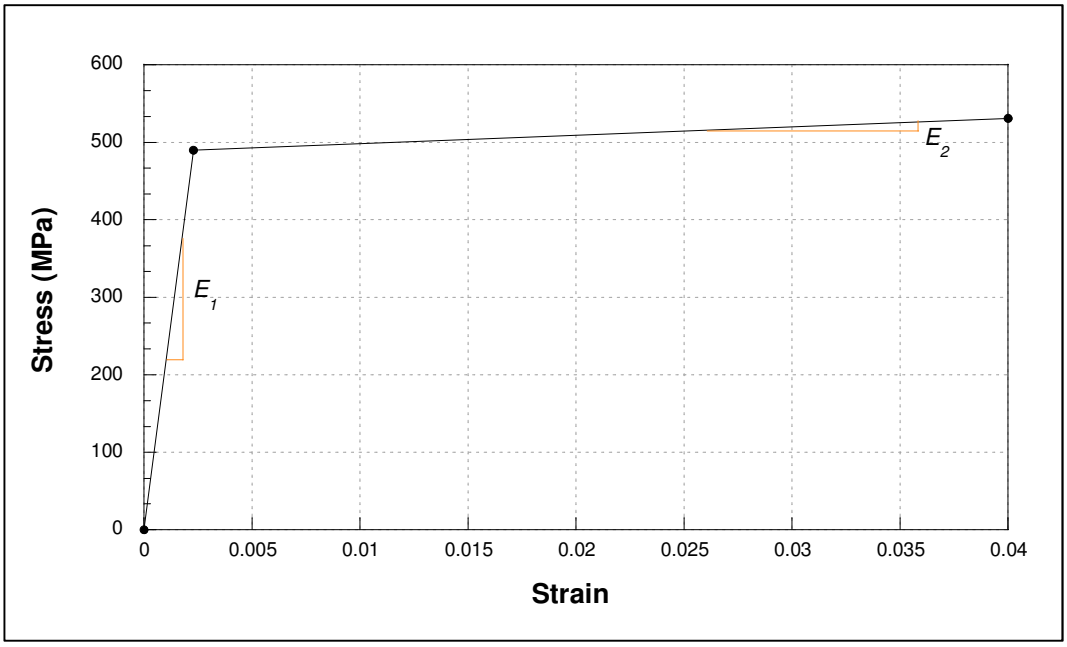

Figure 33: Stress-strain curve of steel pipelines

Based on the literature review performed earlier, Mohr-Coulomb constitutive model is commonly used to represent non-linear material behavior; therefore, for soil and CLSM backfills and in-situ soil material, Mohr-Coulomb constitutive model was chosen for all FE models in this study. Four soil types, Soil (S1) thru Soil (S4), and three selected CLSM mixtures, CLSM (C1) thru CLSM (C3), were evaluated with their elastic properties listed in Table 1. To define material Mohr-Coulomb plasticity in ABAQUS, four additional parameters are required, including friction angle, cohesion stress, dilation angle, and absolute plastic strain. According to Vazouras *et al.* [44], dilation angle of 0.1° was utilized, and the absolute plastic strain was assumed to be zero for all materials evaluated in this study. Friction angle and cohesion stress for the selected soil backfills were based on a study by [33]. It should be noted that in the study by [4], friction angle

and cohesion stress for CLSM mixtures were not evaluated and were not provided. Therefore, the values used in this study were based on CLSM mixtures evaluated by Lee *et al.* [45] with their mixture proportions as shown in Table 21. Inelastic material properties of all materials evaluated in this study are summarized in Table 22.

Table 21: CLSM mixture proportions [45]

ID	Material Description as Listed in References	Optimum Mixing Composition (%)					
		Recycled In-situ Soil	Bottom Ash	Fly Ash	Crumb Rubber	Cement	Water
CLSM (C1)	Type Case 3	25	30	20	-	3	22
CLSM (C2)	Type Case 1	45	20	10	-	3	22
CLSM (C3)	Type Case 4	32	30	10	3	3	22

Table 22: Inelastic properties for soil and CLSM backfills [33, 45]

ID	Material Description as Listed in References	Friction Angle	Cohesion Stress kPa [psi]
Soil (S1)	Loosely Compacted Soil	15º	8 [1.16]
Soil (S2)	Loosely Compacted Sandy Silt	27º	29 [4.21]
Soil (S3)	Loosely Compacted Sandy Silt	25º	30 [4.35]
Soil (S4)	Loosely Compacted Sandy Silt	25º	30 [4.35]
CLSM (C1)	Type Case 3	47.4º	97.7 [14.17]
CLSM (C2)	Type Case 1	43.8º	132 [19.14]
CLSM (C3)	Type Case 4	36.5º	180.7 [26.21]

3.4.3 FE Model Parametric Study

In this study, three FE model parameters placed at FE model boundaries were evaluated to investigate their effects on a uniform pipe axial stress distribution along the pipe. These parameters include:

- Soil spring stiffness (K)
- Dashpot element (c)
- Dashpot element in conjunction with soil spring (c & K)

From the previous results, soil spring was suggested to be used at boundaries to achieve a uniform pipe axial stress along the pipe. For non-linear material behavior, the study further investigated in the use of dashpot element. According to [22], using dashpot element can provide viscous energy dissipation mechanisms and can be useful in FE model convergence in non-linear analysis. Table 23 thru Table 25 show FE variables used in this parametric study for soil backfills, Soil (S1) thru Soil (S4).

Table 23: FE model variables evaluated for boundary soil spring

FE Model Constants	
Model:	Steel pipe embedded in soil backfills
FE Model Dimensions:	$W_d = 30D$, $D_d = 35D$, and $L_d = 200D$
Soil-Pipe Interface:	Friction interface with coefficient of friction (f_1) = 0.5
FE Model Variables	
Boundary Condition:	Soil (S1): spring stiffness (K) ranging from 87.56 kN/m [500 lb/in] to 700.51 kN/m [4000 lb/in] Soil (S2): spring stiffness (K) ranging from 245.18 kN/m [1400 lb/in] to 2626.90 kN/m [15000 lb/in] Soil (S3): spring stiffness (K) ranging from 875.63 kN/m [5000 lb/in] to 4378.17 kN/m [25000 lb/in] Soil (S4): spring stiffness (K) ranging from 1751.27 kN/m [10000 lb/in] to 5253.81 kN/m [30000 lb/in]

Table 24: FE model variables evaluated for boundary dashpot element

FE Model Constants	
Model:	Steel pipe embedded in Soil (S2) backfill
FE Model Dimensions:	$W_d = 30D$, $D_d = 35D$, and $L_d = 200D$
Soil-Pipe Interface:	Friction interface with coefficient of friction (f_1) = 0.5
FE Model Variables	
Boundary Condition:	Dashpot element (c) with values ranging from 5 to 1000 (in term of force per velocity)

Table 25: FE model variables evaluated for boundary soil spring and dashpot element

FE Model Constants	
Model:	Steel pipe embedded in Soil (S2) backfill
FE Model Dimensions:	$W_d = 30D$, $D_d = 35D$, and $L_d = 200D$
Soil-Pipe Interface:	Friction interface with coefficient of friction (f_1) = 0.5
FE Model Variables	
Boundary Condition:	Spring stiffness with dashpot element [c, K]: - [5, 600] - [5, 800] - [5, 2000]

3.5 Results and Discussions with Inelastic Materials

3.5.1 FE Model Parametric Study

3.5.1.1 Soil Spring Stiffness

Several soil spring stiffness values, as shown in Table 23, placed at FE model boundaries were evaluated for FE models with non-linear material behavior to

investigate their effects on a uniform pipe axial stress distribution along the pipe. Figure 34 shows the pipe axial stress along the pipe length for various soil spring stiffness evaluated.

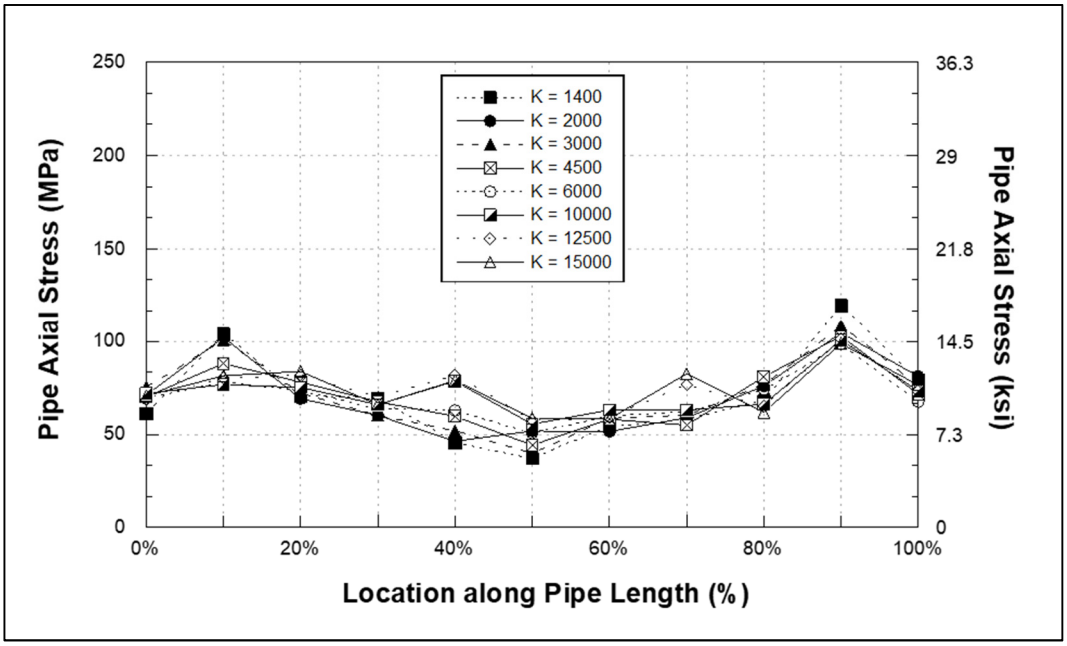

Figure 34: Pipe axial stress along the pipe for various soil spring stiffness at boundaries for inelastic materials Soil (S2) backfill

Results clearly showed that a uniform pipe axial distribution along the pipe was not achieved with any value of soil spring stiffness, unlike results from elastic materials. This could be due to that under seismic loads the materials had gone into inelastic range and had experienced plastic deformations, particularly soil backfill material. This effect was even more dramatic at locations near boundaries as shown by the higher pipe axial stress. From the previous results, the optimal soil spring stiffness (K_{opt}) for Soil (S2)

backfill was equal to 1400 lb/in. It was also observed from Figure 34 that axial stress variation along the pipe was greater with the higher soil spring stiffness utilized.

Since results near boundaries were greatly affected from non-linear material behavior, only results from 30% to 70% of the pipe length were investigated to determine of a better uniform pipe axial distribution along the pipe could be achieved. Figure 29 shows the same results as Figure 28, excluding results near boundaries, and it showed that pipe axial stress along the pipe was more uniform. Figure 36 thru Figure 38 show all results of the pipe axial stress along the pipe length for various soil spring stiffness for Soil (S1), Soil (S3), and Soil (S4) backfills, respectively. Figure 39 thru Figure 41 show the same results for Soil (S1), Soil (S3), and Soil (S4) backfills, respectively, excluding results near boundaries. It was observed that for all soil backfills evaluated using results from 30% to 70% of the pipe length provided a better uniform pipe axial distribution that can be used to determine the pipe seismic performance.

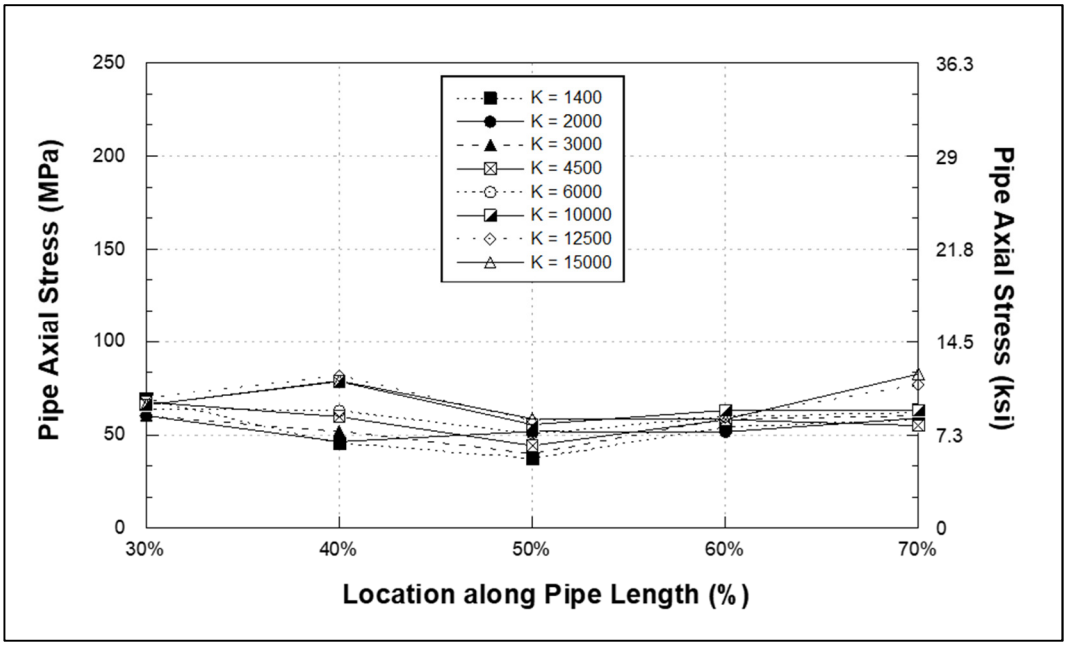

Figure 35: Pipe axial stress along the pipe for various soil spring stiffness at boundaries for inelastic materials Soil (S2) backfill, excluding results near boundaries

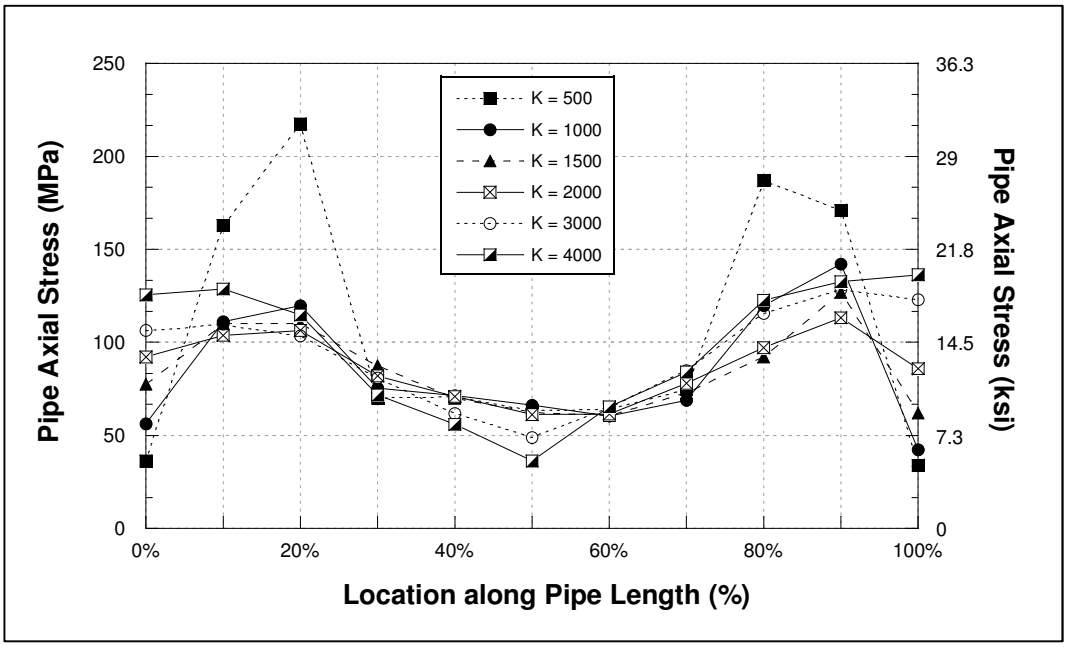

Figure 36: Pipe axial stress along the pipe for various soil spring stiffness at boundaries for inelastic materials Soil (S1) backfill

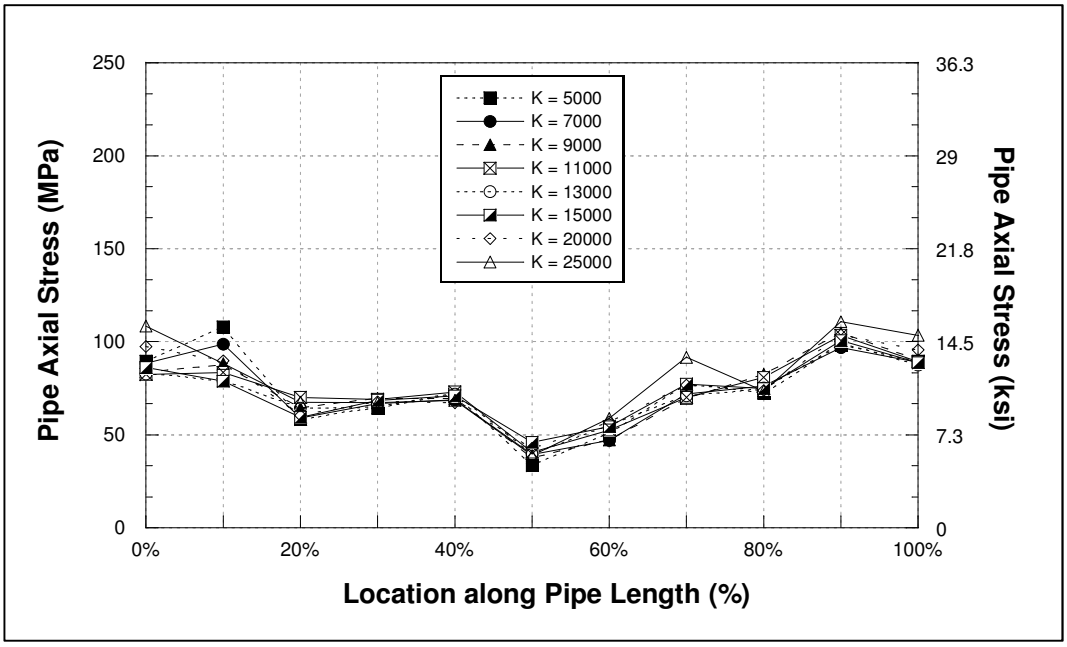

Figure 37: Pipe axial stress along the pipe for various soil spring stiffness at boundaries for inelastic materials Soil (S3) backfill

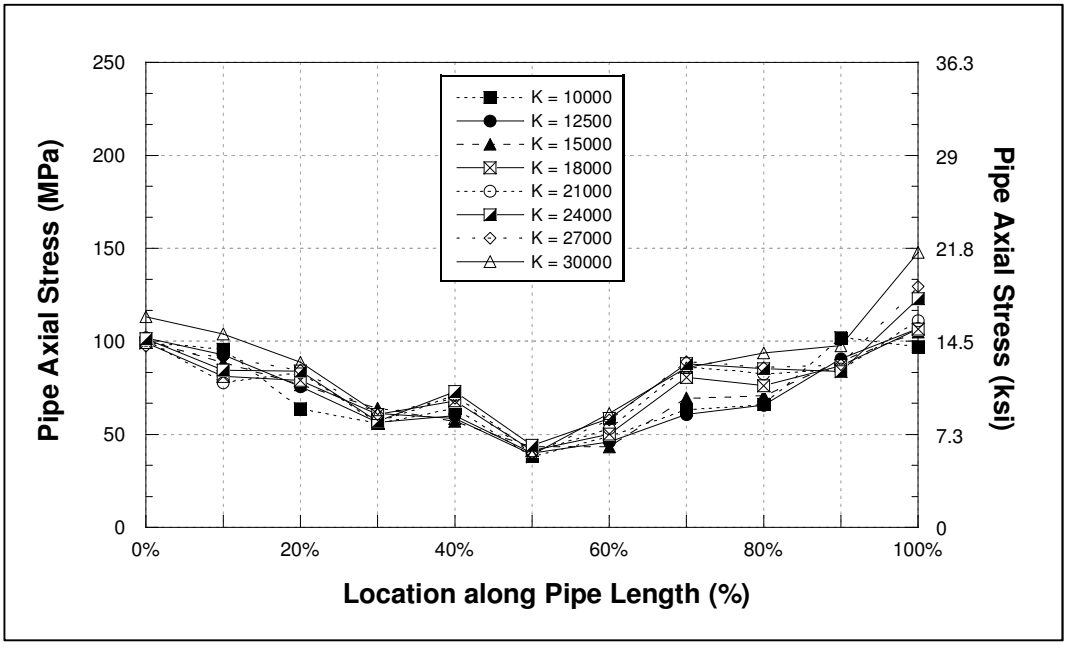

Figure 38: Pipe axial stress along the pipe for various soil spring stiffness at boundaries for inelastic materials Soil (S4) backfill

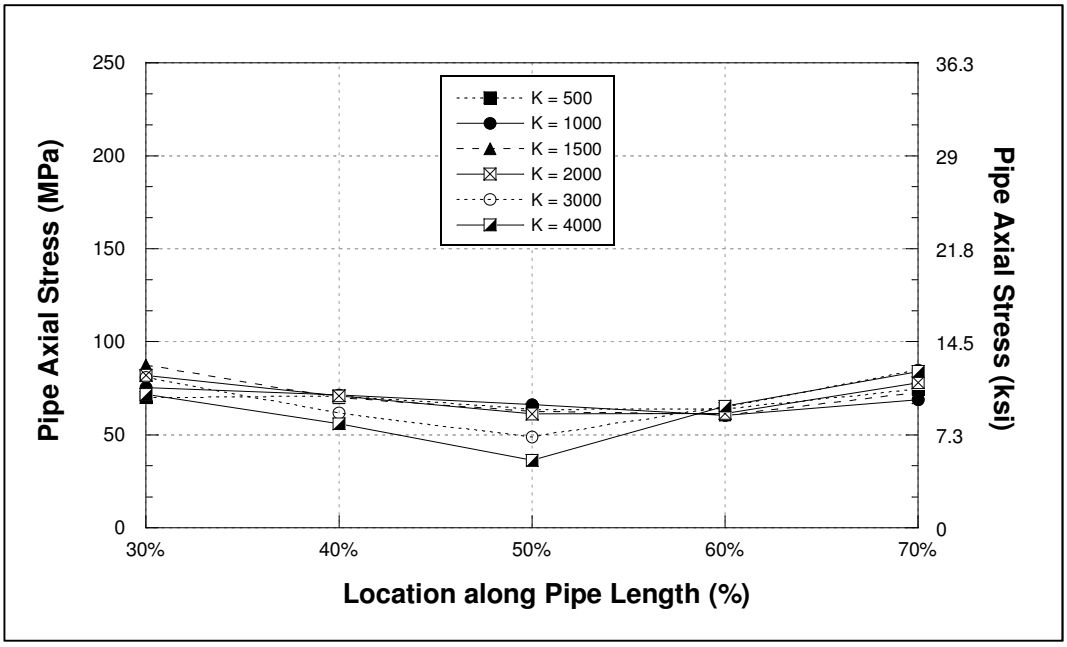

Figure 39: Pipe axial stress along the pipe for various soil spring stiffness at boundaries for inelastic materials Soil (S1) backfill, excluding results near boundaries

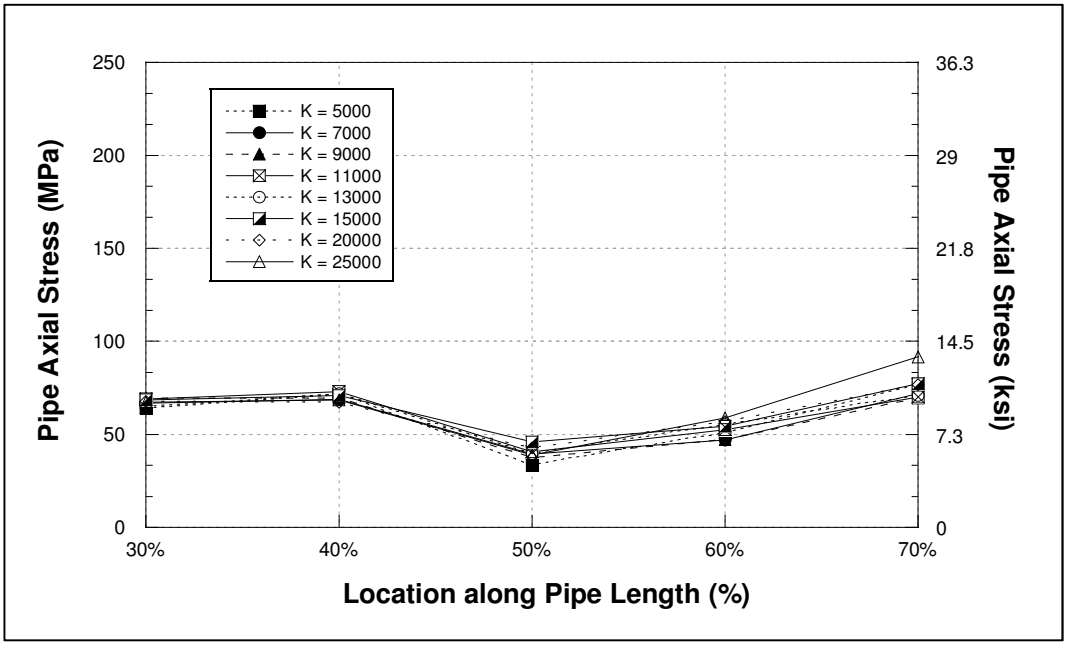

Figure 40: Pipe axial stress along the pipe for various soil spring stiffness at boundaries for inelastic materials Soil (S3) backfill, excluding results near boundaries

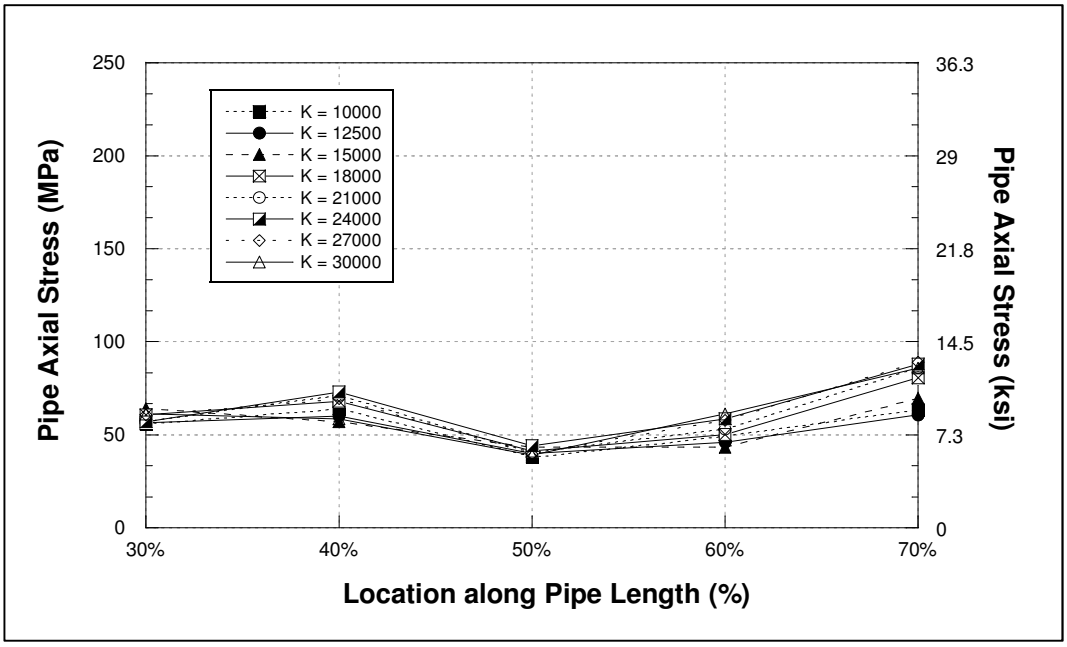

Figure 41: Pipe axial stress along the pipe for various soil spring stiffness at boundaries for inelastic materials Soil (S4) backfill, excluding results near boundaries

3.5.1.2 Dashpot Element

Figure 42 shows all results of the pipe axial stress along the pipe length for pipe embedded in Soil (S2) backfill, and Figure 43 shows the same plot excluding results near boundaries when using dashpot element at FE model boundaries. Similar to results of using soil spring stiffness, results indicated that a uniform pipe axial distribution was not achieved when considering all results. A more uniform distribution would be expected when excluding results near boundaries. Table 26 shows the average pipe axial when considering results only from 30% to 70% of the pipe length compared between using soil spring and dashpot element. It was observed that when using a high value of dashpot element, the average pipe axial stress could be under estimated.

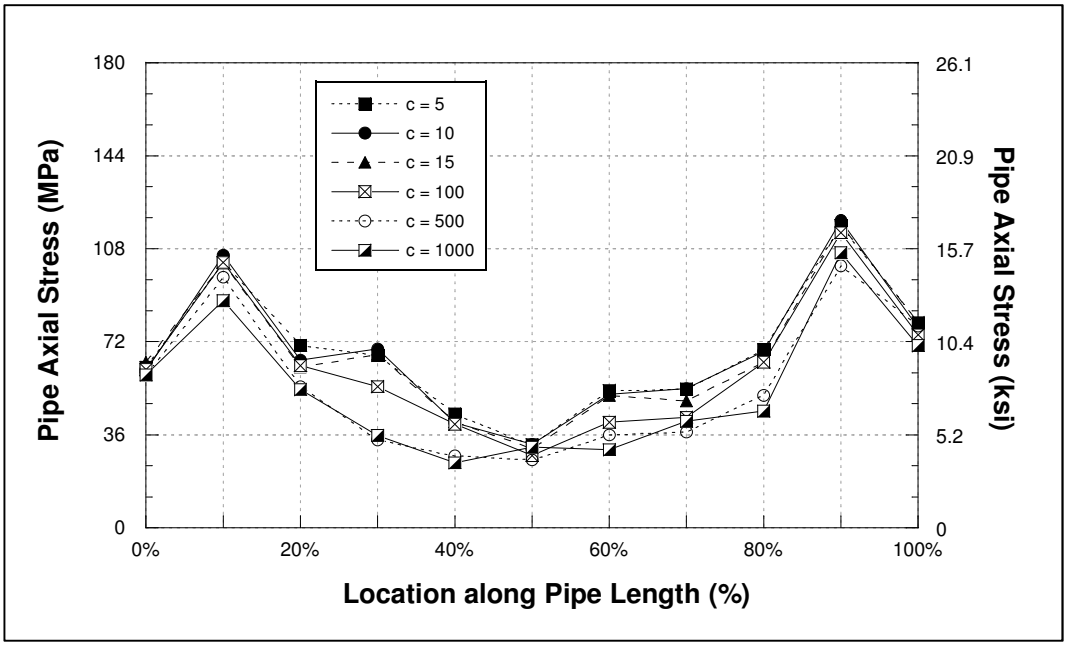

Figure 42: Pipe axial stress along the pipe for various dashpot at boundaries for inelastic materials Soil (S2) backfill

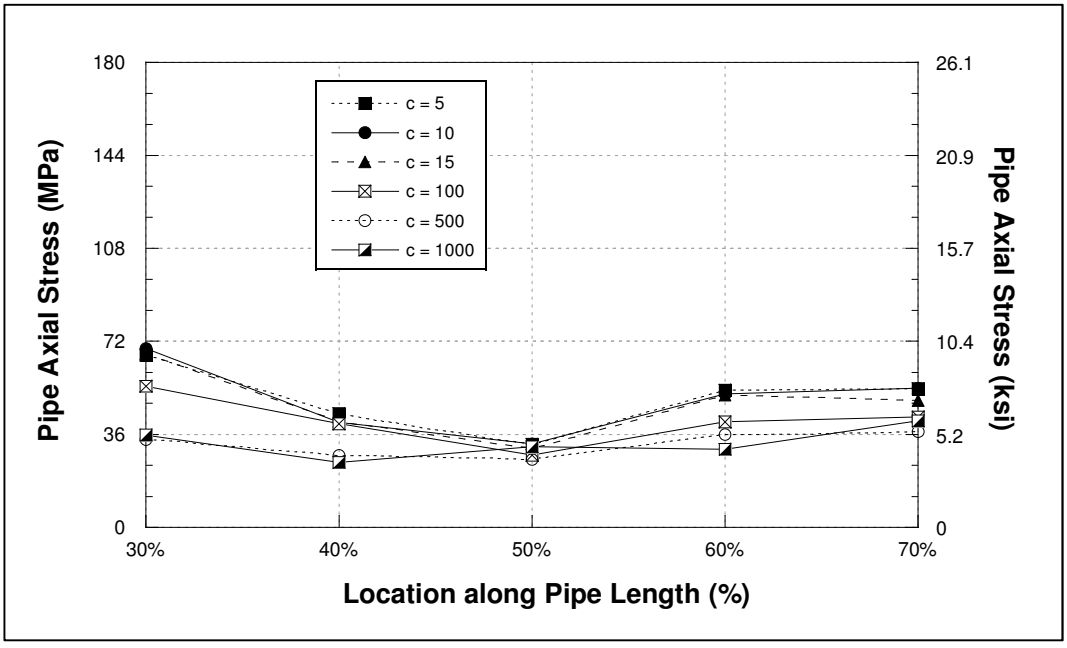

Figure 43: Pipe axial stress along the pipe for various dashpot at boundaries for inelastic materials Soil (S2) backfill, excluding results near boundaries

Table 26: Average pipe axial stress when using soil spring stiffness and dashpot elements at boundaries for inelastic materials Soil (S2) backfill

Soil Spring (*K*)	**Avg. Pipe Axial Stress (30% - 70%) ksi**	**Dashpot (*c*)**	**Avg. Pipe Axial Stress (30% - 70%) ksi**	**Dashpot & Soil Spring (*K* & *c*)**	**Avg. Pipe Axial Stress (30% - 70%) ksi**
1400	7.663	5	7.258	(5, 600)	7.435
2000	7.795	10	7.189	(5, 800)	7.539
3000	7.856	15	6.938	(5, 2000)	8.685
4500	8.249	100	5.983		
6000	8.683	500	4.676		
10000	9.464	1000	4.751		
12500	10.003				
15000	9.981				

3.5.1.3 Dashpot Element & Soil Spring

Similar to results seen previously, a uniform pipe axial distribution was not achieved when considering all results along the pipe length but would be expected when considering results only from 30% to 70% of the pipe length. The average pipe axial stresses for the values considered were similar to results from using soil spring or using dashpot element at boundaries, as shown in Table 26. Figure 44 shows all results of the pipe axial stress along the pipe length for pipe embedded in Soil (S2) backfill, and Figure 45 shows the same plot excluding results near boundaries when using dashpot element in conjunction with soil spring at FE model boundaries.

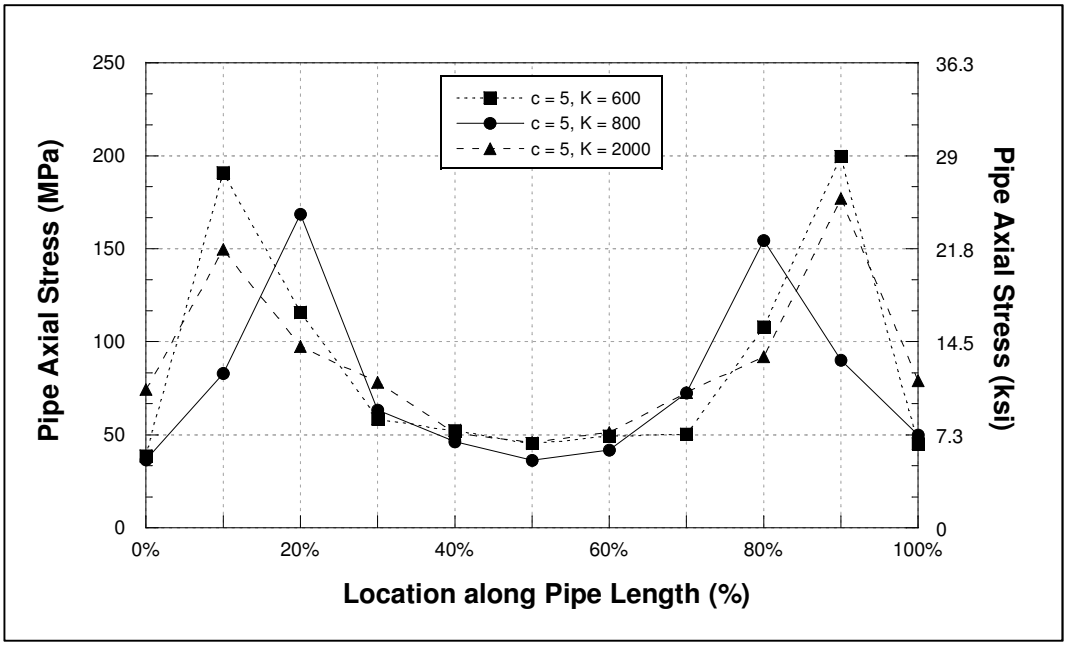

Figure 44: Pipe axial stress along the pipe for various dashpot and soil spring at boundaries for inelastic materials Soil (S2) backfill

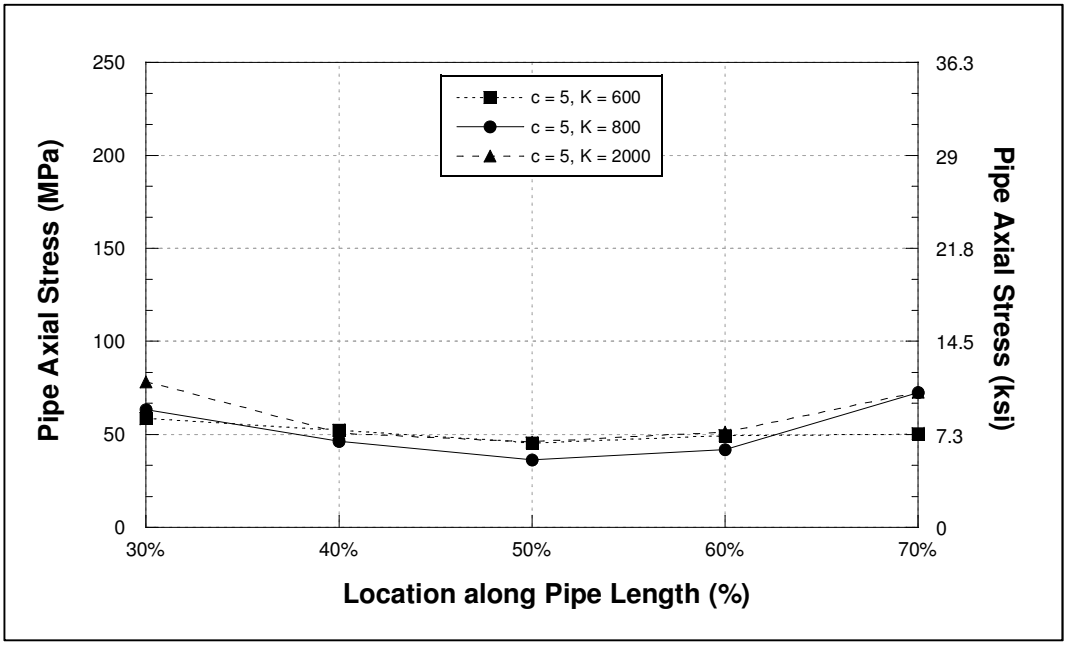

Figure 45: Pipe axial stress along the pipe for various dashpot and soil spring at boundaries for inelastic materials Soil (S2) backfill, excluding results near boundaries

3.5.2 Pipe Seismic Performance of Various Backfill Materials

After evaluating the effects on non-linear material behavior from FE model parameters, the developed FE models were utilized to determine the pipe seismic performance of various backfills, including Soil (S2) and CLSM (C1) thru CLSM (C3) backfills, for an infinitely long pipe free on both ends. From the previous findings, only results in the range from 30% to 70% of the pipe length were considered. The value for soil spring stiffness utilized at FE model boundaries was obtained from the study with elastic materials. For pipe embedded in Soil (S2) backfill and all CLSM backfills, soil spring stiffness, K_{opt}, is equal to 1400 lb/in and 800 lb/in, respectively. The developed FE model for this study also accounted for three-directional seismic wave applied simultaneously. Figure 46 shows the pipe axial stress along the pipe length for buried pipes for various backfill materials accounting for non-linear behavior. Table 27 shows the average pipe axial stresses compared to values obtained earlier from the study with elastic materials.

Similar to results from elastic materials, pipes embedded in CLSM backfills experienced lower pipe axial stresses compared to the soil backfill. Also, the pipe axial stresses decreased with increasing stiffness (Young's modulus) of the backfill materials. For soil backfill, when accounting for non-linear material behavior, the pipe axial stress was lower compared to elastic materials. This could have been the result of soil backfill material undergone plastic deformations. The material plastic deformation may have created more separation between the soil backfill and the pipe allowing the pipe to freely deform more than elastic materials, which resulted in a lower pipe axial stress.

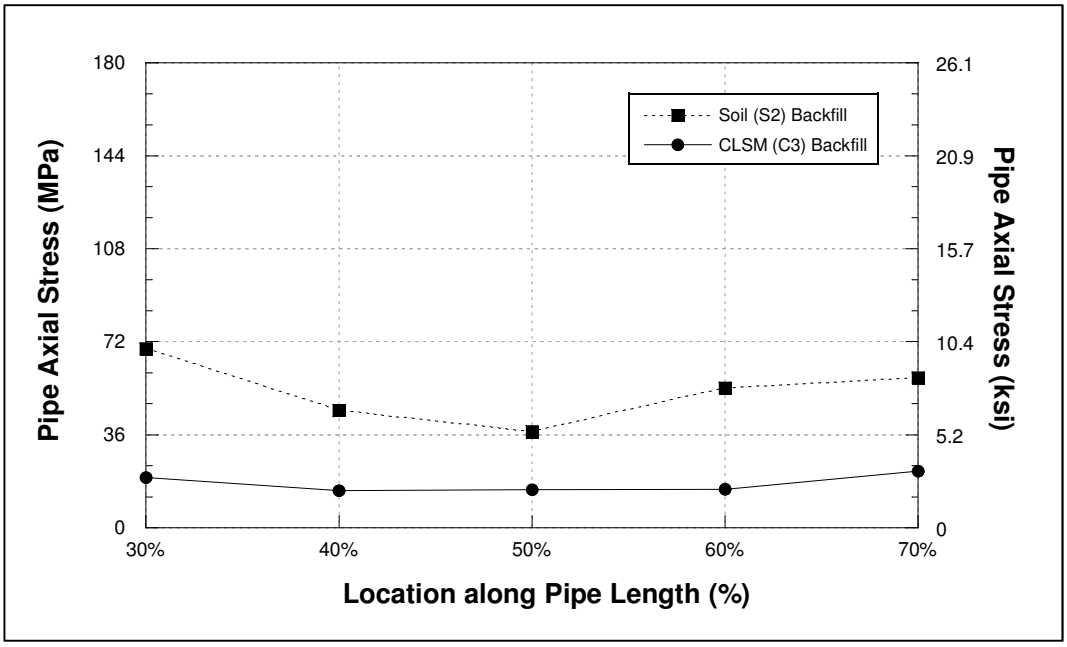

Figure 46: Pipe axial stress along the pipe for various backfill materials considering non-linear material behavior

Table 27: Summary of average pipe axial stress for various backfills considering non-linear material behavior

Description	Elastic Materials		Inelastic Materials
	Subject to 1-Dir. Seismic Wave	Subject to 3-Dir. Seismic Wave	Subject to 3-Dir. Seismic Wave
FE model with Soil (S2) backfill	49.69 [7.206]	60.94 [8.838]	52.83 [7.663]
FE model with CLSM (C1) backfill	31.26 [4.533]	---	32.41 [4.70]
FE model with CLSM (C2) backfill	26.79 [3.886]	---	23.74 [3.443]
FE model with CLSM (C3) backfill	19.85 [2.879]	15.12 [2.198]	17.13 [2.484]

For CLSM backfills, results when accounting for non-linear material behavior were not inclusive. This may be due to the fact that CLSM backfills evaluated in this study are much stiffer compared to soil backfill and may have not undergone plastic deformations. It was also observed that for all backfill material, soil and CLSM, steel pipe remained in elastic range as determined by the pipe axial stress that was well below material yield strength. As shown in Table 27, the changes in pipe axial stress for pipes embedded in CLSM backfills from elastic to inelastic materials were minimal. It was concluded that the pipe axial stress would be affected from non-linear material behavior if the material would extend into inelastic range and would result in lower pipe axial stress. Therefore, the analysis considering only elastic materials would still be conservative.

CHAPTER 4

BURIED PIPELINES SUBJECT TO REVERSE-SLIP FAULT RUPTURE

4.1 Introduction

This chapter focuses on seismic performance of pipelines embedded in CLSM when subjected to permanent ground deformations caused by a reverse-slip fault rupture. This study utilized a 3D finite element model to compare the seismic performance of pipelines embedded in CLSM to the performance of pipelines embedded in compacted soils.

4.2 Research Methodology

As stated earlier, pipelines are more vulnerable to reverse fault due to local buckling based on a study by [18]. Under reverse-slip fault rupture, buried pipelines are subjected to shear and bending, primarily in compression, and can significantly deform causing high stresses and strains beyond the elastic range of pipe material. This study evaluates the seismic performance of pipes embedded in CLSM backfill using a 3D finite element approach considering soil-pipe interactions, material nonlinearity, large deformations, and local failures. In 2016, Jalali *et al.* [23] carried out a full-scale laboratory testing of steel pipes buried in a sand split-box subjected to a reverse faulting and also used these experimental results to compare with 3D FE model analyzes.

This study first developed a 3D FE model with model parameters matching [23], including model dimensions, steel pipe diameter and thickness, pipe and soil backfill properties, boundary conditions, and total applied fault movement. The maximum pipe longitudinal strain, the maximum pipe deformation, and the pipe deformation shape

obtained from the FE model were compared to the experimental results reported by [23]. After validating the developed FE model, it was further used to assess the seismic performance of steel pipes backfilled with CLSM.

Model results, including pipe longitudinal strain, the amount of fault movement causing pipe failure, and the pipe failure location were used to evaluate and compare the seismic performance of pipes. Effects of different model parameters on the pipe seismic performance are evaluated. These parameters include; 1) various soil and CLSM backfill material properties, 2) pipe diameter-to-thickness ratios, and 3) backfill-pipe friction coefficients. Another model parameter evaluated in this study was the CLSM trench continuity through the fault plane. Depending on the strength of the CLSM mixture used to backfill a pipe, the CLSM backfill can be modeled as one continuous component through the fault plane or as two components separated by the fault plane. The effect of this model parameter on the pipe seismic performance was discussed.

4.2.1 3D Finite Element Model

Similar to the previous study outlined in Chapter 3, ABAQUS software was used to develop a 3D FE model that mainly consists of three components; 1) a steel pipeline, 2) a backfill trench, and 3) surrounding in-situ soil. All components were modeled using eight-node reduced-integration brick elements (C3D8R). For backfill trench and in-situ soil, a larger mesh sizes, with the maximum size of $2D$ (where D is the pipe outside diameter), were defined to minimize computational run-time. A smaller mesh size was defined in some areas to improve model mesh quality. For steel pipe, a smaller mesh size, equal to approximately $0.5D$, was specified along the entire pipe length for

improved accuracy of results. Friction contact with various friction coefficients was utilized on all interfaces including soil-pipe, CLSM-pipe, soil-CLSM, and soil-soil at the fault plane. Figure 47 shows an example of the developed FE model consisting of all model components.

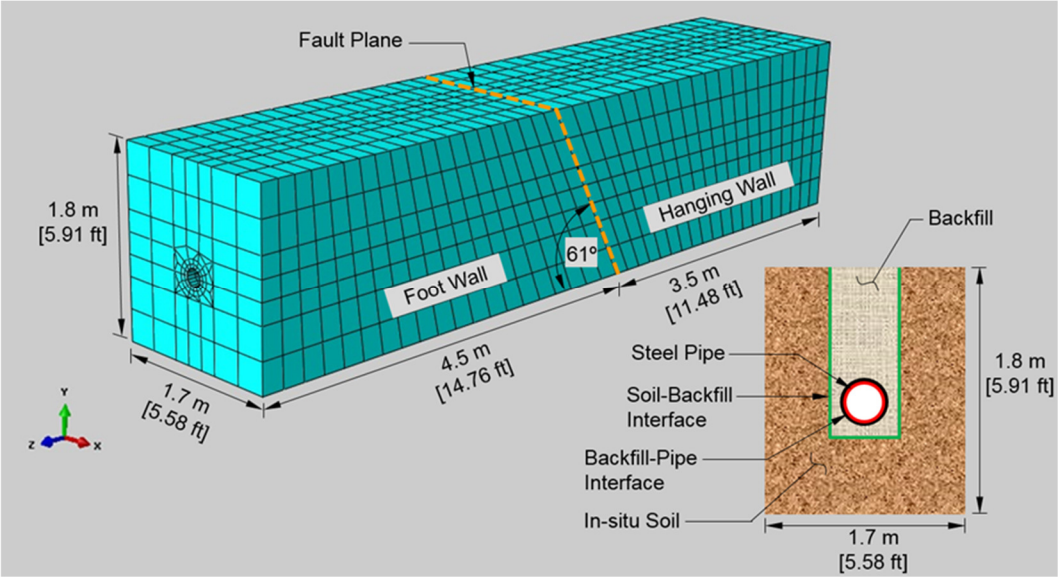

Figure 47: Developed 3D FE model for pipe subject to seismic fault rupture

FE model parameters that were used in this study are listed below:

- Total soil mass dimensions: 1700 mm [66.93 in.] x 1800 mm [70.87 in.] x 8000 mm [314.96 in.], (width x height x length), with a fault angle of 61° in relation to the horizontal plane as shown in Figure 47.

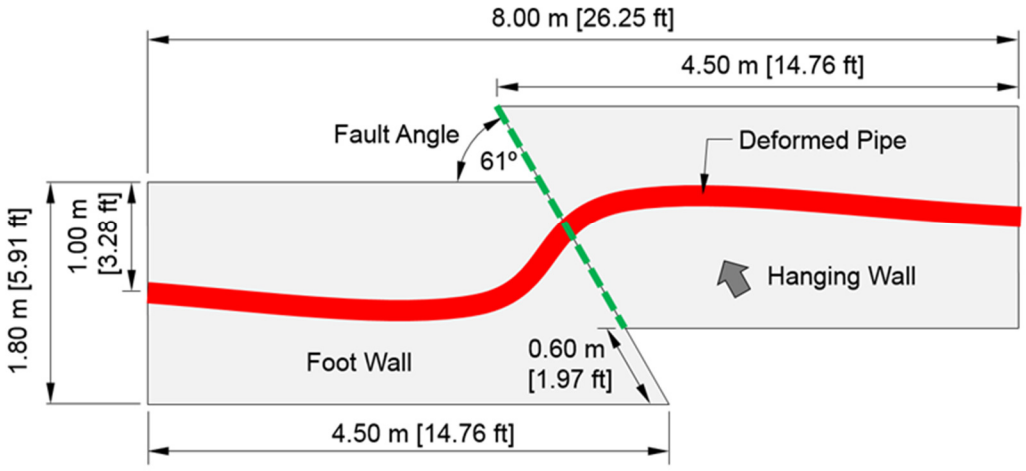

Figure 48: 3D FE model dimensions for pipe subject to seismic fault rupture

- Steel pipeline: API-5L Grade B with a 168.3 mm [6.625 in.] pipe outside diameter, 4.4 mm [0.173 in.] pipe thickness, 8000 mm [314.96 in.] length, and a pipe embedment depth of 1000 mm [39.37 in.] to the centerline of the pipe from the top of the backfill surface. Steel pipeline was modeled in ABAQUS with an elastic-plastic material behavior.
- Backfill trench dimensions: trench width of 500 mm [19.69 in.] and trench depth of 1200 mm [47.24 in.].
- Boundary conditions: pinned boundary condition restraining displacement in all directions was used at the bottom plane to simulate bedrock condition. Roller boundary condition restraining displacement only in the direction normal to the plane was used at all other planes (front, side, and back).

- Load applications: after application of gravitational forces, reverse fault simulation in the FE model was performed by moving the hanging wall block in the total amount of 600 mm [23.62 in.] along the fault plane, as shown in Figure 48.

All the FE model parameters matched the experimental work by [23] except the backfill trench dimensions since there was not a backfill trench in that study. The experimental work used pipe end-clamps at both ends of a sand split-box. Tie constraints were used in our FE model at both pipe ends between the steel pipe and the surrounding soil elements to match the end conditions of the experimental work.

Table 28 shows the material properties of the soil and different CLSM mixtures used in this study. The properties of the soil (S1) matched the soil used in the experimental work by [23]. Material properties of three CLSM mixtures, C1 thru C3, were based on air-entrained CLSM mixtures reported in the Technical Bulletin 1104 document by GCP Applied Technologies for CLSM mixtures containing DaraFill [46]. Material properties of C4 are based on a mixture reported by Shah in the literature [4]. CLSM mixtures, C5 thru C8, were generated by modifying certain properties of mixtures C2 thru C5.

Table 28: Material properties of soil and CLSM used in the FE model for pipe subject to seismic fault rupture [4, 23, 46]

ID	Material Description	Unit Weight (γ) kg/m^3 [lbf/ft^3]	Young's Modulus (E) MPa [kip/in^2]	Poisson Ratio (υ)	Friction Angle (ϕ)	Cohesion (c) MPa [lbf/in^2]	Shear Strength (τ) MPa [lbf/in^2]
Soil (S1)	Well graded sand (SW)	1907 [120.1]	8.4 [1.22]	0.30	33.5	0.005 [0.73]	0.016 [2.32]
CLSM (C1)	DaraFill CLSM Mix 1	1636 [102.1]	21 [3.05]	0.30*	39.3	0.043 [6.24]	0.055 [7.98]
CLSM (C2)	DaraFill CLSM Mix 2	1586 [99.0]	21 [3.05]	0.30*	36.4	0.047 [6.82]	0.058 [8.41]
CLSM (C3)	DaraFill CLSM Mix 3	2083 [130.0]	25* [3.63]*	0.30*	39.4	0.058 [8.41]	0.073 [10.59]
CLSM (C4)	CLSM Mix ID – S3	1776 [110.9]	689.5 [100]	0.13	47.4	0.098 [14.21]	0.115 [16.68]
CLSM (C5)	DaraFill CLSM Mix 1	1636 [102.1]	21 [3.05]	0.30*	39.3	0.030* [4.35]*	0.042* [6.09]*
CLSM (C6)	DaraFill CLSM Mix 1	1636 [102.1]	50* [7.25]*	0.30*	39.3	0.043 [6.24]	0.055 [7.98]
CLSM (C7)	DaraFill CLSM Mix 1	1636 [102.1]	75* [10.88]*	0.30*	39.3	0.043 [6.24]	0.055 [7.98]
CLSM (C8)	CLSM Mix ID – S3	1776 [110.9]	100* [14.5]*	0.13	47.4	0.098 [14.21]	0.115 [16.68]

* denoted modified material properties

4.2.2 Effect of CLSM Trench Continuity through the Fault Plane

Based on several 3D FEA of buried pipelines under seismic fault rupture, soil is typically modeled as two components separated by a fault plane simulating permanent ground deformation [21, 23, 47, 48]. Based on the mixture designs, CLSM mechanical

properties could be somewhere between loosely compacted soils and concrete. High strength CLSM mixtures may behave similar to concrete, which may crack but may not separate under loads, especially under small fault rupture events. With no separation at fault plane, CLSM trench could potentially protect pipelines from fault loads better than conventional soil backfill since CLSM trench and pipe would behave as a combined section.

The effect of CLSM trench continuity through fault plane on the pipe seismic performance was evaluated using two FE models. The two models are identical in terms of model dimensions, CLSM backfill material properties, and friction coefficient values at all interfaces. The only difference between the two models is how the CLSM trench was modeled at the fault plane. In the first model, the CLSM trench was modeled as one continuous component through the fault plane. In the second model, two CLSM trench components were modeled that are separated by a fault plane. Figure 49 shows the two configurations of the developed FE models for this investigation. Friction contact was utilized at the fault plane interface for soil-soil or CLSM-CLSM, providing some shear resistance to fault loads but still allowing ground (or CLSM trench) separation under fault rupture. For each developed FE model, three CLSM mixtures (C1 thru C3) were evaluated on the seismic performance affected by this model parameter.

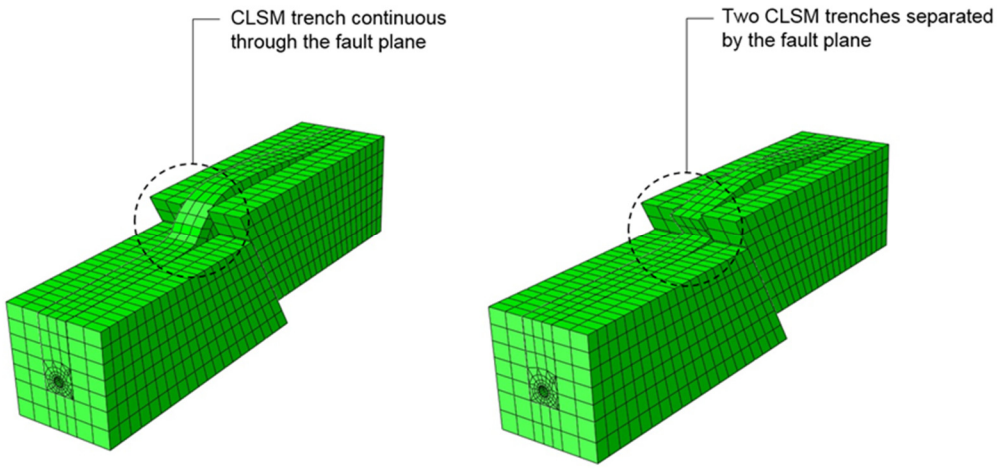

Figure 49: Effect of CLSM trench continuity through the fault plane

4.2.3 Effect of CLSM-Pipe Friction Coefficient

All interfaces were modeled with friction contact coupling with a hard contact feature that allows for a separation after the two surfaces have come into contact but prevents one component from penetrating into the other component. There are four friction interfaces in all developed FE models; 1) CLSM-pipe, 2) soil-CLSM, 3) soil-soil at the fault plane, and 4) CLSM-CLSM at the fault plane, as shown in Figure 50. The experimental work that evaluated a steel pipe under reverse slip fault reported the friction coefficient at the soil-pipe interface to be 0.41.[23] Due to the cementitious content of CLSM, the friction coefficient, *f*, at the CLSM-pipe interface was modeled to be higher than 0.41. Three friction coefficient values, including 0.55, 0.65, and 0.75, were used at the CLSM-soil interface. The friction coefficient for CLSM-CLSM interface at the fault plane was set to be the same as the CLSM-pipe interface. The friction coefficient at soil-CLSM and soil-soil interface at the fault plane were set to be 0.53 and 0.30, respectively.

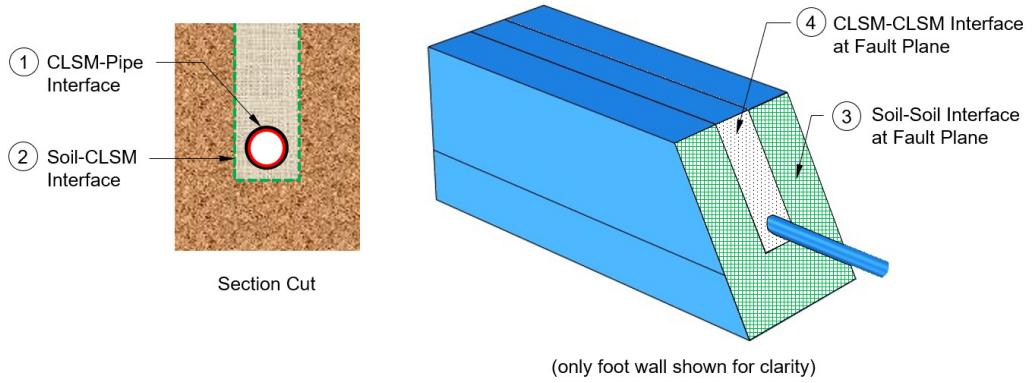

Figure 50: Friction interfaces at various locations

4.2.4 Effect of Backfill Material Shear Strength

A seismic fault rupture often results in large ground deformations and is expected to cause deformations beyond the elastic range of backfill materials. An elastic-perfectly plastic Mohr-Coulomb behavior was used to account for material nonlinearity, as expressed by Eq. (1). The developed FE model was used to evaluate the effect of backfill material shear strength, τ, on the seismic performance of embedded steel pipe, including soil (S1) and five CLSM mixtures (C1 thru C5). The normal stress (σ) at the pipe crown was computed based on the backfill material unit weight (γ) and the pipe embedment depth. The backfill material shear strength values were computed using Eq. (1) and the material properties listed in Table 28.

4.2.5 Effect of Backfill Material Young's Modulus

The Young's modulus of the backfill is another parameter required for the Mohr-Coulomb constitutive material model. The Young's modulus value is independent from the material shear strength. The soil (S1) and the four CLSM mixtures (C1, C6 thru C8)

were used to evaluate the effect of Young's Modulus on the seismic performance of pipes.

4.2.6 Effect of Pipe *D/t* Ratio

The outside diameter to thickness ratio, *D/t,* of the pipe was 38.3. The effect of changing the *D/t* ratio was also evaluated using the FE model. The pipe outside diameter was kept constant and the pipe thickness was changed to 3 mm [0.118 in.], 6.5 mm [0.256 in.], and 8 mm [0.315 in.] resulting in three different pipe *D/t* ratios of 56.1, 25.9, and 21.0, respectively. The pipe seismic performance was evaluated for soil (S1) compared to CLSM mixtures (C1).

4.3 Results and Discussion

4.3.1 FE Model Validation using Experimental Results

Figure 51 shows soil and pipe deformations obtained using the developed FE model for a pipe embedded in soil (S1) after 0.6 m [23.62 in.] applied fault movement. All model parameters including the soil material properties were matched to the experimental work reported by [23].

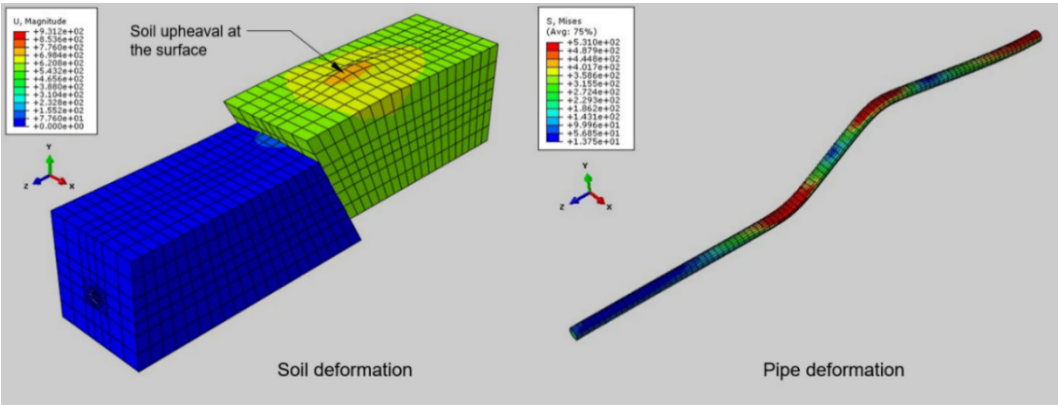

Figure 51: Soil and pipe deformation for pipe embedded in soil backfill after fault movement

The observed soil upheaval at the surface of the hanging wall is consistent with the results of the experimental work. The pipe exhibited an S-shape deformation with unsymmetrical pipe buckling locations with respect to the fault plane, again consistent with the reported experimental results. Although the experimental work did not measure the maximum pipe deformation, the authors used an FE model to report the maximum pipe deformation to be 0.74 m [29.13 in.]. The FE model created by the authors of the experimental work used a shear band preventing model discontinuity at the fault plane. On the contrary, our FE model uses friction interfaces at the fault plane providing resistance but allowing a true separation between the two soil components. The maximum pipe deformation obtained from our FE model was 0.93 m [36.61 in.], which is still comparable to the FE model results of the authors of the experimental work.

Figure 52 shows pipe longitudinal strains measured at the pipe crown along the pipe length in the experimental work and strain values obtained using our FE model.

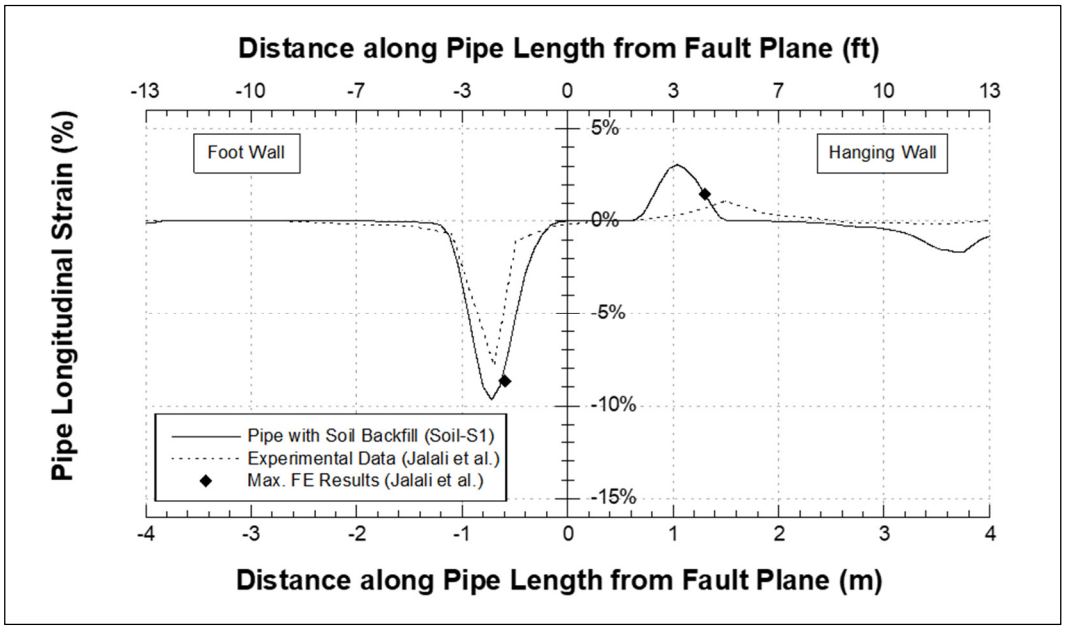

Figure 52: FE model validation with experimental work [23]

The maximum pipe longitudinal strain reported from Jalali et al.'s FE model is also shown in Figure 52. In the foot wall (left quadrant), the maximum pipe longitudinal strain from the experiment, experimental work's FE model, and our FE model are -7.8%, -8.7%, and -9.7%, respectively. Negative values indicate compressive strain and positive values indicate tensile strain. The location of the maximum pipe longitudinal strain is also the location of pipe buckling away from the fault plane. The pipe buckling locations in the foot wall from the experiment, experimental work's FE model, and our FE model are 0.70 m [27.56 in.], 0.60 m [23.62 in.], and 0.72 m [28.35 in.], respectively. In the hanging wall (right quadrant), strains at the pipe crown obtained from our FE model did not match with the reported experimental results as well as they did in the foot wall. However, it should be noted that the pipe longitudinal strain was much lower in the

hanging wall compared to the foot wall and strains did not reach the ultimate pipe strain and therefore would not govern the pipe design. In addition, the maximum pipe longitudinal strain may be beyond the pipe failure point that is normally used for a pipe design, but it is still comparable to the experimental data. More importantly, the results were utilized to evaluate the pipe seismic performance from different backfills rather than to provide a design guideline of the buried pipe.

Overall, the soil upheaval at the surface, the maximum pipe deformation and deformation shape, pipe longitudinal strain, and pipe buckling locations predicted by our FE model were similar to the experimental results reported in Jalali et al.'s study. Therefore, the developed model was further used to compare the seismic performance of pipes backfilled with soils and performance of pipes backfilled with different CLSM mixtures.

4.3.2 Effect of CLSM Trench Continuity through the Fault Plane

The effect of CLSM trench continuity through the fault plane was evaluated using CLSM mixtures C1, C2, and C3. Figure 53 shows the pipe longitudinal strain obtained at the crown along the pipe length after 0.6 m [23.62 in.] applied fault movement for mixtures C1 and C3. Results indicated that modelling the CLSM trench as one continuous trench or as two trench components separated by the fault plane did not have a significant effect on the obtained maximum strain values neither in the foot wall nor in the hanging wall. Modeling the CLSM trench as one continuous trench caused a shift of the pipe buckling locations in the same direction of the fault movement but the distance between the two buckling locations remained constant for the same CLSM mixture.

Results obtained from CLSM mixture C2 were the same as C1 and C3. The horizontal shift of buckling locations was the same for all three CLSM mixtures, approximately 0.48 m [18.90 in.] in the foot wall and 0.4 m [15.75 in.] in the hanging wall. Because the CLSM trench continuity in the model did not affect the maximum strain value but only shifted the location by a constant amount, it was decided to model the trench as two separate components similar to the model used for soil backfill material.

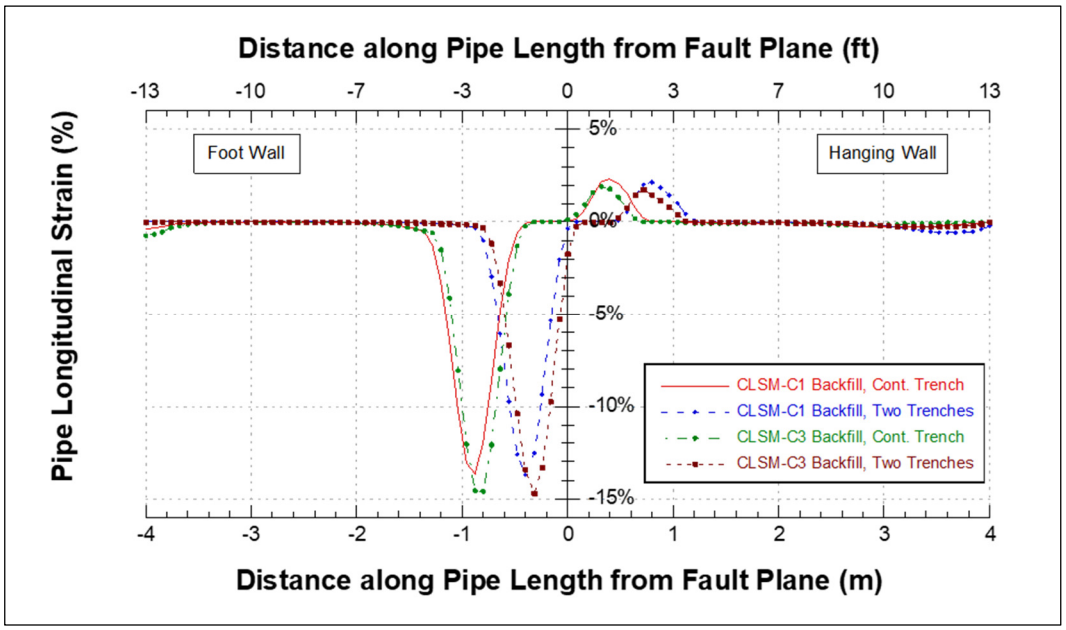

Figure 53: Effect of CLSM trench continuity on pipe longitudinal strain

4.3.3 Effect of CLSM-Pipe Friction Coefficient

Results in Chapter 3 evaluating seismic performance of pipes embedded in CLSM and subjected to seismic wave propagation reported that the pipe axial stresses increased with increasing friction coefficient at CLSM-pipe interface. Therefore, the effect of friction coefficient at the CLSM-pipe interface was also evaluated in this study

when pipes are subjected to reverse slip fault movements. Figure 54 shows the pipe longitudinal strain obtained at the crown along the pipe length for a pipe embedded in CLSM mixture C1 after 0.6 m [23.62 in.] applied fault movement using three different friction coefficient values (f = 0.55, 0.65, and 0.75).

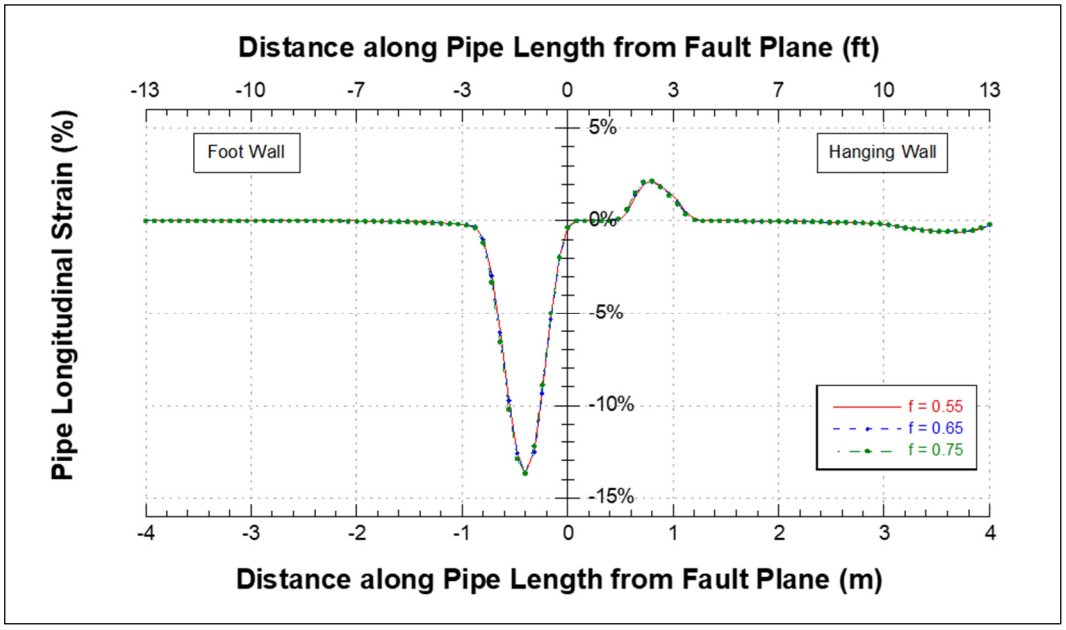

Figure 54: Pipe longitudinal strain for a study on CLSM-pipe friction coefficient

Results showed that for all friction coefficients, the longitudinal strain, buckling locations in the foot wall and the hanging wall, and the distance between the two buckling locations were nearly identical. The same friction coefficients were also evaluated in CLSM mixtures C2 and C3 and results exhibited the same trend. Therefore, it was concluded that CLSM-pipe friction coefficient had a negligible effect on the pipe seismic performance when subjected to seismic fault rupture.

4.3.4 Effect of Backfill Material Shear Strength

After validation of the developed FE model with experimental work, it was used to compare seismic performance of pipes backfilled with soils and CLSM mixtures. Soil and CLSM elements were modeled using elastic-perfectly plastic Mohr-Coulomb material model with different shear strength values. The amount of fault movement to cause the initial pipe failure was determined for soil and CLSM mixtures. The pipe is considered to have a better seismic performance when a larger fault movement is required to fail the pipe. The pipe failure was defined when any segment of the pipe reaches the ultimate pipe strain of 4% as specified in the stress-strain curve of the steel pipe. The ultimate pipe strain of 4% is consistent with the ASCE recommendation in Engineering Practice No. 119 [49], which recommends less than 5% for seismic pipeline design. Table 28 shows the calculated shear strength, τ, values for soil (S1) and CLSM mixtures (C1 to C5) using Eq. (1). Figure 55 shows the relation between the backfill material shear strength on a logarithmic scale and the amount of fault movement causing the pipe failure. Results clearly showed that as the backfill material shear strength increased, the pipe could tolerate a smaller fault movement before reaching the pipe failure. This is due to the increase of system stiffness provided by a CLSM trench surrounding the pipe. This behavior is similar to a building system under seismic loads where a stiffer system would draw higher loads compared to a more flexible system.

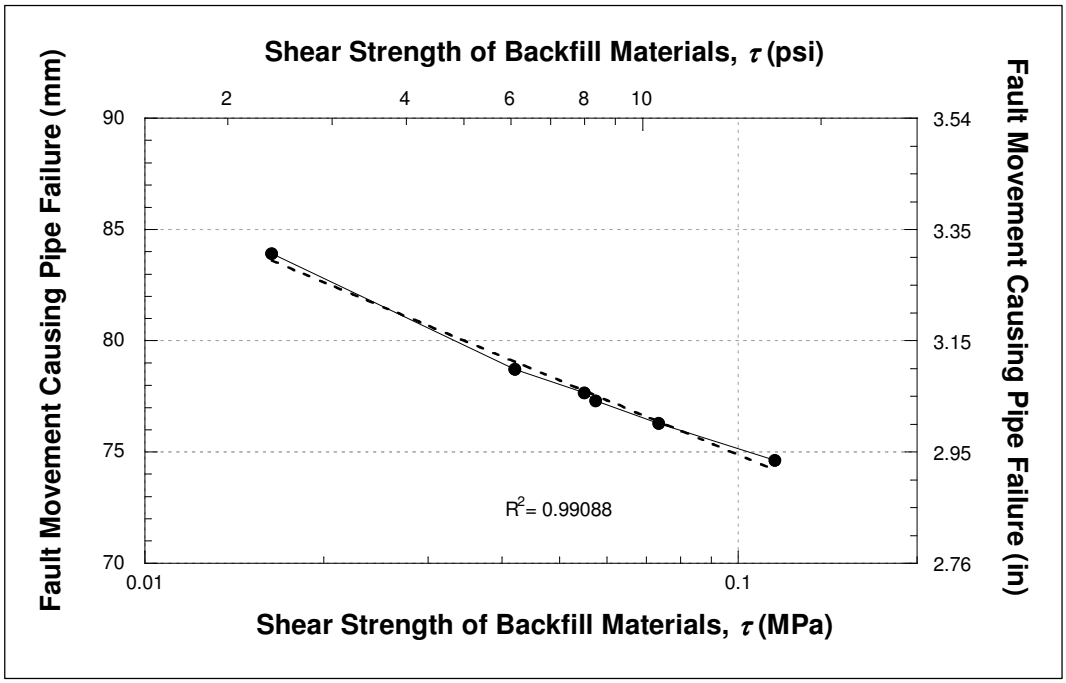

Figure 55: Relation between backfill material shear strength and fault movement at pipe failure

Figure 56 shows the longitudinal strain measured at pipe crown along the pipe length for pipes backfilled with soil (S1) and three CLSM mixtures (C1, C2, and C3). Similar to results shown in Figure 55, the maximum pipe longitudinal strain increased with increasing backfill shear strength. The locations of the maximum longitudinal strain moved closer to the fault plane both in the foot wall and hanging wall as the backfill material shear strength increased. Both figures show that the performance of pipes backfilled with CLSM mixtures was worse in terms of observed maximum longitudinal strain and the pipe strain values increased with increasing shear strength of the CLSM mixture.

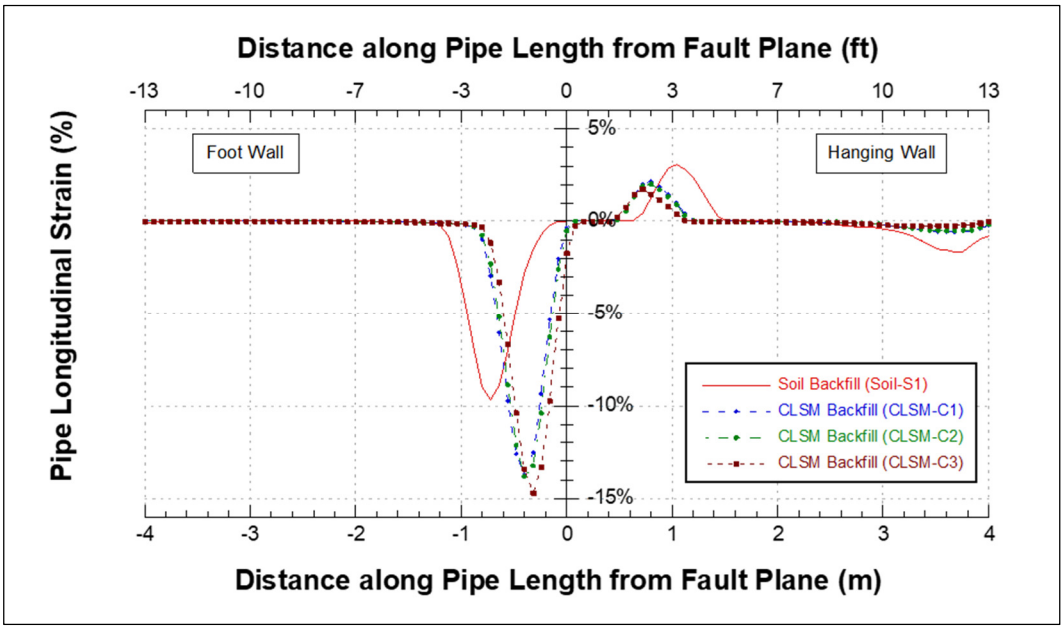

Figure 56: Pipe longitudinal strain for pipe with soil and CLSM backfills

4.3.5 Effect of Backfill Material Young's Modulus

The effect of the backfill material Young's modulus, *E*, on the seismic performance of the pipe was also evaluated based on the amount of fault movements required to cause pipe failure. Figure 57 shows the relation between the backfill material's *E* and the amount of fault movement causing the pipe failure for a pipe embedded in soil (S1) and the CLSM mixtures (C1, C6, C7, and C8). Soil (S1) has a lower *E* value compared to all the evaluated CLSM mixtures. Similar to shear strength values, the amount of fault movement to cause pipe failure decreased with increasing *E* values. It should be noted that the *E* value of the backfill material is independent of its shear strength and therefore both of these variables were evaluated. Evaluation of *E* values also indicated that the seismic performance of the steel pipe backfilled with soil

and exposed to the reverse slip fault was better compared to the pipes backfilled with CLSM mixtures evaluated in this study.

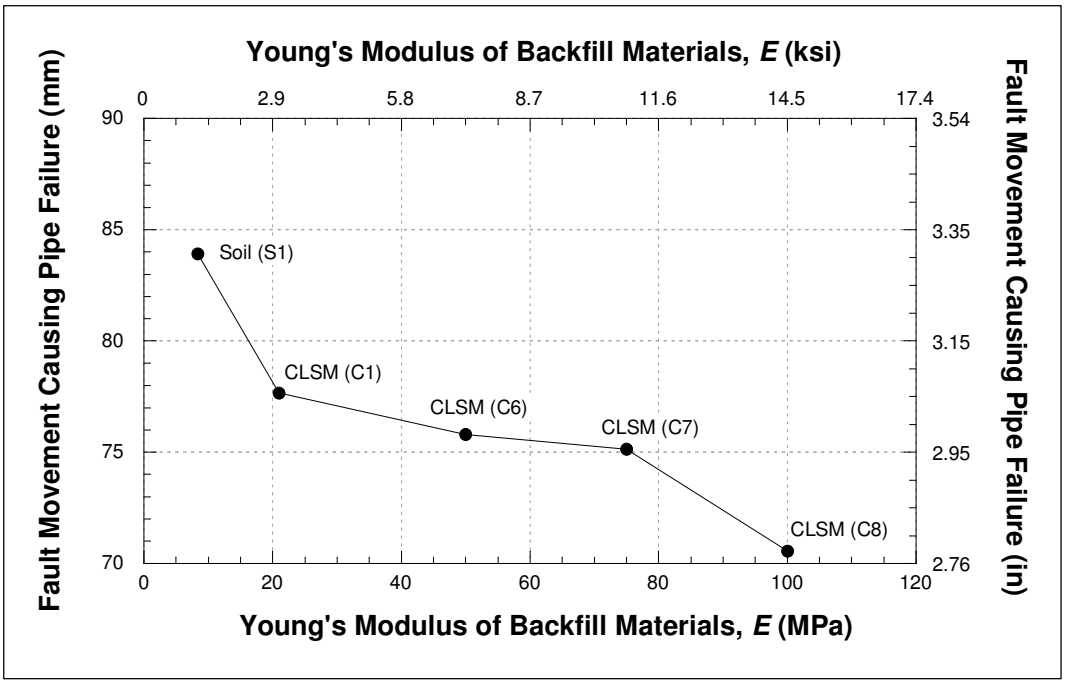

Figure 57: Relation between backfill material *E* and fault movement at pipe failure

4.3.6 Effect of Pipe D/t Ratio

Figure 58 shows the relation between the pipe outside diameter to thickness ratio, *D*/*t,* and the amount of fault movement to cause pipe failure for soil (S1) and CLSM mixture (C1). The steel pipe used in the FE model had a pipe *D*/*t* ratio of 38.3, and at this *D*/*t* value the fault movement to cause pipe failure in CLSM (C1) was smaller compared to the fault movement in soil (S1). Similar to earlier results, this indicated a better pipe seismic performance of pipes backfilled with soils due to higher stiffness of the CLSM backfill.

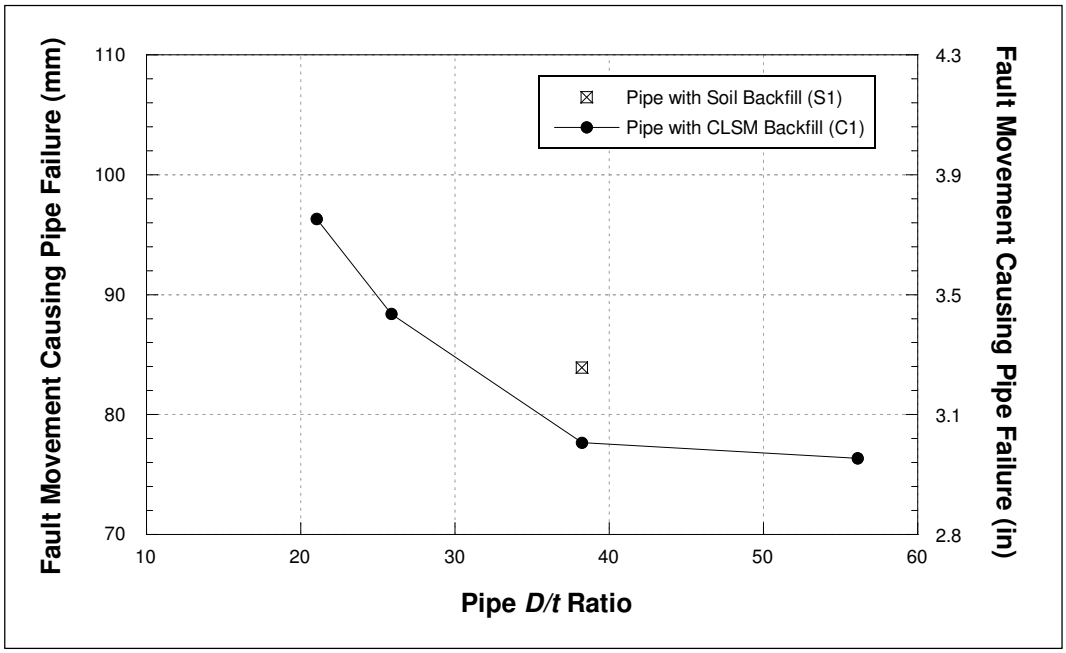

Figure 58: Relation between pipe *D/t* ratio and fault movement at pipe failure

One measure a designer can use to improve the seismic performance of the pipe is to increase the pipe wall thickness. Three different *D*/*t* ratios were evaluated for CLSM backfills by changing the wall thickness of the pipe while keeping the outside diameter constant. As shown in Figure 58, decreasing the *D*/*t* ratio improved the seismic performance of the steel pipe backfilled with CLSM by increasing the necessary fault movement to cause a pipe failure. Increasing the pipe thickness from 4.4 mm [0.173 in.] to 6.5 mm [0.256 in.] changed the *D/t* ratio from 38.3 to 25.9 and changed the fault movement to cause failure from 77.7 mm [3.06 in.] to 88.4 mm [3.48 in.]. The fault movement required to cause a pipe failure in soil (S1) was 84.1 mm [3.31 in.]. These results indicate that pipes embedded in CLSM mixtures can have a seismic performance as well as or better than pipes backfilled with soils with simple changes in the design.

Increasing the pipe wall thickness would increase the material cost but would make the advantages of using CLSM available to contractors and owners. These advantages include better safety during construction, lower cost of construction, and improved construction speed.[6]

CHAPTER 5

SUMMARY

5.1 Research Summary

One of the two main objectives of this research was to provide recommendations on 3D FE modeling parameters and their effects on model results for buried pipelined embedded in soil and CLSM backfills subject to seismic loads. Several FE model parameters were evaluated including soil-pipe interaction, boundary condition, FE model dimensions and scale factors, various friction coefficients at interfaces, relationship between soil spring and material Young's modulus, the effect of three-directional seismic wave, pipe end condition, and the effect of material nonlinearity. The other research objective was to evaluate the use of CLSM mixtures to backfill steel pipelines for earthquake resistance compared to conventional compacted soils. The performance of buried pipes embedded in various soil and CLSM backfills were analyzed under seismic wave propagation as well as seismic reverse fault rupture.

5.2 Summary of Research Findings

5.2.1 Buried Pipelined Subject to Seismic Wave Propagation

The study in Chapter 3 evaluated the seismic performance of steel pipe embedded in CLSM backfill subject to seismic wave propagation compared to compacted soil backfill. The study was performed in two phases, 1) with all materials considered in elastic range and 2) with all materials considered in inelastic range.

5.2.1.1 Research Findings with Elastic Materials

The study started with the evaluation of the existing ASCE guidelines for designing pipelines when subjected to seismic wave propagation. Then, a parametric study on various FE model parameters was conducted to evaluate their effects on FE model results. After evaluating the effects of different FE model parameters, the FE model parameters were set to obtain a similar pipe axial stress as predicted by the ASCE guidelines for pipes buried in soils. Next, the developed FE model was utilized to evaluate various FE model parameters as well as the pipe seismic performance of pipes embedded in CLSM backfills compared to soil backfills. Analysis of results indicated:

- Pipe axial stress prediction from the developed FE model matched well with results computed from the ASCE guidelines.
- FE models using tie constraint for soil-pipe interaction resulted in much higher pipe axial stress along the pipe, approximately 10-15 times, than FE models using friction interface. Friction interface should be used for more realistic results.
- To achieve a uniform pipe axial stress distribution along the pipe, soil spring support should be used at FE model boundaries rather than roller support.
- FE model width does not have a significant impact to FE model results. A minimum FE model width of 20*D* was recommended to minimize computational run-time.
- The peak axial stress at mid-pipe location increased as the FE model depth increased and started to be constant after a certain model depth. Modeling with too

shallow of FE model depth could under estimate the peak axial stress. A minimum FE model depth of 35*D* was suggested.

- For soil backfills, the peak axial stress at mid-pipe location first increased with increasing FE model length and decreased after it reached the critical FE model length. The critical FE model length decreased as the soil-pipe friction coefficient increased. In addition, the maximum pipe axial stress at the critical length increased as the friction coefficient increased. Therefore, a model should be created with a sufficient FE model length based on soil-pipe friction coefficient to capture the peak axial stress that a pipeline could experience under seismic loads.
- Similar to soil backfills, for CLSM backfills, the pipe axial stress initially increased as the FE model length increased and it remained constant after reaching the critical model length. The maximum pipe axial stress increased with increasing CLSM-pipe friction coefficient. However, the critical FE model length did not vary with the CLSM-pipe friction coefficient. For the evaluated CLSM backfills a minimum model length of 200*D* is recommended to have a complete transfer of loads resulting in a uniform axial stress along the pipe.
- Friction coefficients of both interfaces, CLSM-pipe (f_1) and CLSM-soil (f_2), affected the pipe axial stress. The pipe axial stress increases as CLSM-soil friction coefficient (f_2) increases for the same CLSM-pipe friction coefficient (f_1). Similarly, the pipe axial stress increases as CLSM-pipe friction coefficient (f_1) increases for the same CLSM-soil friction coefficient (f_2).

- Soil springs should be used at FE model boundary planes to obtain uniform axial stress distribution along the pipe for both soil and CLSM backfills. In case of soil backfill, there is an optimum soil spring stiffness value related to the soil Young's modulus to minimize stress variation. For the evaluated CLSM backfills in this study a soil spring stiffness of 140.2 kN/m [800 lb/in] was recommended.
- Increasing or decreasing the model dimensions by a scale factor increased or decreased the observed axial stresses by a similar factor as long as the dimension ratios were kept constant.
- Under the same seismic wave propagation, pipes embedded in the evaluated CLSM backfills exhibited as much as 2.5 times lower in pipe axial stresses compared to pipes embedded in soils. The pipe axial stress decreased as the strength of backfill materials increased.
- Embedded pipes subject to seismic wave propagation are more likely to fail in pipe crushing rather than bending failure due to much higher axial stresses compared to bending stresses.
- Under the same seismic load conditions, lower pipe axial stresses in CLSM backfill would allow engineers to use a smaller pipe diameter or a thinner pipe wall thickness providing a cost saving to a project. However, it should be noted that pipe crushing under seismic wave propagation is not the only failure mode typically considered for seismic design of buried pipelines. It should also be noted that the results are valid for the CLSM mixtures similar to the ones evaluated in this study and could not be applied for any CLSM mixture.

- For the evaluated soil and CLSM backfill materials in this study, pipes embedded in soils or CLSM may experience 5 to 7 times higher axial stresses at a rigid connection compared to the free end of the pipe. However, the maximum axial stress at the rigid end was significantly lower for pipes embedded in a stiff CLSM mixture compared to a pipe embedded in a soil backfill.

5.2.1.2 Research Findings with Inelastic Materials

The study started the parametric study on various FE model parameters to determine their effects on a uniform pipe axial stress distribution along the pipe. Then, the developed FE model was utilized to evaluate the pipe seismic performance of pipes embedded in CLSM backfills compared to soil backfills. Analysis of results indicated:

- Unlike FE models with elastic materials, the use of soil spring stiffness, dashpot element, or dashpot element with soil spring at FE model boundaries did not provide a uniform pipe axial stress distribution along the pipe.
- Recommendations obtained from the study with elastic materials still applied that soil spring should be used at FE model boundaries with the optimal soil spring stiffness (K_{opt}) based on material Young's modulus.
- For a better uniform pipe axial stress distribution, results near boundaries should be excluded due to material plastic deformation. In this study, results from 30% to 70% of the pipe length were utilized.
- Similar to results from the study of elastic materials, pipes embedded in CLSM backfills experienced as much as 3 times lower in pipe axial stress compared to pipes embedded in soil.

- For soil backfill, non-linear material behavior resulted in the lower pipe axial stress. For CLSM backfill, results were not inclusive, which could have been because CLSM materials did not extend into plastic range under seismic loads in this study. Therefore, an elastic analysis would still be conservative for a pipe design.

5.2.2 Buried Pipelined Subject to Reverse-Slip Fault Rupture

This study in Chapter 4 evaluated the seismic performance of steel pipes embedded in CLSM backfill and subjected to a reverse-slip fault and compared their performance to pipes embedded in compacted soil backfill. A 3D FE model was used to perform the evaluations and comparisons. The developed FE model was first validated by modeling an experimental work reported in the literature and comparing the predicted results with the results of the experimental work.[23] It should be noted that although the evaluated materials represent a wide range of commonly used CLSM mixtures and allow to make general conclusions based on material properties, specific results are only valid for the specific soil and CLSM mixtures evaluated in this study and may be different for different soils and differently designed CLSM mixtures. Evaluation of certain model parameters and the comparison of seismic performance of pipes resulted in the following conclusions:

- Under reverse-slip fault rupture in soil backfill, the steel pipe exhibited an S-shape deformation with unsymmetrical pipe buckling locations with respect to the fault plane similar to the observations in the experimental work. The soil upheaval at the surface, maximum pipe deformation, pipe longitudinal strain, and buckling

location matched the experimental observations in the foot wall where the pipe failure occurred.

- Modelling the CLSM trench continuously through the fault plane did not change the maximum pipe longitudinal strain neither in the foot wall nor in the hanging wall. It only caused a shift in the location of the maximum pipe longitudinal strain in the direction of the fault movement. A seismic fault rupture often causes a true ground separation; therefore, it is more realistic to model the CLSM trench as two FE model components separated by the fault plane.
- CLSM-pipe interface friction coefficient had no impact on the seismic performance of the pipe embedded in CLSM backfill regardless of CLSM backfill material strength.
- As the backfill material shear strength and Young's modulus increased, the maximum pipe longitudinal strain increased and the fault movement to cause initial pipe failure decreased. This indicated that a steel pipe embedded in a soil backfill which will typically have a lower shear strength and lower Young's modulus may have a better seismic performance compared to steel pipes backfilled with CLSM. This assumes that the soil is properly compacted all around the steel pipe similar to the case of CLSM backfill.
- By increasing the pipe thickness (or decreasing the pipe *D/t* ratio), the seismic performance of the pipe embedded in CLSM backfill can be improved to allow the use of CLSM backfill with all its inherent advantages in zones prone to reverse-slip faults.

5.3 Conclusions

Seismic resistance of pipelines is a very important topic in terms of public safety and economic impact. This study analyzed steel buried pipelines embedded in CLSM backfills compared to compacted soil backfill when subjected to seismic wave propagation and reverse-slip fault rupture. Several FE model parameters, such as soil-pipe interaction, boundary condition, FE model dimensions, friction coefficients at interfaces, material nonlinearity, etc., and their effects on the results were discussed in great details.

Under seismic wave propagation, results clearly indicated that steel pipes embedded in CLSM had a better seismic performance compared to soil backfills as indicated by a lower pipe axial stress. A better pipe seismic performance would allow engineers to use a smaller pipe diameter or a thinner pipe wall thickness providing a cost saving to a project. On the contrary, under reverse-slip fault rupture, results showed that steel pipes embedded in CLSM had a lower seismic performance compared to soil backfills due to the increase in system stiffness from CLSM trench surrounding the pipe. One measure that the study suggested was to increase the pipe wall thickness. Although this option would increase the material cost, it would make the advantages of using CLSM available to contractors and owners.

In conclusion, with a proper design buried steel pipe with CLSM backfill with all its inherent advantages can perform as well as or better than soils in seismic prone areas. The improvement in pipe earthquake resistant could prevent loss to human life as well as reduce economic impact.

5.4 Future Research

Although CLSM has been increasingly utilized as a pipe backfill material due to its inherent benefits compared to conventional soil backfill, the study of its use particularly in seismic prone areas has not been done. This research provides a better understandings of the pipe seismic performance with CLSM backfill in several design aspects, but there are some additional studies that could be conducted to provide more insights of its application in seismic prone areas including:

- Under seismic wave propagation, buried pipes are more likely to fail in pipe crushing. Crushing in steel pipe may not control a design due to its ductility. Other materials, such as concrete pipe, that may be more sensitive to pipe crushing could be evaluated.
- It was assumed in this study that steel pipe is continuous with no joints. Sections of pipes embedded in CLSM considering joint details could be analyzed under seismic loads.
- The Mohr-Coulomb constitutive model was used for all CLSM mixtures evaluated in this study. For high strength CLSM mixtures, it may behave similar to concrete, and some other material constitutive models may be better represented, e.g. Concrete Damaged Plasticity (CDP).
- Under seismic fault rupture, the ultimate tensile was utilized to define pipe failure limit. Different criteria, e.g. local buckling strain, could be used to determine its effect on results.

- Full-scale laboratory testing for pipes embedded in CLSM backfills could be performed for additional result verifications.
- A more commonly used or a wider range of CLSM mixtures could be evaluated to establish a recommended guideline.
- Future research could extend to different pipe configurations, e.g. pipes with bends embedded in CLSM.

REFERENCES

[1] *Where Are Pipelines Located?*, Pipeline 101. Accessed: Jan. 27, 2018. [Online]. Avaialble: https://pipeline101.org/Where-Are-Pipelines-Located

[2] J. Boschert and A. Howard, "Importance of haunching," in *Pipelines 2014: From Underground to the Forefront of Innov. and Sustain.*, Aug. 2014, pp. 393-404, doi: 10.1061/9780784413692.036.

[3] M. Nataraja and Y. Nalanda, "Performance of industrial by-products in controlled low-strength materials (CLSM)," *Waste Manage.*, vol. 28, no. 7, pp. 1168-1181, 2008, doi: 10.1016/j.wasman.2007.03.030.

[4] H. Shah, "Controlled low strength material (CLSM) produced from limestone fines and other byproducts," M.S. Thesis, Dept. Civil Eng., Univ. of Missouri-Kansas City, Kansas City, 2012.

[5] R. Siddique, "Utilization of waste materials and by-products in producing controlled low-strength materials," *Resour., Conserv. and Recycling,* vol. 54, no. 1, pp. 1-8, Nov. 2009, doi: 10.1016/j.resconrec.2009.06.001.

[6] *Report on Controlled Low-Strength Materials*, ACI Committee 229, American Concrete Institute, Farmington Hills, MI, 2013.

[7] J. Liang and S. Sun, "Site effects on seismic behavior of pipelines: a review," *J. Pressure Vessel Technol.*, vol. 122, no. 4, pp. 469-475, Nov. 2000.

[8] T. O'Rourke and M. Palmer, "Earthquake performance of gas transmission pipelines," *Earthq. Spectra,* vol. 12, no. 3, pp. 493-527, Aug. 1996, doi: 10.1193/1.1585895.

[9] S. Toprak and F. Taskin, "Estimation of earthquake damage to buried pipelines caused by ground shaking," *Natural Hazards,* vol. 40, no. 1, pp. 1-24, Jan. 2007, doi: 10.1007/s11069-006-0002-1.

[10] R. T. Eguchi, "Earthquake performance of water supply components during the 1971 San Fernando Earthquake," in *Prepared for the Nat. Sci. Found*. Redondo Beach, CA: JH Wiggins Company, Mar. 1982.

[11] *What Are Seismic Waves?*, UPSeis – An Educational Site for Budding Seismologists. Accessed: Mar. 31, 2017. [Online]. Avaialble: http://www.geo.mtu.edu/UPSeis/waves.html

[12] *Seismic Waves*, allanawheeler. Accessed: Jun. 5, 2014. [Online]. Avaialble: https://allanawheeler.wordpress.com/2011/05/18/23/

[13] *M7.0 Loma Prieta Earthquake of 17 Oct 1989*, Center for Engineering Strong Motion Data. Accessed: Sep. 26, 2012. [Online]. Avaialble: https://strongmotioncenter.org/cgi-bin/CESMD/Multiplesearch_eq_D.pl?staID=%&statype=%&material=Any&height=%&PMix=-10000&PMax=3&DMix=0&DMax=1000&SFlag=&iqrid=LomaPrieta_17Oct1989

[14] *Earthquake Glossary*, United States Geological Survey. Accessed: May 14, 2014. [Online]. Avaialble: https://earthquake.usgs.gov/learn/glossary/?term=fault

[15] N. M. Newmark and W. J. Hall, "Pipeline design to resist large fault displacement," in *Proc. US Nat. Conf. Earthq. Eng.*, Jun. 1975, pp. 416-425.

[16] R. P. Kennedy, A. Chow, and R. A. Williamson, "Fault movement effects on buried oil pipeline," *Transp. Eng. J. ASCE,* vol. 103, no. 5, pp. 617-633, 1977.

[17] L. R. L. Wang and Y. H. Yeh, "A refined seismic analysis and design of buried pipeline for fault movement," *Earthq. Eng. & Struct. Dyn.,* vol. 13, no. 1, pp. 75-96, Jan./Feb. 1985, doi: 10.1002/eqe.4290130109.

[18] S. Takada, J.-W. Liang, and T. Li, "Shell-mode response of buried pipelines to large fault movements," *J. Struct. Eng.,* vol. 44A, pp. 1637-1646, Mar. 1998.

[19] V. Bolvardi and A. Bakhshi, "A study on seismic behavior of buried steel pipelines crossing active faults," in *Pipelines 2010: Climbing New Peaks to Infra. Rel.: Renew, Rehab, and Reinvest*, Aug. 2010, pp. 1-12, doi: 10.1061/41138(386)1.

[20] R. Paolucci, S. Griffini, and S. Mariani, "Simplified modelling of continous buried pipelines subject to earthquake fault rupture," *Earthq. and Struct.*, vol. 1, no. 3, pp. 253-267, 2010, doi: 10.12989/eas.2010.1.3.253.

[21] R. Tarinejad, A. Mahdavi, and N. Jahangir, "Buried pipeline response analysis to reverse-slip fault displacements," in *15th World Conf. Earthq. Eng., Lisbon, Portugal*, 2012.

[22] *ABAQUS.* (2014). Dassault Systèmes Simulia Corp. Accessed: Apr. 4, 2015. [Online]. Avaialble:

https://www.sharcnet.ca/Software/Abaqus/6.14.2/v6.14/books/usb/default.htm?startat=pt10eli03.html

[23] H. H. Jalali, F. R. Rofooei, N. K. A. Attari, and M. Samadian, "Experimental and finite element study of the reverse faulting effects on buried continuous steel gas pipelines," *Soil Dyn. and Earthq. Eng.,* vol. 86, pp. 1-14, Jul. 2016, doi: 10.1016/j.soildyn.2016.04.006.

[24] C. Zhan and B. Rajani, "Load transfer analyses of buried pipe in different backfills," *J. Transp. Eng.,* vol. 123, pp. 447-453, Nov. 1997, doi: 10.1061/(ASCE)0733-947X(1997)123:6(447).

[25] T. Masada and S. M. Sargand, "Measured structural performance of HDPE pipe installed in CLSM-CDF," in *Pipelines 2002: Beneath Our Feet: Challenges and Solutions*, Aug. 2002, pp. 1-12, doi: 10.1061/40641(2002)73.

[26] M. S. Dezfooli, A. Abolmaali, Y. Park, M. Razavi, and F. Bellaver, "Staged construction modeling of steel pipes buried in controlled low-strength material using 3D nonlinear finite-element analysis," *Int. J. Geomech.,* vol. 15, no. 6, pp. 1-13, Dec. 2015, doi: 10.1061/(ASCE)GM.1943-5622.0000436.

[27] V. Alizadeh, S. Helwany, A. Ghorbanpoor, M. Oliva, and R. Ghaderi, "CLSM bridge abutments - Finite element modeling and parametric study," *Comput. and Geotech.,* vol. 64, pp. 61-71, Mar. 2015, doi: 10.1016/j.compgeo.2014.10.015.

[28] K. Abdel-Rahman, T. Gerlach, and M. Achmus, "Behavior of pipelines embedded in self-compacting materials under traffic loads," in *Int. Congr. and Exhib. "Sustain. Civil Infra.: Innov. Infra. Geotech."*, May 2017, pp. 89-99, doi: 10.1007/978-3-319-63889-8_7.

[29] *Guidelines for the Seismic Design of Oil and Gas Pipeline Systems*, American Society of Civil Engineers, New York, NY, 1984.

[30] N. M. Newmark, "Problem in wave propagation in soil and rock," in *Proc. Int. Symp. Wave Propag. and Dyn. Properties of Earth Mater.*, 1968, pp. 7-26.

[31] D. H. Lee, B. H. Kim, H. Lee, and J. S. Kong, "Seismic behavior of a buried gas pipeline under earthquake excitations," *Eng. Struct.,* vol. 31, no. 5, pp. 1011-1023, May 2009, doi: 10.1016/j.engstruct.2008.12.012.

[32] H. Lee, "Finite element analysis of a buried pipeline," M.S. thesis, Dept. Mech. Aerosp. and Civil Eng., Univ. of Manchester, Manchester, UK, 2010.

[33] R. Yang and S. Zhang, "Study on mechanical behaviors of buried pipelines subjected to three-dimensional earthquake input motions," in *Int. Conf. Pipelines and Trenchless Technol. 2011*, Oct. 2011, pp. 1802-1809, doi: 10.1061/41202(423)190.

[34] S. Sahoo, B. Manna, and K. Sharma, "Seismic behaviour of buried pipelines: 3D finite element approach," *J. Earthq.,* vol. 2014, Aug. 2014, Art. no. 818923, doi: 10.1155/2014/818923.

[35] F. Zhang and Y.-Y. Wang, "Assess the seismic wave influence on buried pipelines with ASCE soil-spring model," in *Proc. ASME 2014 33rd Int. Conf. Ocean, Offshore and Arctic Eng.*, Jun. 2014, pp. 1-9, doi: 1115/OMAE2014-24650.

[36] S. Joshi, A. Prashant, A. Deb, and S. K. Jain, "Analysis of buried pipelines subjected to reverse fault motion," *Soil Dyn. and Earthq. Eng.,* vol. 31, no. 7, pp. 930-940, Jul. 2011, doi: 10.1016/j.soildyn.2011.02.003.

[37] J. Zhang, Z. Liang, and H. Zhang, "Response analysis of buried pipeline subjected to reverse fault displacement in rock stratum," *Trans. FAMENA,* vol. 40, no. 3, pp. 91-100, 2016, doi: 10.21278/TOF.40308.

[38] L. Xu and M. Lin, "Analysis of buried pipelines subjected to reverse fault motion using the vector form intrinsic finite element method," *Soil Dyn. and Earthq. Eng.,* vol. 93, pp. 61-83, Feb. 2017, doi: 10.1016/j.soildyn.2016.12.004.

[39] A. J. Sadowski and J. M. Rotter, "Solid or shell finite elements to model thick cylindrical tubes and shells under global bending," *Int. J. Mech. Sci.,* vol. 74, pp. 143-153, Sep. 2013, doi: 10.1016/j.ijmecsci.2013.05.008.

[40] X. Liu, H. Zhang, K. Wu, M. Xia, Y. Chen, and M. Li, "Buckling failure mode analysis of buried X80 steel gas pipeline under reverse fault displacement," *Eng. Failure Anal.,* vol. 77, pp. 50-64, Jul. 2017, doi: 10.1016/j.engfailanal.2017.02.019.

[41] *Oil and Gas Pipeline Systems*, Z662-07, Canadian Standards Association, Ontario, Canada, Jun. 2007.

[42] E. C. Goodling, "Buried piping—an analysis procedure update," in *Proc. Int. Symp. Lifeline Earthq. Eng.*, Jun. 1983, pp. 225-237.

[43] N. K. Psyrras and A. G. Sextos, "Safety of buried steel natural gas pipelines under earthquake-induced ground shaking: a review," *Soil Dyn. and Earthq. Eng.,* vol. 106, pp. 254-277, Mar. 2018, doi: 10.1016/j.soildyn.2017.12.020.

[44] P. Vazouras, S. A. Karamanos, and P. Dakoulas, "Mechanical behavior of buried steel pipelines crossing strike-slip seismic faults," in *ASME 2011 30th Int. Conf. Ocean, Offshore and Arctic Eng.*, Jun. 2011, pp. 429-438, doi: 10.1115/OMAE2011-49455.

[45] K.-J. Lee, S.-K. Kim, and K.-H. Lee, "Flowable backfill materials from bottom ash for underground pipeline," *Materials,* vol. 7, no. 5, pp. 3337-3352, Apr. 2014, doi: 10.3390/ma7053337.

[46] "TB-1104 – DARAFILL controlled low strength material technical bulletin," GCP Applied Technologies, Cambridge, MA, USA. Accessed: Aug. 24, 2015. [Online]. Available: https://gcpat.com/en/solutions/products/tb-1104-darafill-controlled-low-strength-material-technical-bulletin.

[47] E. Uckan, B. Akbas, J. Shen, W. Rou, F. Paolacci, and M. O'Rourke, "A simplified analysis model for determining the seismic response of buried steel pipes at strike-slip fault crossings," *Soil Dyn. and Earthq. Eng.,* vol. 75, pp. 55-65, Aug. 2015, doi: 10.1016/j.soildyn.2015.03.001.

[48] P. Vazouras, P. Dakoulas, and S. A. Karamanos, "Pipe–soil interaction and pipeline performance under strike–slip fault movements," *Soil Dyn. and Earthq. Eng.,* vol. 72, pp. 48-65, May 2015, doi: 10.1016/j.soildyn.2015.01.014.

[49] *Buried Flexible Steel Pipe Design and Structural Analysis*, ASCE Manuals and Reports on Engineering Practices No. 119, American Society of Civil Engineers, Reston, VA, 2009.

VITA

Prapon Somboonyanon was born in Chachoengsao, Thailand. He was educated in public schools and completed high school from Bodindecha (Sing Singhaseni) in 1995. He then attended the King Mongkut's University of Technology Thonburi, Bangkok, Thailand, and finished the program in 1999 with a degree of Bachelor of Engineering in Civil Engineering.

In 1999, he began his study abroad at the University of Missouri-Kansas City and obtained another degree of Bachelor of Science in Civil Engineering in 2001. He then continued his education in a Master of Science program in the same year and completed the program in 2003 with the thesis entitled "Model for Behavior of Granular Materials with Pseudo Particle-Potentials". After the graduation, he served as a civil engineer performing roadway and traffic related designs as well as developing Asset Management System for Public Works Department of Jackson County, Independence, Missouri until 2006.

Since 2006, he has worked as a full-time civil/structural engineer in Transmission & Distribution Department at Burns & McDonnell while pursuing a doctoral degree in Interdisciplinary Ph.D. program emphasizing in Civil Engineering and Geosciences as a part-time student. Mr. Somboonyanon is a Professional Engineer registered in several states/provinces in the United States and Canada.